Chapter 4: Elucidating the "Sulfation Code" of Chondroitin Sulfate Glycosaminoglycans*†

Background

Chondroitin sulfate proteoglycans (CSPGs) are complex oligosaccharides that display a variety of sulfation patterns (see Figure 2.1, Chapter 2), and of these sulfation patterns, CS-A and CS-C are the most abundant. In the embryonic rat brain, 30% of the CS glycosaminoglycan (GAG) disaccharide units display CS-C and 67% CS-A. The remaining disaccharides are believed to consist largely of the oversulfated motifs, CS-E and CS-D (Figure 4.1), motifs enriched in the developing brain,[1] and small amounts of CS-K, CS-L, and CS-M (Figure 2.1, Chapter 2).[2]

Paradoxically, CS has been reported both to stimulate and inhibit neuronal growth, depending on the cellular context. For instance, CSPGs can repel migrating neurons or extending axons during brain development or following injury.[3,4] Studies

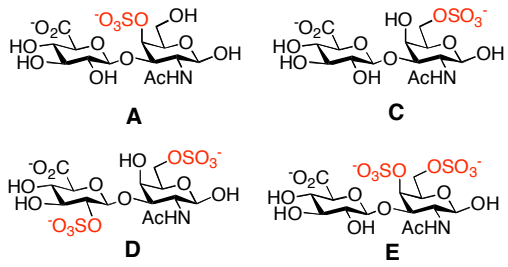

Figure 4.1: Major chondroitin sulfate disaccharides of the embryonic rat brain Ac = acetyl.

* Neurobiological studies were done in collaboration with Cristal I. Gama, a graduate student in the Hsieh-Wilson laboratory, and Naoki Sotogaku, a graduate student in Akinori Nishi's laboratory in the Department of Pharmacology at the Kurume University School of Medicine, Kurume, Fukuoka, Japan. Computational modeling studies were done in collaboration with Peter M. Clark, a graduate student in the Hsieh-Wilson laboratory.

† Portions of this chapter were taken from C.I. Gama *et al*. (2006) *Nat. Chem. Biol.* accepted.

with rat spinal cord injury models show a build-up of CSPGs in the area of the wound, but treatment with the enzyme chondroitinase ABC, which cleaves the CS side chains from the proteoglycans, promotes axonal growth, suggesting that CS prevents neuroregeneration.[4] During development of the neural crest, CSPGs stop migrating neurons from entering specific areas in order to guide them to their proper targets.[5]

However, CS staining also coincides with developing axon pathways, and tissues expressing CS do not always exclude axon entry.[6] The CS-E enriched CS chains of the proteoglycan phosphacan promote neurite outgrowth of both embryonic rat mesecephalic and hippocampal neurons,[7] and CSPGs are also important in promoting growth of developing olfactory bulb neurons.[8] Neuronal cultures grown on CS-E-enriched polysaccharides[9] and on synthetic CS-E tetrasaccharides (Chapter 3) had longer neurite projections than control neurons, and implicate this motif as being growth-promoting. The growth inhibitory or stimulatory properties of CS are most likely associated with the types of sulfation motifs the CS chains display, as they may dictate CS binding partners.

GAGs regulate various growth factors involved in cell growth and development, including fibroblast growth factors (FGF), Hedgehog, Wnt/Wingless, and semaphorins.[3,9-11] The ability of CS polysaccharides to modulate neuronal growth[12,13] suggests that CS may recruit specific growth factors to the cell surface, thereby activating downstream signaling pathways. The structural diversity of GAGs *in vivo* has led to the hypothesis that unique sulfated structures may modulate binding interactions and the activity of growth factors. For example, preparations of polysaccharides enriched in the oversulfated CS-E sequence, with 65% of the disaccharide units displaying the CS-E motif, have been shown to bind preferentially to growth factors, such as pleiotrophin and

midkine, which are crucial for proper brain development.[12] Systematic investigations into the sulfation requirements for protein binding have been hindered due to the complexity and heterogeneity of GAGs.

To elucidate the neurobiological activities of the sulfation patterns CS-A, CS-C, and CS-E, we decided to utilize the synthetic methodology developed in Chapter 3 to expand the CS tetrasaccharide library (Figure 4.2). In addition to the CS-A, CS-C, and CS-E tetrasaccharides, we also generated two unnatural CS molecules, a dimer of CS-E disaccharides linked via an aminooxy linker, and a tetrasaccharide with a sulfation motif not yet observed in nature, CS-R. It is possible that CS-R is present due to the existence of sulfotransferase enzymes that target the C-2 and C-3 hydroxyls.[14] The dimer and CS-R were synthesized as controls, for unlike the CS-A or CS-C tetrasaccharides, they have the same net overall charge as the CS-E tetrasaccharide, but the sulfate groups are displayed in a different manner. These controls will enable us to determine if the exact placement of the sulfate groups is important for biological activity, not just the overall charge.

As in Chapter 3, we decided to use embryonic hippocampal neurons to test the neurite outgrowth promoting effects of the CS oligosaccharides, and we also wanted to discover whether the effects of the CS molecules were unique to specific cell types through use of dopaminergic and dorsal root ganglion neurons. In addition, we began to investigate potential CS binding partners (Chapter 5) and the pathways through which CS activity is regulated.

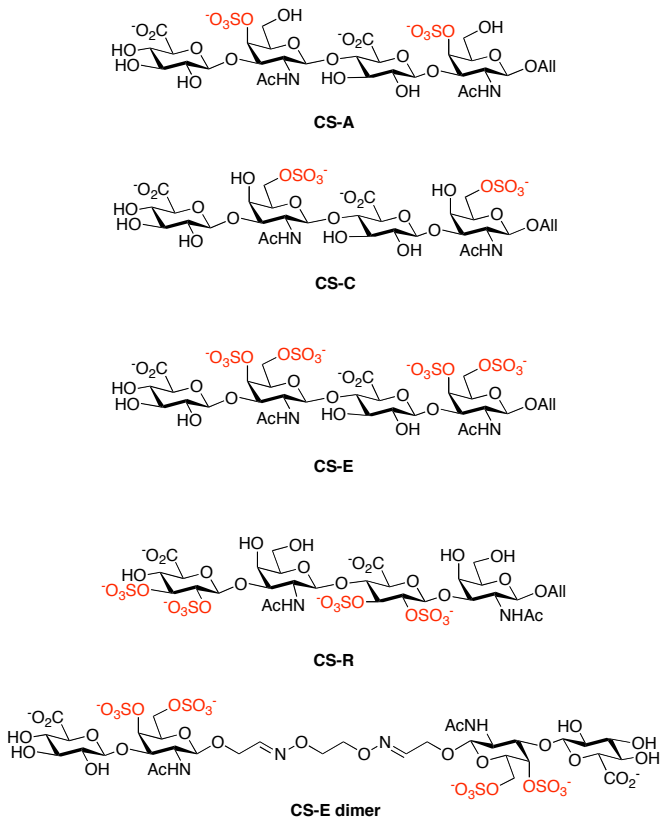

Figure 4.2: Structures of the second library of synthetic CS oligosaccharides. All = allyl, Ac = acetyl.

Completion of the library of CS oligosaccharides

We began the synthesis of CS-A, CS-C, and CS-R tetrasaccharides with tetraol **76**, synthesized in Chapter 3. Due the convergent and modular nature of our synthesis, we were able to generate all of the CS tetrasaccharides using one common intermediate. From tetraol **76**, CS-A was generated in five steps (Scheme 4.1). Selective C-6 benzoylation followed by C-4 sulfation of the *N*-acetylgalactosamine (GalNAc) moieties using excess sulfur trioxide-trimethylamine complex[15] afforded **83** in a 78% yield for the two steps. Cleavage of the silyl group and the esters[16] in a manner similar to that described for **79: CS-E** and **81** (see Chapter 3) gave the final CS-A tetrasaccharide **85**.

The compound was characterized by ^{1}H NMR (Figure 4.3), proton decoupling experiments and ESI-MS, and C-4 sulfation on the GalNAc moieties was confirmed by the presence of doublets with *J* values of 3.0 Hz at 4.79 and 4.74 ppm.

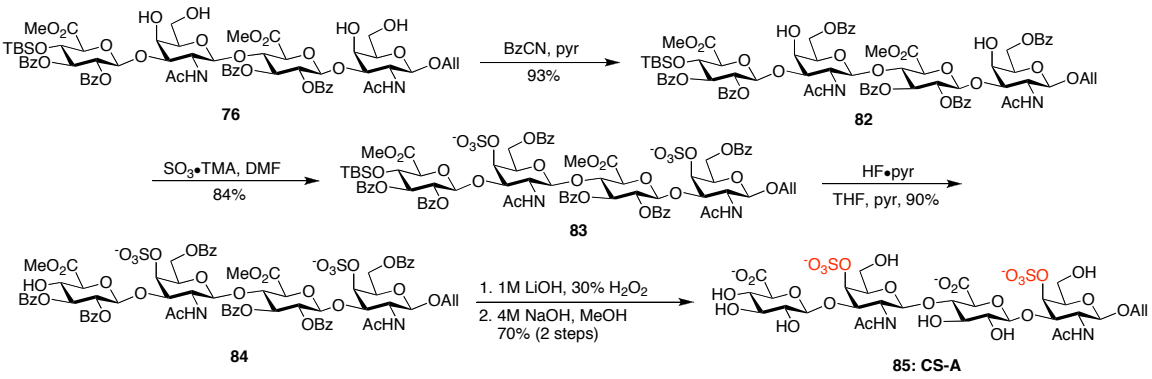

Scheme 4.1: Synthesis of the CS-A tetrasaccharide **85**. TBS = *t*-butyldimethylsilyl, Me = methyl, Bz = benzoyl, Ac = acetyl, BzCN = benzoyl cyanide, pyr = pyridine, All = allyl, TMA = trimethylamine.

The CS-C tetrasaccharide was accessible in four steps from tetraol **76** (Scheme 4.2). With six equivalents of sulfur trioxide-trimethylamine complex and a shorter reaction time than that of the CS-E tetrasaccharide sulfation reaction, selective C-6 sulfation of the GalNAcs was observed to afford **86**. Some trisulfated product was observed and could be avoided using a shorter reaction time, but this product can be used to generate CS-E tetrasaccharide **79**. The silyl and ester groups were removed, as before, to yield CS-C tetrasaccharide **88**. The compound was characterized in the same manner as described for the CS-A tetrasaccharide and the ^{1}H NMR is shown in Figure 4.4.

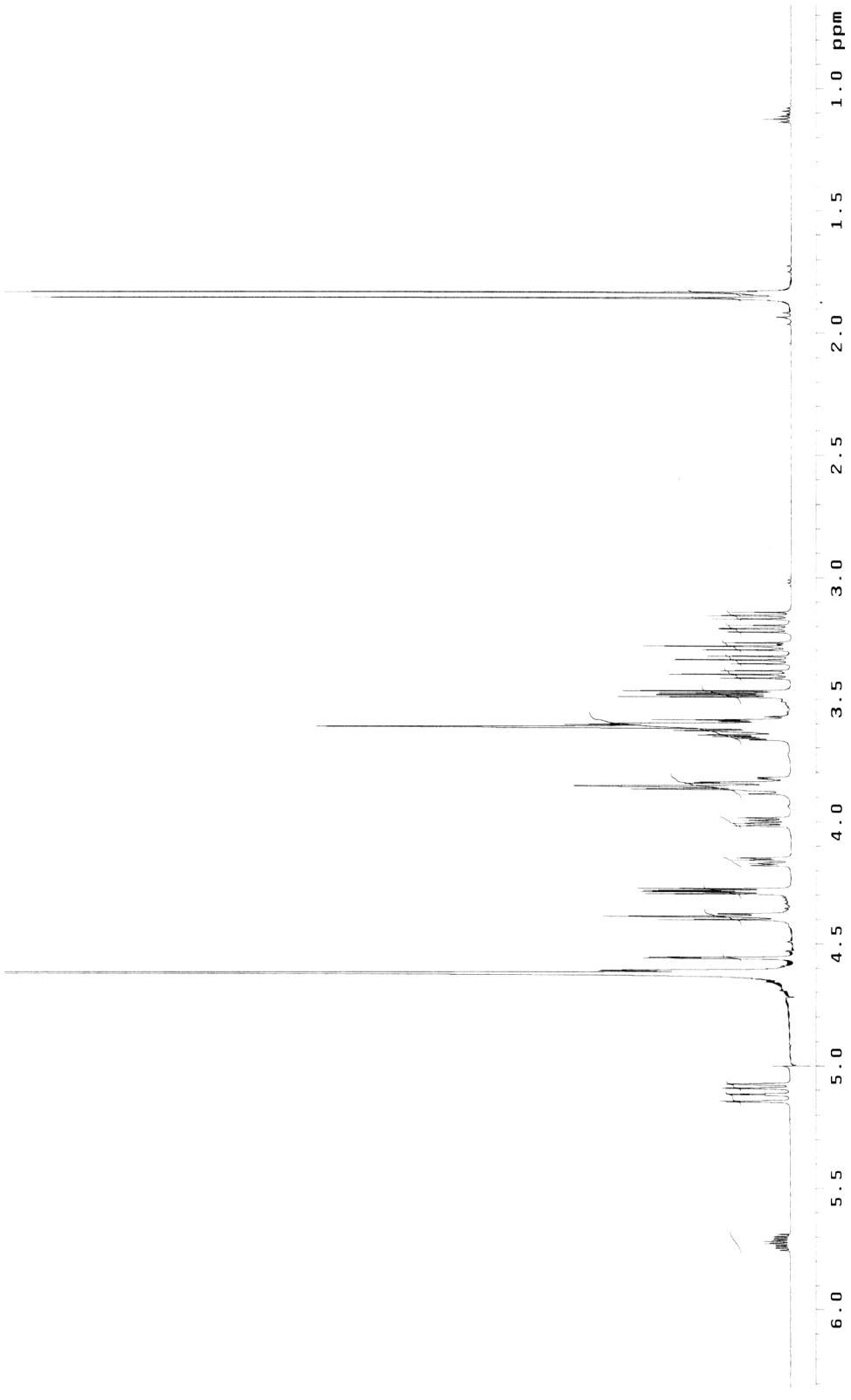

Figure 4.3: ^{1}H NMR (600 MHz, D_2O) of CS-A tetrasaccharide **85**.

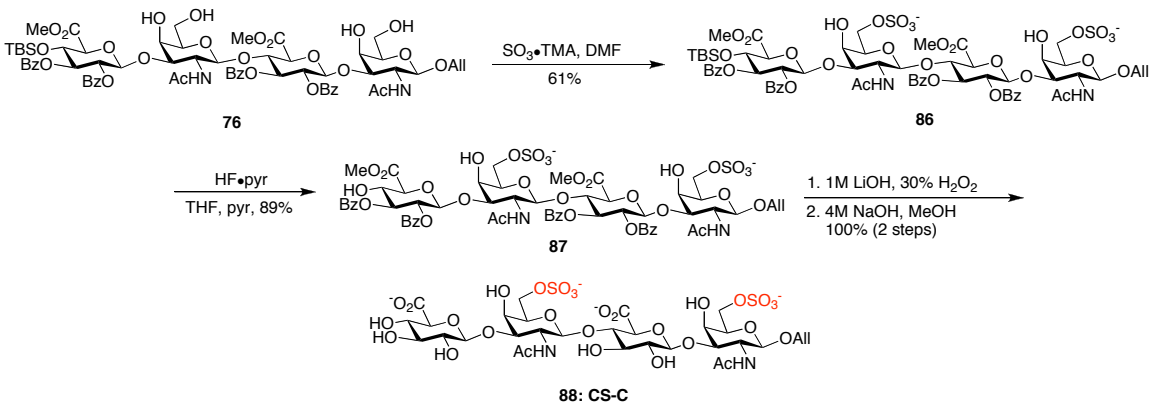

Scheme 4.2: Synthesis of the CS-C tetrasaccharide **88**. TBS = *t*-butyldimethylsilyl, Me = methyl, Bz = benzoyl, Ac = acetyl, TMA = trimethylamine, pyr = pyridine, All = allyl.

Synthesis of the CS-R tetrasaccharide was completed in five steps from **76** (Scheme 4.3). First, the C-4 and C-6 hydroxyl groups of the GalNAc moieties were protected in a benzylidene acetal to afford **89**. The benzylidene acetal proved to be more stable than the *p*-methoxybenzylidene acetal during the sulfation reaction, which can get acidic as the reaction proceeds. The esters were then cleaved using sequential LiOOH-NaOH treatment to give **90** in a yield of 56%. The reduced yield compared to previous reactions using these conditions reflects migration of the TBS group from the C-4 hydroxyl of glucuronic acid (GlcA) to the C-3 hydroxyl. Sulfation was then performed with sulfur trioxide-triethylamine in DMF for 12 h. Sulfur trioxide-triethylamine complex was utilized because it is more activated than sulfur trioxide-trimethylamine complex[17] and is more able to sulfate the hindered C-2 and C-3 hydroxyls of the GlcA units. Longer reaction times, which were necessary when attempts to sulfate with sulfur trioxide-trimethylamine complex were performed, led to degradation of the product to either disaccharides or loss of the TBS group to afford a pentasulfated product. As this reaction can become acidic, these products are presumably due to the electron-withdrawing nature

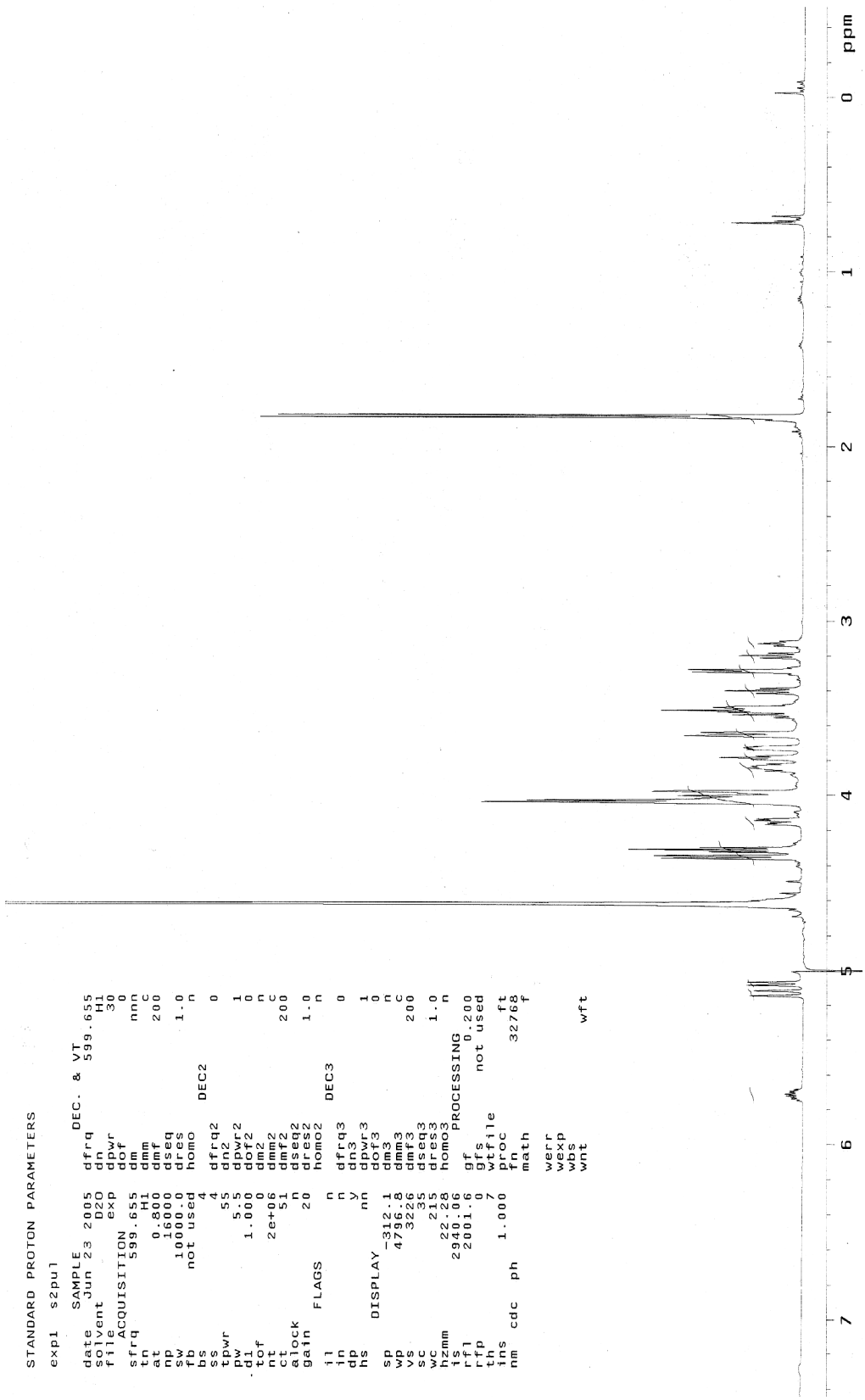

Figure 4.4: ^{1}H NMR (600 MHz, D_2O) of CS-C tetrasaccharide **88**.

of the C-3 sulfate groups. The final CS-R tetrasaccharide **92** was afforded upon acid cleavage of the TBS group and benzylidene acetals. The ^{1}H NMR is shown in Figure 4.5, and the *J* values of 5.4 and 6.0 Hz for the GlcA anomeric protons suggest that these sugars take a conformation different than the standard chair conformation, potentially boat or twist-boat,[18] due to the presence of the C-2 and C-3 sulfates. Typical *J* values for these protons when the sugar is in a chair conformation and the linkage is β are between 7.5 and 10 Hz, and *J* values for the α-linkage are between 3 and 5 Hz. For example, the *J* values for the GlcA anomeric protons of the CS-E tetrasaccharide were 7.8 Hz. The protons for the sulfated GlcA C-2 and C-3 positions are located between 4.45 and 4.10 ppm, as opposed to 3.58 and 3.31 ppm when they are unsulfated, and unlike previous spectra, the GlcA anomeric protons are now shifted downfield compared to the GalNAc anomeric protons.

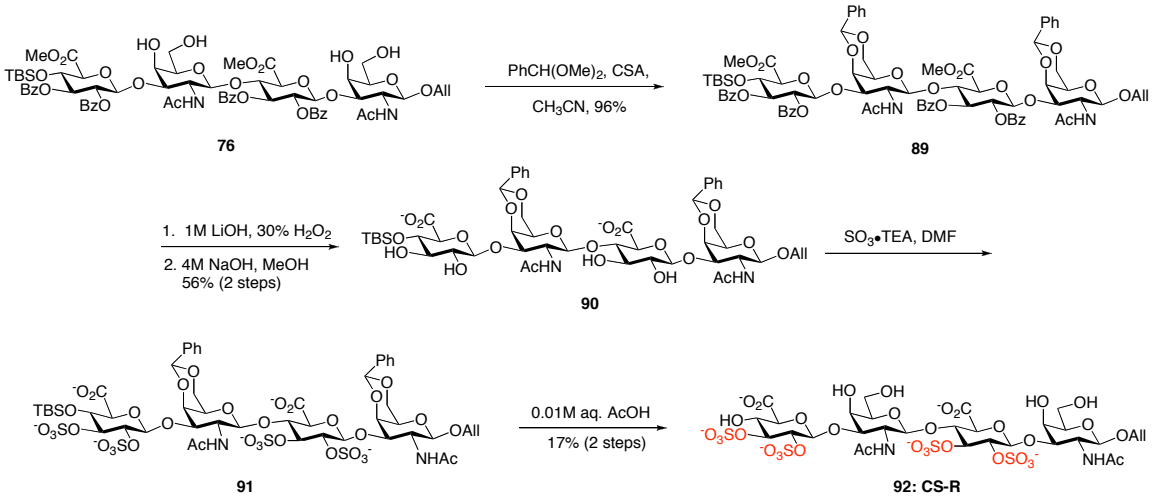

Scheme 4.3: Synthesis of the CS-R tetrasaccharide **92**. TBS = *t*-butyldimethylsilyl, Me = methyl, Bz = benzoyl, Ac = acetyl, TEA = triethylamine, All = allyl, $PhCH(OMe)_2$ = benzaldehyde dimethyl acetal, CSA = (±)-DL-camphor-10-sulfonic acid, Ph = phenyl.

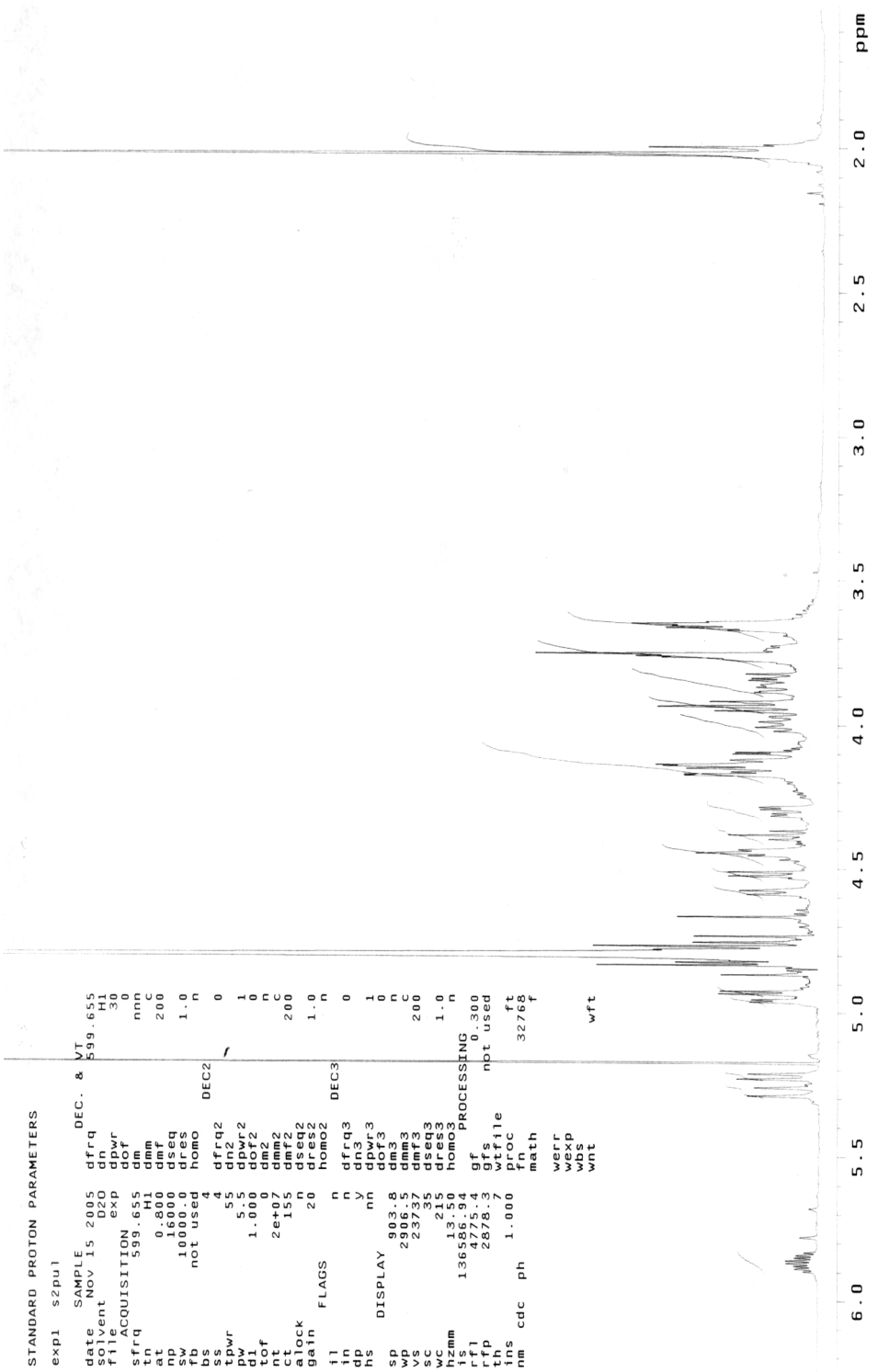

Figure 4.5: ^{1}H NMR (600 MHz, D_2O) of CS-R tetrasaccharide **92**.

The dimer of CS-E disaccharides was produced from CS-E disaccharide **73** (Scheme 4.4). Ozonolysis of the allyl group afforded aldehyde **93**, and two equivalents of the aldehyde were then linked via one equivalent of the aminooxy linker **94**, synthesized in two steps from 1,2-dibromoethane,[19] to yield dimer **95**. The ^{1}H NMR is shown in Figure 4.6.

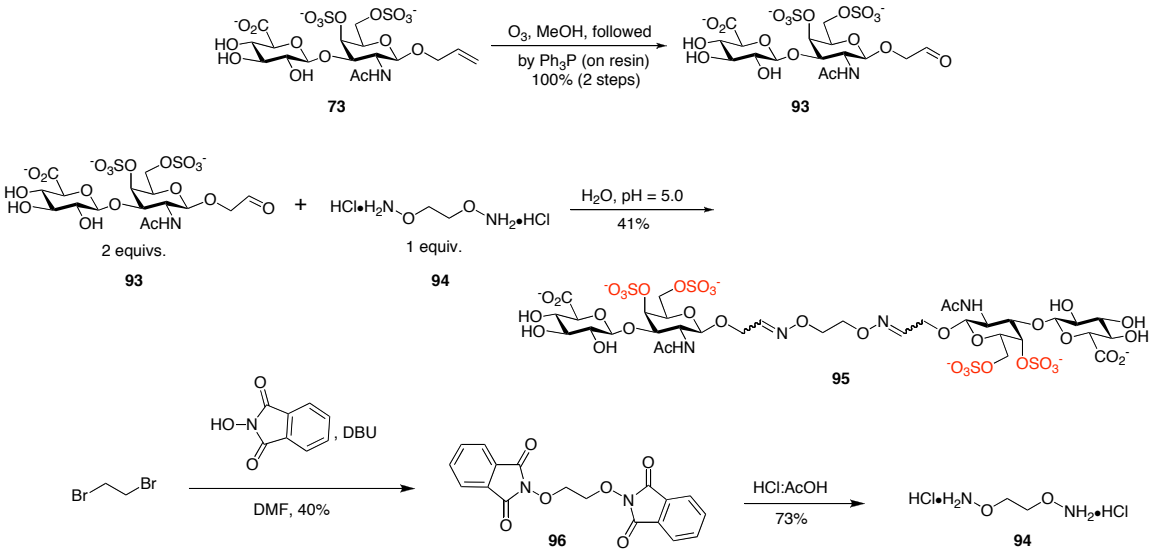

Scheme 4.4: Synthesis of the CS-E dimer **95**. Ac = acetyl, Ph = phenyl, DBU = 1,8-diazabicyclo[5.4.0]undec-7-ene.

Through our synthetic method, we were able to synthesize six CS oligosaccharides (**85: CS-A**, **88: CS-C**, **79: CS-E**, **92: CS-R**, an unsulfated tetrasaccharide **81** and a dimer of CS-E disaccharides **95**) for biological evaluation. Our method was convergent, and we were able to make all of the sulfation motifs from one key disaccharide and one key tetrasaccharide.[13,20] To our knowledge, it is the first time five different CS sulfation patterns were generated from one tetrasaccharide.

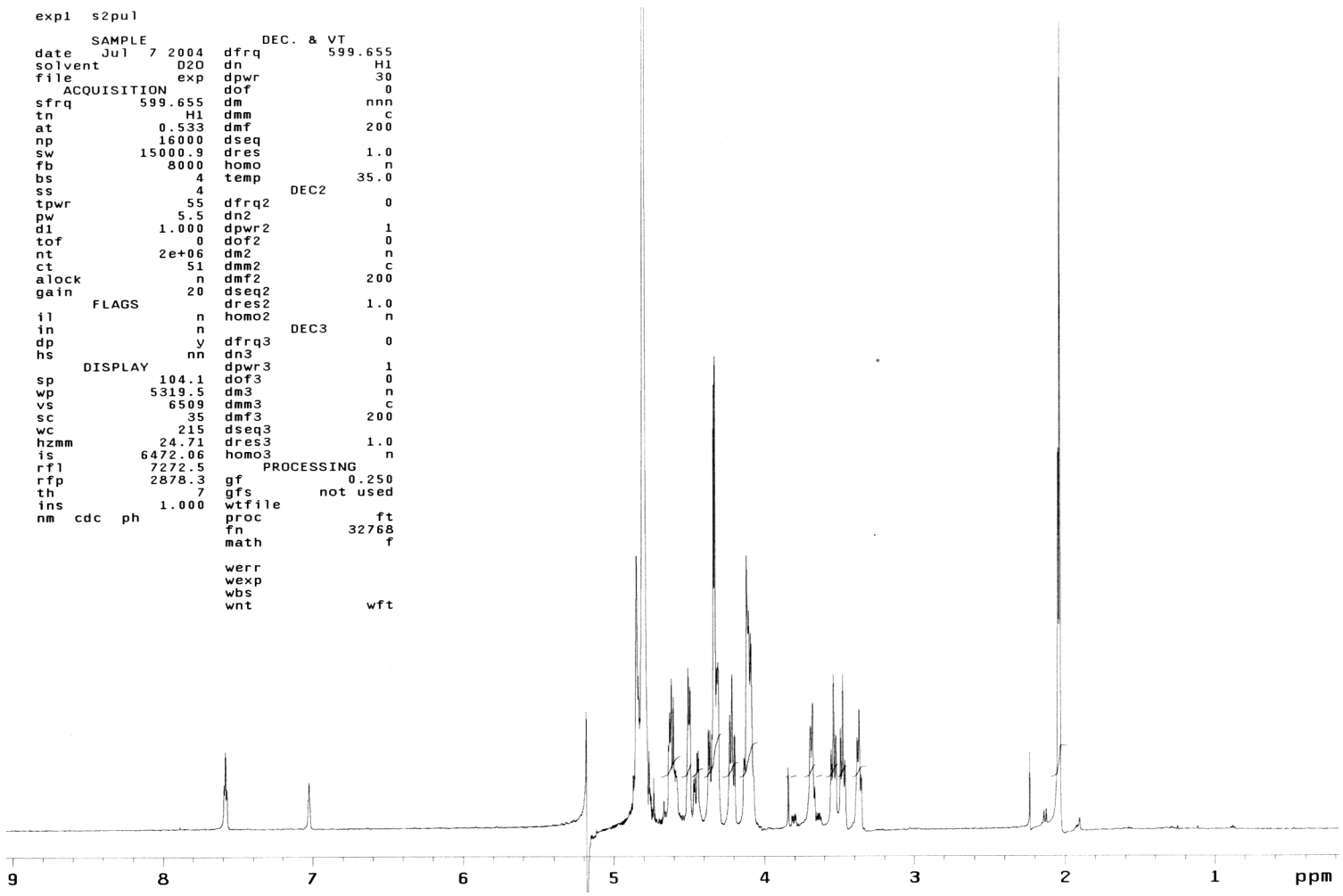

Figure 4.6: ^{1}H NMR (600 MHz, D_2O) of CS-E dimer **95**.

Computational modeling of synthetic chondroitin sulfate oligosaccharides

With the ability to access well-defined CS sequences, we embarked on systematic investigations into the role of sulfation. Peter Clark first investigated computationally whether subtle variations in the sulfation pattern would favor distinct structural conformations of GAGs. We used the Dreiding force field[21] (modified slightly using quantum mechanics) with charges from the Charge Equilibrium[22] (QEq) method and carried out Boltzmann jump simulations[23] on the tetrasaccharides to obtain the lowest energy CS conformations. These conformations were then used to perform molecular dynamics simulations[23] in explicit water to predict the optimum conformation in solution. Interestingly, we found that each CS tetrasaccharide favors a distinct set of torsion angles and presents a unique electrostatic and van der Waals surface for interaction with proteins (Figure 4.7). Whereas the negatively charged sulfate and carboxylate groups on CS-C point toward either the top or bottom face of the molecule as oriented in Figure 4.7, the same charges on CS-A point in multiple different directions. Similarly, although CS-E and CS-R have the same number of sulfate groups, the relative orientation of these groups along the carbohydrate backbone leads to distinctly different predicted solution structures. Whereas the CS-R tetrasaccharide has the sulfate groups distributed along multiple faces of the molecule, the CS-E tetrasaccharide presents all four sulfate groups along a single face, which may position the groups to interact with basic residues characteristic of GAG binding sites on proteins.[24]

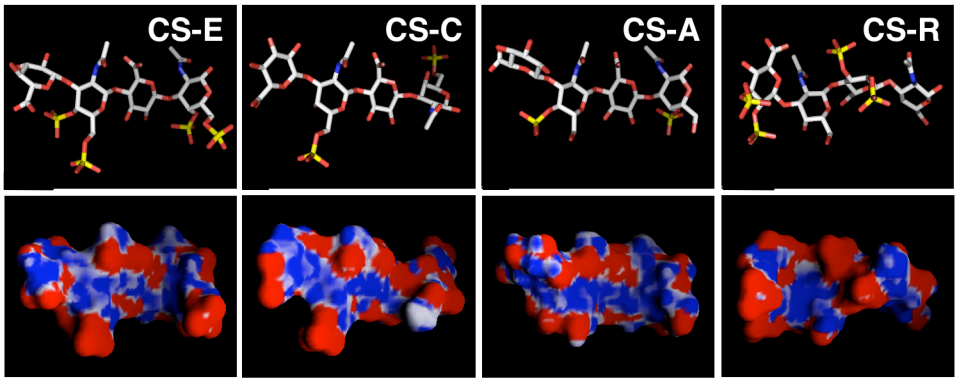

Figure 4.7: Average structures from molecular dynamics simulations of the CS tetrasaccharides in water. The sulfation pattern influences the structure of CS, allowing it to present distinct electrostatic and van der Waals surfaces to proteins. The CS ball-and-stick figures were generated in PyMOL, and the electrostatic maps were created using GRASP.

Biological evaluation of the chondroitin sulfate library

To compare the neuritogenic activity of the tetrasaccharides and the dimer, Cristal Gama cultured primary hippocampal neurons from embryonic day 18 (E18) rats on coverslips coated with polyornithine and each compound. The neurons were fixed after 48 h, immunostained with anti-tubulin antibodies, and examined by confocal fluorescence microscopy. A specific CS sulfation pattern was required for the growth-promoting activity of CS. Whereas the CS-E tetrasaccharide stimulated neurite outgrowth by 48.6 ± 2.3% relative to the polyornithine control, tetrasaccharides representing other CS subclasses found *in vivo*, CS-A and CS-C, and the dimer had no appreciable activity (Figure 4.8, a and b). Importantly, CS-R had no effect on neurite outgrowth, despite having the same overall negative charge as CS-E. These results are consistent with previous reports that CS polysaccharides enriched in the CS-E sulfation pattern possess neuritogenic activity.[25] In this study, we further extend those findings by establishing that a precise orientation of the sulfate groups is critical for the growth-promoting ability of CS.

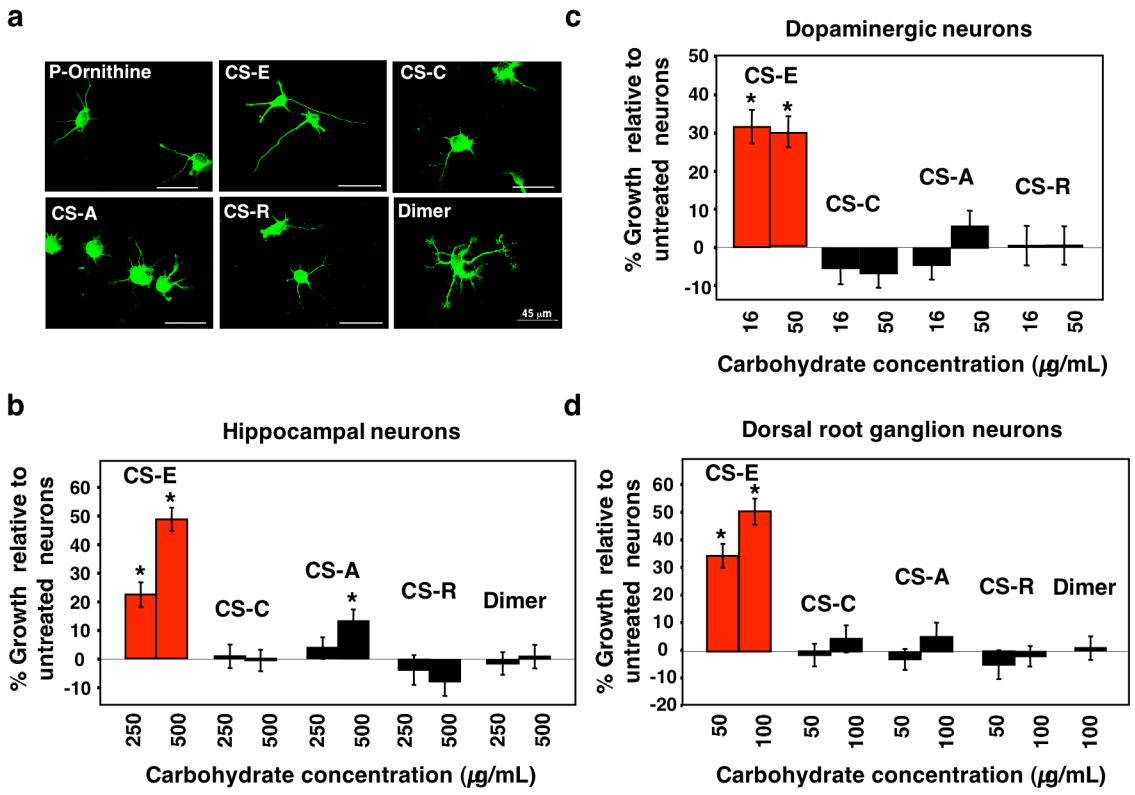

Figure 4.8: The sulfation pattern directs the neuritogenic activity of CS. (**a**) Representative immunofluorescence images of hippocampal neurons cultured on a substratum of polyornithine and the synthetic tetrasaccharides. Scale bar, 50 µm. (**b**) The CS-E tetrasaccharide **1** stimulates the outgrowth of hippocampal neurons. Altering the position of the sulfate groups, but not the overall electrostatic charge, modulates the neuritogenic activity of CS. (**c**, **d**) The specific sulfation pattern directs the activity of CS toward various neuron types. The CS-E tetrasaccharide **1** promotes the outgrowth of dopaminergic (**c**) and dorsal root ganglion (**d**) neurons. Neurons were cultured for 2-5 days on glass coverslips coated with polyornithine and the tetrasaccharides at the indicated concentrations. The tetrasaccharide concentration required to elicit neurite outgrowth varied depending on the neuron type, which likely indicates differences in the expression levels of protein receptors or downstream signaling components. Neurite length (mean ± s.e.m.) was quantified using NIH Image 1.62 or Neurolucida 2000 software after immunostaining with anti-tubulin (**a,b**), anti-tyrosine hydroxylase (**c**) or anti-β tubulin III (**d**) antibodies. Statistical analysis was performed using the one-way ANOVA followed by the Scheffe-test. n = 50-200 cells. Asterisk, $P < 0.0001$, relative to polyornithine control.

We next investigated whether the effects of the CS-E motif were unique to specific cell types and whether growth promotion is dependent on certain sulfation patterns. Dopaminergic neurons, the neurons affected in Parkinson's disease,[26] from the mesencephalon of rat embryos were cultured on a substratum of each oligosaccharide by Naoki Sotogaku. We found that the CS-E tetrasaccharide had a similar activity toward both dopaminergic and hippocampal neurons, inducing the outgrowth of dopaminergic neurons by 29.6 ± 6.0 % (Figure 4.8c). In contrast, the CS-C, CS-A, and CS-R motifs exhibited no significant neuritogenic activity. Similarly, Cristal Gama observed that the CS-E tetrasaccharide, but not other sulfation motifs, stimulated the outgrowth of dorsal root ganglion (DRG) neurons derived from the spinal cord (Figure 4.8d). These neurons are a good model to investigate the effects of CS oligosaccharides on spinal cord neurons. The ability of the CS-E sulfation motif to elicit a response in various cell types suggests that protein receptors are likely present to engage the sugar, which are shared by multiple cell types. These results indicate that the molecular structure of CS GAGs is critical for the function of CS, independent of neuron type.

Growth factors interact with the CS-E sulfation sequence, and these interactions may regulate neuronal growth. Potentially, CSPGs bearing the CS-E motif could recruit specific growth factors to the cell surface and thereby trigger downstream signaling pathways. To elucidate this mechanism, Cristal Gama grew hippocampal neurons on a CS-E tetrasaccharide or polyornithine substratum in the presence or absence of antibodies selective for midkine or brain-derived neurotrophic factor (BDNF) to block the interaction of the endogenous growth factors with the CS-E substratum. These proteins were chosen because through use of CS microarrays displaying our synthetic molecules

(see Chapter 5), we found that CS-E specifically interacts with the growth factors midkine and BDNF.[27] Midkine participates in the development and repair of neural and other tissues[28] and has been shown to bind with nanomolar affinity to heterogeneous polysaccharides enriched in the CS-E motif.[13] The neurotrophin BDNF controls many aspects of mammalian nervous system development and contributes to synaptic plasticity, neurotransmission and neurodegenerative disease.[29]

Antibodies against midkine or BDNF had no effect on neurite outgrowth in the absence of the tetrasaccharide (Figure 4.9a). Importantly, addition of either antibody blocked the neurite outgrowth induced by CS-E. In contrast, a control antibody selective for FGF-1, a growth factor known to not interact with CS-E oligosaccharides based on our microarray results[21] (see Chapter 5) and previous studies,[12] as well as rabbit and goat IgG antibodies, could not abolish the growth-promoting effects of CS-E (Figure 4.10a). We confirmed that the antibodies could disrupt binding of the growth factors to CS-E using carbohydrate microarrays. As expected, the antibodies effectively blocked the interaction between midkine or BDNF and the CS-E tetrasaccharide on the microarray (Figure 4.11).

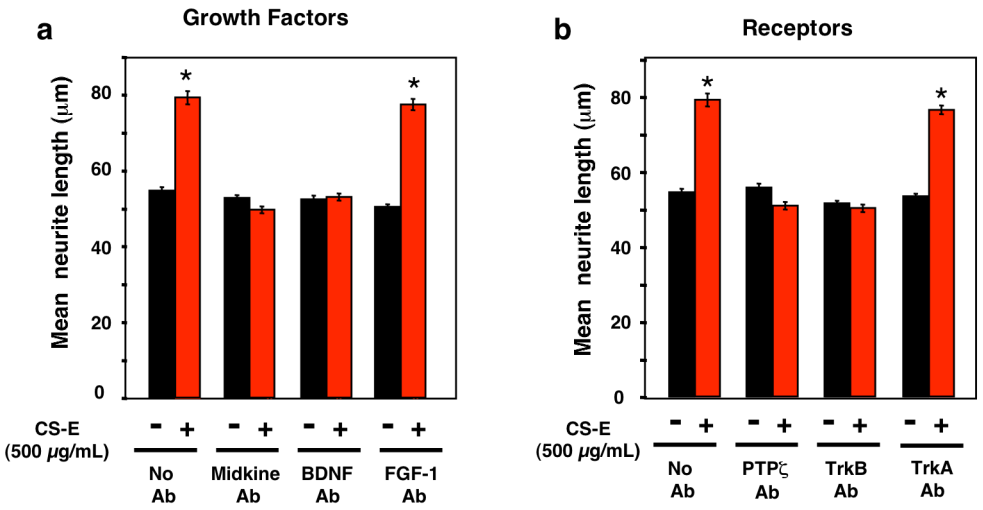

Figure 4.9: The CS-E sulfation motif stimulates neuronal growth through activation of midkine- PTPζ and BDNF-TrkB signaling pathways. (a) Antibodies selective for midkine or BDNF, but not FGF-1, block the neurite outgrowth induced by CS-E. (b) Antibodies against the receptors PTPζ or TrkB, but not TrkA, abolish the growth-promoting effects of CS-E. Hippocampal neurons were cultured on a substratum of poly-DL-ornithine or poly-DL-ornithine plus the CS-E tetraccharide (500 μg/mL). After 24 h, the antibodies (midkine, FGF-1, TrkB, TrkA, 4 μg/mL; BDNF, 1 μg/mL; PTPζ, 2 μg/mL) were added to the medium and incubated with the cells for 24 h. Neurite length (mean ± s.e.m.) was quantified using NIH Image 1.62 software after immunostaining with anti-tubulin antibodies. Asterisk, $P < 0.0001$, relative to the CS-E, no antibody control. n = 150 cells.

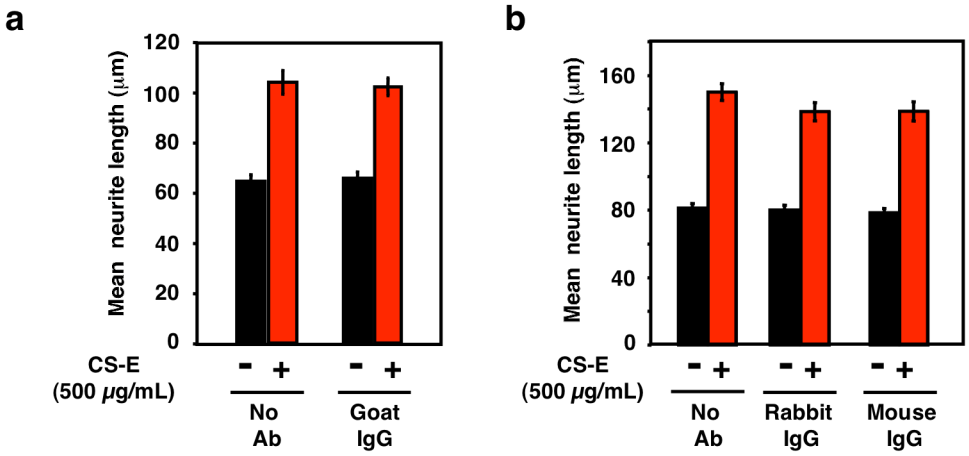

Figure 4.10: Class-matched IgG control antibodies do not effect neurite outgrowth in the presence or absence of CS-E. Hippocampal neurons were cultured on a substratum of poly-DL-ornithine or poly-DL-ornithine plus the CS-E tetraccharide (500 μg/mL). After 24 h, the antibodies (goat IgG, 4 μg/mL; rabbit IgG, 2 μg/mL; mouse IgG, 4 μg/mL) were added to the medium and incubated with the cells for 24 h. Neurite length (mean ± s.e.m.) was quantified using NIH Image 1.62 software after immunostaining with anti-tubulin antibodies. Asterisk, $P < 0.0001$, relative to the CS-E, no antibody control.

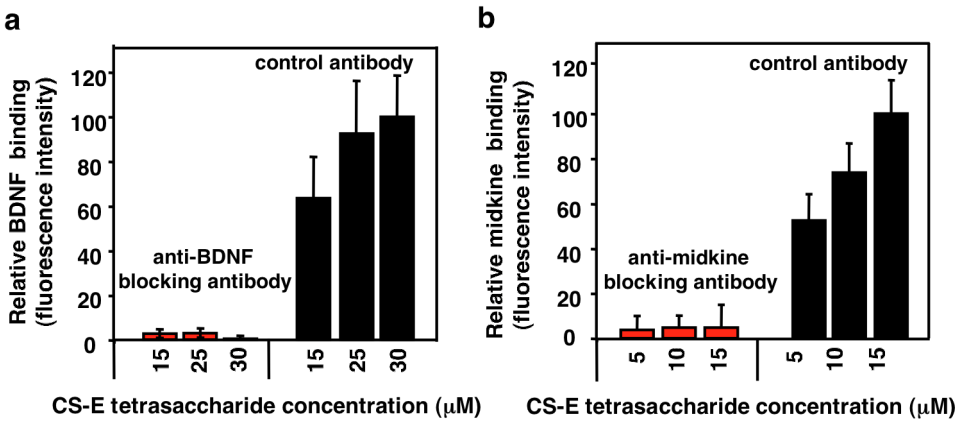

Figure 4.11: Antibodies against BDNF or midkine, but not control IgG antibodies, block the binding of BDNF or midkine to CS-E on the microarray. (**a**) Quantitative analysis of the relative binding of BDNF to the CS-E tetrasaccharide in the presence of a rabbit anti-BDNF IgG antibody (red, left) or a rabbit IgG control antibody (black, right). Data were normalized with respect to the average fluorescence intensity for BDNF binding to 30 μM CS-E in the presence of the control antibody. (**b**) Quantitative analysis of the relative binding of midkine to the CS-E tetrasaccharide in the presence of a goat anti-midkine IgG antibody (red, left) or a goat IgG control antibody (black, right). Data were normalized with respect to the average fluorescence intensity for midkine binding to 15 μM CS-E in the presence of the control antibody.

As further confirmation, Cristal Gama employed antibodies recognizing the extracellular domains of the cell surface receptors, protein tyrosine phosphatase zeta (PTPζ) and tyrosine kinase B receptor (TrkB). Binding of midkine and BDNF to PTPζ and TrkB, respectively, has been shown to promote neuronal outgrowth and survival in various systems by activating intracellular pathways such as mitogen associated protein kinase (MAPK), and phosphatidylinositol-3 kinase (PI3-K) pathways.[27,28] Notably, antibodies against either PTPζ or TrkB blocked the neuritogenic activity of CS-E (Figure 4.9b). In contrast, neither antibody alone had an effect on neurite outgrowth in the absence of CS-E. To demonstrate the specificity of the antibodies, we showed that TrkA and class-matched IgG control antibodies did not influence CS-E-mediated neurite outgrowth (Figure 4.9b and Figure 4.10b). These results indicate that the CS-E sulfation

motif stimulates neuronal growth through activation of midkine-PTPζ and BDNF-TrkB signaling pathways.

Discussion

Together, these studies provide compelling support for a 'sulfation code,' whereby the precise position of sulfate groups along the carbohydrate backbone permits GAGs to encode information in a sequence-specific manner. Using well-defined oligosaccharides, we have shown directly that distinct CS sulfation sequences can function as molecular recognition elements for growth factors and facilitate activation of associated signaling pathways. Moreover, the relative activity of CS-E versus other CS subclasses, CS-R and the dimer, as well as the preservation of activity across different cell types, suggest the importance of specific molecular interactions rather than non-specific, electrostatic effects. Heparan sulfate, a related GAG, has also been proposed to operate through a sulfation code,[29] and the concept finds strong precedent in the sequence-specific manner by which other biopolymers – DNA, RNA and proteins – interact with their molecular targets.

According to the sulfation code hypothesis, chemical modifications to the polysaccharide backbone may be introduced in a temporal- or region-specific manner, such as during neuronal development or in response to injury. Precise modifications to GAGs could facilitate or inhibit ligand-receptor interactions in a highly localized fashion, providing an exquisite mechanism for regulatory control. Indeed, specific sulfation motifs might control the diffusion and efficient signaling of growth factors, establishing concentration gradients and boundaries. In support of this view, the *tout-velu* gene

responsible for HS biosynthesis in *Drosophila* has been shown to be required for Hedgehog diffusion during embryonic patterning.[30] Moreover, specific CS sulfation motifs have been shown to be upregulated during neuronal development and enriched along axon growth tracts.[31]

Conclusion

Understanding the roles of GAGs will require new approaches and reagents to probe and manipulate their structures. We have shown that synthetic chemical approaches are particularly valuable in this regard, enabling the identification of biologically active sulfation motifs, systematic structure-function studies, and the analysis of GAG-protein interactions. While GAGs cannot yet be assembled with the same ease as nucleic acids or proteins, rapid advances in their synthesis and characterization are enabling the first molecular-level investigations of this important class of biopolymers. We anticipate that our approach to systematically exploring the role of sulfation sequences will open numerous opportunities for structural and biophysical studies, as well as facilitate exploration of the roles of GAGs across various proteins and biological contexts.

Experimental Procedures for Chapter 4

General methods

Unless stated otherwise, reactions were performed in flame-dried glassware under a nitrogen or an argon environment, using freshly-distilled solvents. Acetonitrile used for LC/MS was HPLC grade, and all aqueous solutions were made from nanopure water. All other commercially obtained reagents were used as received. Thin-layer chromatography (TLC) was performed using E. Merck silica gel 60 F254 precoated plates (0.25 mm). Visualization of the developed chromatogram was performed by fluorescence quenching, cerium ammonium molybdate stain, or ninhydrin stain, as necessary. ICN silica gel (particle size 0.032 - 0.063 mm) was used for flash chromatography. Gel filtration chromatography (Sephadex® LH-20, G-10 and G-25 ultrafine) and ion exchange chromatography [Sephadex® C-25 (Na^+)] were used in order to achieve purification of the final products.

^1H NMR and proton decoupling spectra were recorded on Varian Mercury 300 (300 MHz) and Varian Mercury 600 (600 MHz) spectrometers and the ^1H NMR spectra are reported in parts per million (δ) relative to the residual solvent peak. Data for ^1H are reported as follows: chemical shift (δ ppm), multiplicity (s = singlet, d = doublet, t = triplet, q = quartet, m = multiplet), coupling constant in Hz, and integration. ^{13}C NMR spectra were obtained on a Varian Mercury 300 (75 MHz) spectrometer and are reported in parts per million (δ) relative to the residual solvent peak. IR spectra were recorded on a Perkin Elmer Paragon 1000 spectrometer and are reported in terms of frequency of absorption (cm^{-1}). A JASCO P-1010 was used to measure optical rotation. Mass spectra

were obtained from the Protein/Peptide MicroAnalytical Laboratory on a Perkin Elmer/Sciex API 365 triple quadrupole/electrospray tandem mass spectrometer and the Mass Spectrometry Facility at the California Institute of Technology on a JEOL JMS-600H High Resolution Mass Spectrometer.

Synthetic methods

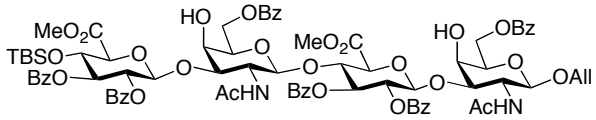

82

Allyl (methyl 2,3-di-*O*-benzoyl-4-*O*-*tert*-butyldimethylsilyl-*β*-D-glucopyranosyluronate)-(1 → 3)-(6-*O*-benzoyl-2-deoxy-2-acetamido-*β*-D-galactopyranosyl)-(1 → 4)-(methyl 2,3-di-*O*-benzoyl-*β*-D-glucopyranosyluronate)-(1 → 3)-6-*O*-benzoyl-2-deoxy-2-acetamido-*β*-D-galactopyranoside (82). Benzoylation of **76** was performed in the manner of Jacquinet *et al.*[15] **76** (60 mg, 0.44 mmol) was dissolved in pyridine (3.0 mL), and to this were added benzoyl cyanide (29 mg, 0.22 mmol) and 4-(dimethylamino)pyridine (13 mg, 0.11 mmol). The reaction stirred at rt for 12 h and was then concentrated to afford a yellow solid. The resulting crude product was purified by flash chromatography (100% EtOAc) to afford **82** (64 mg, 93%). R_f 0.86 (100% EtOAc). ^{1}H NMR (300 MHz, $CDCl_3$): δ = 8.02 – 7.98 (m, 3H, Ar*H*), 7.95 – 7.86 (m, 5H, Ar*H*), 7.58 – 7.30 (m, 22H, Ar*H*), 5.86 – 5.70 (m, 1H, OCH_2CH=CH_2), 5.55 (dd, *J* = 9.0, 9.0 Hz, 2H, H-3 GlcA), 5.47 (d, *J* = 6.9 Hz, 1H, N*H*Ac), 5.40 (dd, *J* = 8.4, 8.4 Hz, 2H, H-2 GlcA, N*H*Ac), 5.32 (dd, *J* = 8.4, 8.7 Hz, 1H, H-2 GlcA), 5.15 (dd, *J* = 1.4, 17.3 Hz, 1H, OCH_2CH=CH_2), 5.08 (dd, *J* = 1.4, 10.4 Hz, 1H, OCH_2CH=CH_2), 5.02 (d, *J*

= 8.1 Hz, 1H, H-1 GalNAc), 4.94 (d, *J* = 8.4 Hz, 1H, H-1 GalNAc), 4.88 (d, *J* = 7.5 Hz, 1H, H-1 GlcA), 4.83 (d, *J* = 7.8 Hz, 1H, H-1 GlcA), 4.68 (dd, *J* = 3.2, 10.7 Hz, 1H, H-3 GalNAc), 4.61 (dd, *J* = 3.2, 10.7 Hz, 1H, H-3 GalNAc), 4.56 – 4.54 (m, 2H), 4.30 – 4.23 (m, 3H), 4.11 – 4.01 (m, 5H), 3.92 – 3.84 (m, 2H), 3.68 – 3.59 (m, 8H, CO_2CH_3), 3.20 – 3.12 (m, 1H, H-5 GalNAc), 3.06 – 2.97 (m, 1H, H-5 GalNAc), 1.33 (s, 3H, HNC(O)CH_3), 1.33 (s, 3H, HNC(O)CH_3), 0.70 (s, 9H, $(CH_3)_3CSi$), -0.07 (s, 3H, CH_3Si), -0.21 (s, 3H, CH_3Si). ESI MS: *m/z*: calcd for $C_{81}H_{91}N_2O_{29}Si$: 1583.6; found 1583.2 [*M* + H]$^+$.

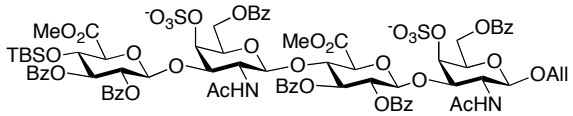

83

Allyl (methyl 2,3-di-*O*-benzoyl-4-*O*-*tert*-butyldimethylsilyl-*β*-D-glucopyranosyluronate)-(1 → 3)-(4-*O*-sulfonato-6-*O*-benzoyl-2-deoxy-2-acetamido-*β*-D-galactopyranosyl)-(1 → 4)-(methyl 2,3-di-*O*-benzoyl-*β*-D-glucopyranosyluronate)-(1 → 3)-4-*O*-sulfonato-6-*O*-benzoyl-2-deoxy-2-acetamido-*β*-D-galactopyranoside (83). 82 (64 mg, 0.040 mmol) was dissolved in DMF (3.2 mL), to this was added $SO_3 \bullet$ TMA (170 mg, 1.2 mmol), and the reaction stirred at 50 °C for 2 d. It was then cooled to rt and loaded onto a Sephadex LH-20 column (50% CH_2Cl_2:MeOH, 30 mL resin, 1 cm x 30 cm column). The resulting crude product was purified by flash chromatography (6:0.5:0.5 EtOAc:MeOH:H_2O) to afford **83** as a white solid (59 mg, 84%). R_f 0.40 (6:0.5:0.5 EtOAc:MeOH:H_2O). ^{1}H NMR (300 MHz, CD_3OD): δ = 8.06 (d, *J* = 7.5 Hz, 2H, Ar*H*), 7.99 (d, *J* = 7.5 Hz, 2H, Ar*H*), 7.96 – 7.92 (m, 4H, Ar*H*), 7.87 (d, *J*

= 7.5 Hz, 2H, Ar*H*), 7.80 (d, *J* = 7.5 Hz, 2H, Ar*H*), 7.62 – 7.32 (m, 16H, Ar*H*), 7.26 (dd, *J* = 7.5, 7.5 Hz, 2H, Ar*H*), 5.84 – 5.71 (m, 1H, OCH_2CH=CH_2), 5.55 (dd, *J* = 9.0, 9.0 Hz, 1H, H-3 GlcA), 5.49 (dd, *J* = 9.0, 9.3 Hz, 1H, H-3 GlcA), 5.34 (dd, *J* = 7.8, 9.3 Hz, 1H, H-2 GlcA), 5.29 (dd, *J* = 8.1, 8.1 Hz, 1H, H-2 GlcA), 5.16 – 5.14 (m, 3H), 5.06 (d, *J* = 13.5 Hz, 1H, OCH_2CH=CH_2), 4.98 (d, *J* = 10.2 Hz, 1H, OCH_2CH=CH_2), 4.93 (s, 1H, H-4 GalNAc), 4.78 (s, 1H, H-4 GalNAc), 4.75 – 4.67 (m, 3H, H-1 GlcA, H-1 GalNAc) 4.51 (d, *J* = 7.8 Hz, 1H, H-1 GlcA), 4.43 (dd, *J* = 9.0, 9.0 Hz, 1H, H-4 GlcA), 4.29 (dd, *J* = 7.5, 9.3 Hz, 1H), 4.21 – 4.10 (m, 4H), 4.02 – 3.89 (m, 5H), 3.74 – 3.66 (m, 7H, CO_2CH_3), 3.47 (dd, *J* = 6.3, 6.3 Hz, 1H), 1.65 (s, 3H, $HNC(O)CH_3$), 1.54 (s, 3H, $HNC(O)CH_3$), 0.71 (s, 9H, $(CH_3)_3CSi$), -0.02 (s, 3H, CH_3Si), -0.19 (s, 3H, CH_3Si). ESI MS: *m/z*: calcd for $C_{81}H_{89}N_2O_{35}S_2Si$: 1741.5; found 1742.0 $[M - H]^-$.

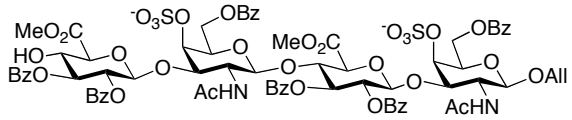

84

Allyl (methyl 2,3-di-*O*-benzoyl-*β*-D-glucopyranosyluronate)-(1 → 3)-(4-*O*-sulfonato-6-*O*-benzoyl-2-deoxy-2-acetamido-*β*-D-galactopyranosyl)-(1 → 4)-(methyl 2,3-di-*O*-benzoyl-*β*-D-glucopyranosyluronate)-(1 → 3)-4-*O*-sulfonato-6-*O*-benzoyl-2-deoxy-2-acetamido-*β*-D-galactopyranoside (84). 83 (59 mg, 0.034 mmol) in a plastic centrifuge tube was dissolved in pyridine (1.3 mL) and THF (1.3 mL). The reaction was cooled to 0 °C and and HF • pyridine (210 μL, 11.6 mmol) was added. After stirring at 0 °C for 1 h and at rt overnight, the reaction mixture was loaded onto a Sephadex LH-20 column (50% CH_2Cl_2:MeOH, 30 mL resin, 1 cm x 30 cm column). The product was

concentrated, dissolved in H_2O, and lyophilized to afford a white solid (50 mg, 90%) that was immediately used in the next reaction. R_f 0.46 (6:1:0.5 EtOAc:MeOH:H_2O). ESI MS: *m/z*: calcd for $C_{75}H_{75}N_2O_{35}S_2$: 1627.4; found 1627.6 [*M* - H]$^-$.

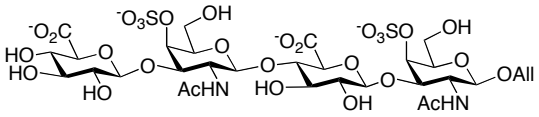

85: CS-A

Allyl (*β*-D-glucopyranosyluronate)-(1 → 3)-(4-*O*-sulfonato-2-deoxy-2-acetamido-*β*-D-galactopyranosyl)-(1 → 4)-(*β*-D-glucopyranosyluronate)-(1 → 3)-4-*O*-sulfonato-2-deoxy-2-acetamido-*β*-D-galactopyranoside (85: CS-A). 84 (50 mg, 0.031 mmol) was dissolved in THF (3.3 mL) and H_2O (2.5 mL) and cooled to 0 °C. To this were added 1 M aq. LiOH (370 μL, 0.37 mmol) and 30% H_2O_2 (250 μL, 0.0022 mmol), and the reaction stirred at 0 °C for 1 h and at rt for 12 h. At this time, 4 M NaOH (330 μL, 1.3 mmol) and MeOH (2.5 mL) were added and the reaction stirred for another 12 h. It was then neutralized with Amberlyst IR-120 resin, filtered, and lyophilized to afford an orange solid. The product was purified by Sephadex G-25 UF (0.9 % NaCl in H_2O, 30 mL resin, 1 cm x 20 cm column) and desalted with Sephadex G-25 UF (100% H_2O, 30 mL resin, 1 cm x 20 cm column) to afford **85: CS-A** as a white solid upon lyophilization (21 mg, 70%). For complete assignment of the ^{1}H NMR spectra of this compound, ^{1}H decoupling experiments were performed. ^{1}H NMR (600 MHz, D_2O): δ = 5.94 – 5.86 (m, 1H, OCH_2CH=CH_2), 5.31 (dd, *J* = 1.5, 17.7 Hz, 1H, OCH_2CH=CH_2), 5.27 (dd, *J* = 1.2, 10.2 Hz, 1H, OCH_2CH=CH_2), 4.79 (d, *J* = 3.0 Hz, 1H, H-4 GalNAc), 4.74 (d, *J* = 3.0 Hz, 1H, H-4 GalNAc), 4.58 (d, *J* = 7.8 Hz, 1H, H-1 GalNAc), 4.56 (d, *J* = 7.8 Hz, 1H, H-1

GalNAc), 4.47 (d, *J* = 7.8 Hz, 1H, H-1 GlcA), 4.46 (d, *J* = 7.8 Hz, 1H, H-1 GlcA), 4.34 (dd, *J* = 5.1, 13.5 Hz, 1H, OC*H*$_2$CH=CH$_2$), 4.18 (dd, *J* = 3.3, 13.2 Hz, 1H, OC*H*$_2$CH=CH$_2$), 4.07 – 4.00 (m, 4H, H-2 GalNAc, H-3 GalNAc), 3.85 – 3.77 (m, 7H, H-4 GlcA, H-6 GalNAc, H-5 GalNAc), 3.66 (d, *J* = 9.6 Hz, 1H, H-5 GlcA), 3.66 (d, *J* = 10.2 Hz, 1H, H-5 GlcA), 3.58 (dd, *J* = 9.0, 9.0 Hz, 1H, H-3 GlcA), 3.52 (dd, *J* = 9.0, 9.6 Hz, 1H, H-3 GlcA), 3.46 (dd, *J* = 9.0, 9.0 Hz, 1H, H-4 GlcA), 3.39 (dd, *J* = 8.4, 8.4 Hz, 1H, H-2 GlcA), 3.34 (dd, *J* = 8.4, 8.4 Hz, 1H, H-2 GlcA), 2.04 (s, 3H, HNC(O)C*H*$_3$), 2.01 (s, 3H, HNC(O)C*H*$_3$). ESI MS: *m/z*: calcd for $C_{31}H_{46}N_2NaO_{29}S_2$: 997.2; found 997.2 $[M + Na - 2H]^-$.

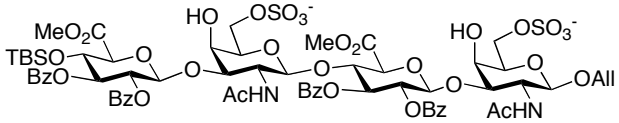

86

Allyl (methyl 2,3-di-*O*-benzoyl-4-*O*-*tert*-butyldimethylsilyl-*β*-D-glucopyranosyluronate)-(1 → 3)-(6-*O*-sulfonato-2-deoxy-2-acetamido-*β*-D-galactopyranosyl)-(1 → 4)-(methyl 2,3-di-*O*-benzoyl-*β*-D-glucopyranosyluronate)-(1 → 3)-6-*O*-sulfonato-2-deoxy-2-acetamido-*β*-D-galactopyranoside (86). 76 (25 mg, 0.018 mmol) was dissolved in DMF (1.0 mL), to this was added $SO_3 \bullet$ TMA (17 mg, 0.12 mmol), and the reaction stirred at 50 °C for 3 h. The reaction was then cooled to rt and eluted through a Sephadex LH-20 column (50% CH_2Cl_2:MeOH, 30 mL resin, 1 cm x 30 cm column). The resulting crude product was purified by flash chromatography (6:1:1 EtOAc:MeOH:H_2O) to afford **86** as a white solid (17 mg, 61%). R_f 0.32 (6:1:1 EtOAc:MeOH:H_2O). Also observed was allyl (methyl 2,3-di-*O*-benzoyl-4-*O*-*tert*-

butyldimethylsilyl-*β*-D-glucopyranosyluronate)-(1 → 3)-(6-*O*-sulfonato-2-deoxy-2-acetamido-*β*-D-galactopyranosyl)-(1 → 4)-(methyl 2,3-di-*O*-benzoyl-*β*-D-glucopyranosyluronate)-(1 → 3)-4,6-di-*O*-sulfonato-2-deoxy-2-acetamido-*β*-D-galactopyranoside (8.6 mg, 31%) which could be used to generate **79: CS-E** upon further sulfation. R_f 0.16 (6:1:1 EtOAc:MeOH:H_2O). Desired product ^{1}H NMR (600 MHz, CD_3OD): δ = 7.88 (dd, *J* = 6.0, 6.6 Hz, 4H, Ar*H*), 7.82 (dd, *J* = 6.6, 7.2 Hz, 4H, Ar*H*), 7.53 – 7.49 (m, 4H, Ar*H*), 7.40 – 7.33 (m, 8H, Ar*H*), 5.80 – 5.73 (m, 1H, OCH_2CH=CH_2), 5.60 (dd, *J* = 8.4, 9.0 Hz, 1H, H-3 GlcA), 5.56 (dd, *J* = 9.0, 9.6 Hz, 1H, H-3 GlcA), 5.27 (dd, *J* = 8.4, 8.4 Hz, 2H, H-2 GlcA), 5.16 (d, *J* = 16.8 Hz, 1H, OCH_2CH=CH_2), 5.04 – 5.00 (m, 3H), 4.48 (d, *J* = 7.8 Hz, 1H, H-1 GalNAc), 4.32 – 4.29 (m, 2H, H-1 GlcA, H-1 GalNAc), 4.25 – 4.20 (m, 3H), 4.17 – 4.08 (m, 5H), 3.98 – 3.95 (m, 3H), 3.84 – 3.72 (m, 9H, CO_2CH_3), 3.69 – 3.60 (m, 2H), 3.52 (dd, *J* = 5.4, 6.0 Hz, 1H), 1.19 (s, 6H, $HNC(O)CH_3$), 0.70 (s, 9H, $(CH_3)_3CSi$), -0.05 (s, 3H, CH_3Si), -0.21 (s, 3H, CH_3Si). ESI MS: *m/z*: calcd for $C_{67}H_{81}N_2O_{33}S_2Si$: 1533.4; found 1533.6 [*M* - H]$^-$.

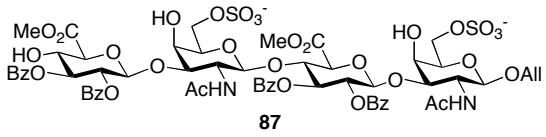

87

Allyl (methyl 2,3-di-*O*-benzoyl-*β*-D-glucopyranosyluronate)-(1 → 3)-(6-*O*-sulfonato-2-deoxy-2-acetamido-*β*-D-galactopyranosyl)-(1 → 4)-(methyl 2,3-di-*O*-benzoyl-*β*-D-glucopyranosyluronate)-(1 → 3)-6-*O*-sulfonato-2-deoxy-2-acetamido-*β*-D-galactopyranoside (87). 86 (4.6 mg, 0.0030 mmol) in a plastic centrifuge tube was dissolved in pyridine (55 μL) and THF (55 μL). The reaction was cooled to 0 °C and to

this was added HF•pyridine (15 μL, 0.83 mmol). It was stirred at 0 °C for 1 h and at rt overnight, and following this, was loaded onto a Sephadex LH-20 column (50% CH_2Cl_2:MeOH, 30 mL resin, 1 cm x 30 cm column). The product was concentrated, dissolved in H_2O, and lyophilized to afford a white solid (3.8 mg, 89%) that was immediately used in the next reaction. R_f 0.44 (6:2:1 EtOAc:MeOH:H_2O). ESI MS: *m/z*: calcd for $C_{61}H_{67}N_2O_{33}S_2$: 1419.3; found 1419.6 [*M* - H]$^-$.

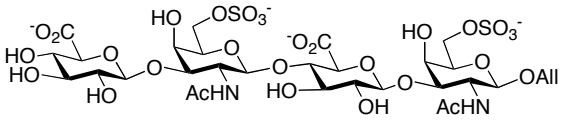

88: CS-C

Allyl (*β*-D-glucopyranosyluronate)-(1 → 3)-(6-*O*-sulfonato-2-deoxy-2-acetamido-*β*-D-galactopyranosyl)-(1 → 4)-(*β*-D-glucopyranosyluronate)-(1 → 3)-6-*O*-sulfonato-2-deoxy-2-acetamido-*β*-D-galactopyranoside (88: CS-C). 87 (1.2 mg, 0.00084 mmol) was dissolved in THF (70 μL) and H_2O (50 μL) and cooled to 0 °C. To this were added 1 M aq. LiOH (10.0 μL, 0.010 mmol) and 30% H_2O_2 (5.0 μL, 0.044 μmol), and the reaction was stirred at 0 °C for 1 h and at rt for 12 h. At this time, 4 M NaOH (7.0 μL, 0.028 mmol) and MeOH (50 μL) were added and the reaction stirred for another 12 h. It was then neutralized with Amberlyst IR-120 resin, filtered, and lyophilized to afford an orange solid. The product was purified by Sephadex G-25 UF (0.9 % NaCl in H_2O, 30 mL resin, 1 cm x 20 cm column) and desalted with Sephadex G-25 UF (100% H_2O, 30 mL resin, 1 cm x 20 cm column) to afford **88: CS-C** as a white solid upon lyophilization (0.8 mg, 100%). For complete assignment of the ^{1}H NMR spectra of this compound, ^{1}H decoupling experiments were performed. ^{1}H NMR (600 MHz, D_2O): δ = 5.93 – 5.86 (m,

1H, $OCH_2CH{=}CH_2$), 5.31 (d, J = 17.4 Hz, 1H, $OCH_2CH{=}CH_2$), 5.26 (d, J = 10.8 Hz, 1H, $OCH_2CH{=}CH_2$), 4.53 (d, J = 8.4 Hz, 2H, H-1 GalNAc), 4.50 (d, J = 7.2 Hz, 1H, H-1 GlcA), 4.49 (d, J = 7.2 Hz, 1H, H-1 GlcA), 4.34 (dd, J = 5.1, 13.5 Hz, 1H, $OCH_2CH{=}CH_2$), 4.23 – 4.16 (m, 7H, $OCH_2CH{=}CH_2$, H-4 GalNAc, H-6 GalNAc), 4.04 – 4.00 (m, 2H, H-2 GalNAc), 3.99 (dd, J = 6.0, 6.0 Hz, 1H, H-5 GalNAc), 3.92 – 3.90 (m, 1H, H-5 GalNAc), 3.83 (d, J = 11.4 Hz, 2H, H-3 GalNAc), 3.72 – 3.67 (m, 3H, H-4 GlcA, H-5 GlcA), 3.58 (dd, J = 8.4, 9.0 Hz, 1H, H-3 GlcA), 3.49 (dd, J = 8.4, 9.0 Hz, 2H, H-3 GlcA, H-4 GlcA), 3.38 (dd, J = 8.4, 9.0 Hz, 1H, H-2 GlcA), 3.31 (dd, J = 8.4, 8.4 Hz, 1H, H-2 GlcA), 2.02 (s, 3H, $HNC(O)CH_3$), 2.00 (s, 3H, $HNC(O)CH_3$). ESI MS: *m/z*: calcd for $C_{31}H_{46}N_2NaO_{29}S_2$: 997.2; found 997.2 $[M + Na - 2H]^-$.

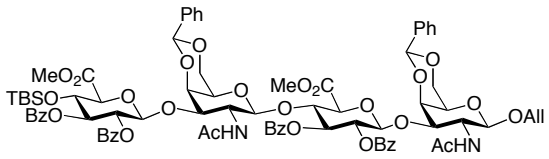

89

Allyl (methyl 2,3-di-*O*-benzoyl-4-*O*-*tert*-butyldimethylsilyl-*β*-D-glucopyranosyluronate)-(1 → 3)-(4,6-*O*-benzylidene-2-deoxy-2-acetamido-*β*-D-galactopyranosyl)-(1 → 4)-(methyl 2,3-di-*O*-benzoyl-*β*-D-glucopyranosyluronate)-(1 → 3)-4,6-*O*-benzylidene-2-deoxy-2-acetamido-*β*-D-galactopyranoside (89). 76 (22 mg, 0.016 mmol) was dissolved in CH_3CN (1.2 mL) and to this were added benzaldehyde dimethyl acetal (120 μL, 0.78 mmol) and DL-10-camphorsulfonic acid (3 mg). The reaction was stirred at rt for 12 h, quenched with TEA, and concentrated to afford an orange solid. The product was purified by flash chromatography (80% → 100% EtOAc:hexanes) to afford **89** (23 mg, 96%) as a white crystalline solid. R_f 0.71 (100%

EtOAc). ^{1}H NMR (300 MHz, $CDCl_3$): δ = 7.94 – 7.85 (m, 4H, Ar*H*), 7.86 (d, *J* = 8.1 Hz, 4H, Ar*H*), 7.58 – 7.42 (m, 7H, Ar*H*), 7.38 – 7.27 (m, 15H, Ar*H*), 5.89 – 5.76 (m, 1H, OCH_2CH=CH_2), 5.62 (dd, *J* = 7.8, 8.1 Hz, 1H, H-3 GlcA), 5.56 (s, 1H, MeOPhC*H*), 5.49 (dd, *J* = 8.7, 8.7 Hz, 1H, H-3 GlcA), 5.43 (d, *J* = 6.9 Hz, 1H, N*H*Ac), 5.34 – 5.23 (m, 4H, H-2 GlcA, H-1 GalNAc, OCH_2CH=CH_2, MeOPhC*H*), 5.17 – 5.06 (m, 3H, H-2 GlcA, H-1 GalNAc, OCH_2CH=CH_2), 4.98 (d, *J* = 6.6 Hz, 1H, N*H*Ac), 4.91 (d, *J* = 8.4 Hz, 1H, H-1 GlcA), 4.90 (d, *J* = 7.2 Hz, 1H, H-1GlcA), 4.77 (dd, *J* = 3.6, 11.1 Hz, 1H, H-3 GalNAc), 4.51 (dd, *J* = 8.4, 9.3 Hz, 1H, H-4 GlcA), 4.39 – 4.28 (m, 5H, OCH_2CH=CH_2, H-3 GalNAc, H-4 GalNAc, H-4 GlcA, H-6 GalNAc), 4.16 (d, *J* = 9.6 Hz, 1H, H-5 GlcA), 4.07 – 3.99 (m, 4H, OCH_2CH=CH_2, H-5 GlcA, H-6 GalNAc), 3.79 – 3.70 (m, 7H, $PhOCH_3$), 3.57 (d, *J* = 11.4 Hz, 1H), 3.48 (s, 1H, H-5 GalNAc), 3.35 – 3.29 (m, 2H), 2.87 (s, 1H, H-5 GalNAc), 1.54 (s, 3H, $HNC(O)CH_3$), 1.51 (s, 3H, $HNC(O)CH_3$), 0.70 (s, 9H, $(CH_3)_3CSi$), -0.11 (s, 3H, CH_3Si), -0.25 (s, 3H, CH_3Si). ESI MS: *m/z*: calcd for $C_{81}H_{90}N_2NaO_{27}Si$: 1573.5; found 1573.6 $[M + Na]^+$.

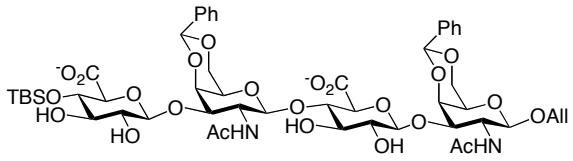

90

Allyl (methyl 4-*O*-*tert*-butyldimethylsilyl-*β*-D-glucopyranosyluronate)-(1 → 3)-(4,6-*O*-benzylidene-2-deoxy-2-acetamido-*β*-D-galactopyranosyl)-(1 → 4)-(methyl *β*-D-glucopyranosyluronate)-(1 → 3)-4,6-*O*-benzylidene-2-deoxy-2-acetamido-*β*-D-galactopyranoside (90). 89 (23 mg, 0.015 mmol) was dissolved in THF (2.0 mL) and H_2O (1.0 mL) and cooled to 0 °C. To this were added 1 M aq. LiOH (175 μL, 0.175

mmol) and 30% H_2O_2 (120 μL, 1.1 μmol), and the reaction was stirred at 0 °C for 1 h and at rt for 12 h. At this time, 4 M NaOH (1.5 mL, 6.0 mmol) and MeOH (1.2 mL) were added and the reaction stirred for another 12 h. It was then neutralized with Amberlyst IR-120 resin, filtered, and lyophilized to afford an orange solid. The product was purified by flash chromatography (6:2:1 EtOAc:MeOH:H_2O) to afford **90** (9.3 mg, 56%). The yield was reduced due to partial migration of the *tert*-butyldimethylsilyl protecting group during the reaction. R_f 0.75 (6:2:1 EtOAc:MeOH:H_2O). ^{1}H NMR (600 MHz, CD_3OD): δ = 7.50 – 7.49 (m, 4H, Ar*H*), 7.35 – 7.31 (m, 6H, Ar*H*), 5.92 – 5.86 (m, 1H, OCH_2CH=CH_2), 5.66 (s, 1H, MeOPhC*H*), 5.58 (s, 1H, MeOPhC*H*), 5.28 (d, *J* = 17.4 Hz, 1H, OCH_2CH=CH_2), 5.14 (d, *J* = 11.4 Hz, 1H, OCH_2CH=CH_2), 4.66 (d, *J* = 8.4 Hz, 1H, H-1 GalNAc), 4.58 (d, *J* = 7.8 Hz, 1H, H-1 GlcA), 4.52 (d, *J* = 8.4 Hz, 1H, H-1 GalNAc), 4.42 – 4.32 (m, 4H), 4.27 – 4.22 (m, 1H), 4.17 – 4.07 (m, 5H), 3.88 – 3.84 (m, 2H), 3.70 (dd, *J* = 9.0, 9.6 Hz, 1H), 3.64 – 3.61 (m, 3H), 3.53 – 3.52 (m, 3H), 3.45 (dd, *J* = 8.4, 9.0 Hz, 1H, H-3 GlcA), 3.43 (dd, *J* = 7.2, 9.0 Hz, 1H, H-3 GlcA), 3.37 (dd, *J* = 9.0, 9.0 Hz, 1H, H-2 GlcA), 3.16 (dd, *J* = 7.8, 8.4 Hz, 1H, H-2 GlcA), 2.01 (s, 3H, HNC(O)CH_3), 1.93 (s, 3H, HNC(O)CH_3), 0.87 (s, 9H, (CH_3)$_3$CSi), 0.09 (s, 3H, CH_3Si), 0.08 (s, 3H, CH_3Si). ESI MS: *m/z*: calcd for $C_{51}H_{69}N_2O_{23}Si$: 1105.4; found 1105.6 [*M* - H]$^-$.

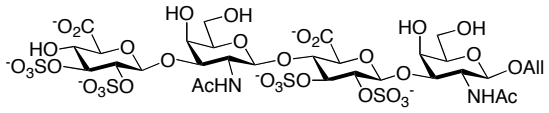

92: CS-R

Allyl (2,3-di-*O*-sulfonato-*β*-D-glucopyranosyluronate)-(1 → 3)-(2-deoxy-2-acetamido-*β*-D-galactopyranosyl)-(1 → 4)-(2,3-di-*O*-sulfonato-*β*-D-

glucopyranosyluronate)-(1 → 3)-2-deoxy-2-acetamido-*β*-D-galactopyranoside (92: CS-R). 90 (9.3 mg, 0.0084 mmol) was dissolved in DMF (500 μL) and to this was added $SO_3 \bullet$ TEA (30 mg, 0.17 mmol), and the reaction stirred at 65 °C for 36 h. It was then cooled to rt and loaded onto a Sephadex LH-20 column (50% CH_2Cl_2:MeOH, 30 mL resin, 1 cm x 30 cm column). The product was concentrated, dissolved in H_2O, and lyophilized to afford a yellow solid (7.5 mg) that was immediately used in the next reaction. Prolonged reaction times or greater amounts of sulfating reagent led to degradation of the product during the reaction to afford a mixture of the desired product, various sulfated disaccharides, and loss of the *tert*-butyldimethylsilyl protecting group to afford the pentasulfated product. ESI MS: *m/z*: calcd for $C_{57}H_{83}N_3O_{35}S_4Si$: 1526.6; found 1526.4 $[M + \text{TEA} - 2\text{H}]^-$.

The tetrasulfated product (7.5 mg, 0.053 mmol) was dissolved in 0.01 M AcOH, pH 3.0 (500 μL), and the reaction stirred at rt for 4 d. During this time, the pH was carefully monitored to prevent loss of the allyl group. The reaction was then quenched with TEA and concentrated to afford a yellow syrup, and the product was purified by Sephadex G-25 UF (H_2O, 30 mL resin, 1 cm x 20 cm column) and Sephadex SP C-25 (Na^+) (H_2O, 30 mL resin, 1 cm x 20 cm column) chromatography. **92: CS-R** was afforded as a white solid upon lyophilization (1.6 mg, 17%, 2 steps). For complete assignment of the ^{1}H NMR spectra of this compound, ^{1}H decoupling experiments were performed. ^{1}H NMR (600 MHz, D_2O): δ = 5.90 – 5.83 (m, 1H, OCH_2CH=CH_2), 5.28 (d, *J* = 17.4 Hz, 1H, OCH_2CH=CH_2), 5.22 (d, *J* = 10.8 Hz, 1H, OCH_2CH=CH_2), 4.96 (d, *J* = 5.4 Hz, 1H, H-1 GlcA), 4.93 (d, *J* = 6.0 Hz, 1H, H-1 GlcA), 4.58 (d, *J* = 7.8 Hz, 1H, H-1 GalNAc), 4.52

(d, J = 8.4 Hz, 1H, H-1 GalNAc), 4.45 – 4.44 (m, 2H, H-2 GlcA), 4.38 (dd, J = 9.0, 9.0 Hz, 1H, H-4 GlcA), 4.30 (dd, J = 5.4, 13.2 Hz, 1H, OCH_2CH=CH_2), 4.18 – 4.10 (m, 4H, OCH_2CH=CH_2, H-4 GlcA, H-3 GlcA), 4.02 – 3.97 (m, 2H, H-2 GalNAc), 3.94 (dd, J = 8.7, 10.2 Hz, 2H, H-5 GlcA), 3.89 – 3.82 (m, 3H, H-3 GalNAc, H-4 GalNAc), 3.77 –3.73 (m, 3H, H-3 GalNAc, H-6 GalNAc), 3.67 – 3.64 (m, 4H, H-5 GalNAc, H-6 GalNAc), 2.02 (s, 6H, HNC(O)CH_3). ESI MS: *m/z*: calcd for $C_{31}H_{46}N_2O_{35}S_4$: 567.0; found 567.0 $[M - 2H]^{2-}$. In addition to the previously described conditions, CS-R could also be purified by liquid chromatography/mass spectrometry (LC/MS).[32] Separations were performed on a Hewlett Packard (Agilent) 1100 LC-MSD with an Agilent Zorbax Stable Bond C18 column (80 Å pore, 4.6 x 250 mm). Eluent A was water/acetonitrile (80:20) and eluent B was water/acetonitrile (35:65). Tributylamine (15 mM) and ammonium acetate (50 mM) were added to both eluents. The mobile phase pH was adjusted to 7.0 with acetic acid. Sample injection sizes were 40 μL, and a linear gradient (from 0 to 100% eluent B in 120 min) at a flow rate of 0.5 mL/min was used for elution. ESI mass spectra were obtained with the electrospray interface set in negative ionization mode with a fragmentor voltage of 60 V, a capillary voltage of –3500 V, and a source temperature of 350 °C. Nitrogen was used as a drying (12 L/min) and nebulizing gas (60 p.s.i.). Total ion chromatograms and mass spectra were processed using Agilent Chemstation. Optimization of the method was performed with pure CS-A (22 min), CS-E (34 min), and mixtures of CS-A and CS-E tetrasaccharides. CS-R eluted at 28 min.

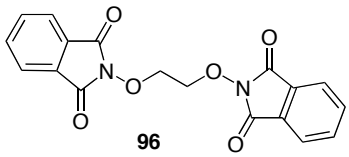

96

1,2-Diphthalimidooxyethane (96).[19] To a solution of *N*-hydroxyphthalimide (1.74 g, 10.6 mmol) in DMF (10.6 mL) was added dropwise 1,8-diazabicyclo[5.4.0]undec-7-ene (1.6 mL, 10.6 mmol) with stirring. A deep red color change was observed. 1,2-dibromoethane (0.46 mL, 5.3 mmol) was added, and the reaction stirred at 85 °C for 2 h. It turned colorless and was then cooled to rt and poured onto ice to afford a precipitate. The precipitate was collected and recrystallized from *n*-butanol to afford **96** as white crystals (0.69 g, 40%). The spectral data agreed with published data. ^{1}H NMR (300 MHz, $CDCl_3$): δ = 7.85 – 7.82 (m, 4H, Ar*H*), 7.75 – 7.72 (m, 4H, Ar*H*), 4.63 (s, 4H, OCH_2, OCH_2). ESI MS: *m/z*: calcd for $C_{18}H_{13}N_2O_6$: 353.3; found 353.0 $[M + H]^+$.

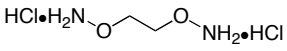

94

1,2-(Bisaminooxy)ethane hydrochloride (94).[19] **96** (0.69 g, 1.9 mmol) was dissolved in HCl:AcOH (3 mL:4.5 mL) and heated to 115 °C for 1.5 h. The mixture was at first a suspension that became clear throughout the reaction. It was then cooled to rt, and concentrated to afford a yellow solid. The solid was dissolved in H_2O, and the suspension filtered and washed with 6 *N* HCl. The combined filtrates were concentrated to afford a yellow solid, and recrystallization from H_2O:EtOAc afforded **94** as a white solid (0.24 g, 73%). The spectral data agreed with published data. ^{1}H NMR (300 MHz, D_2O): δ = (s, 4H, OCH_2, OCH_2); ^{13}C NMR (75 MHz, D_2O): δ = 64.6.

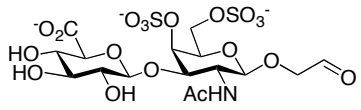

93

Ethyl aldehyde (*β*-D-glucopyranosyluronate)-(1 → 3)-4,6-di-*O*-sulfonato-2-deoxy-2-acetamido-*β*-D-galactopyranoside (93). Disaccharide **73** (1 mg, 1.5 μmol) was dissolved in MeOH (500 μL) and cooled to –78 °C. O_3 was bubbled through the reaction until a blue color persisted (1 min), and the reaction was then purged with N_2 until colorless, quenched with Ph_3P beads (3 mg), and gradually warmed to rt over 12 h. It was filtered and the product concentrated to afford the desired aldehyde **93** as a white solid (1 mg, 100%). ^{1}H NMR (300 MHz, D_2O): δ = 4.87 (s, 1H, H-4 GalNAc), 4.56 (d, *J* = 8.1 Hz, 1H , H-1 GalNAc), 4.46 (d, *J* = 7.5 Hz, 1H, H-1 GlcA), 4.28 (dd, *J* = 5.4, 11.1 Hz, 1H, H-3 GalNAc), 4.18 (dd, *J* = 8.7, 11.1 Hz, 1H, H-2 GalNAc), 4.07 – 4.04 (m, 3H, H-5 GalNAc, H-6 GalNAc, H-6 GalNAc), 3.77 (dd, *J* = 4.6, 11.3 Hz, 1H, OC*H*$_2$CHO), 3.64 (d, *J* = 8.7 Hz, 1H, H-5 GlcA), 3.59 (dd, *J* = 5.5, 11.0 Hz, 1H, OC*H*$_2$CHO), 3.50 (dd, *J* = 9.0, 9.3 Hz, 1H, H-4 GlcA), 3.43 (dd, *J* = 8.7, 8.7 Hz, 1H, H-3 GlcA), 3.34 (dd, *J* = 7.5, 9.0 Hz, 1H, H-2 GlcA), 1.99 (s, 3H, HNC(O)C*H*$_3$). ESI MS: *m/z*: calcd for $C_{17}H_{28}NO_{20}S_2$: 630.5; found 630.4 [*M* + MeOH – H]$^-$.

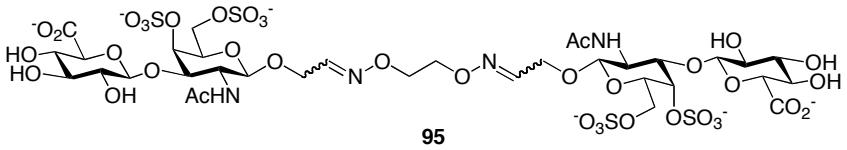

95

1,2-Dioxime [ethyl (*β*-D-glucopyranosyluronate)-(1 → 3)-4,6-di-*O*-sulfonato-2-deoxy-2-acetamido-*β*-D-galactopyranosyl] ethane (95). The aldehyde **93** (3 mg, 5 μmol) was reacted for 14 h at rt with 1,2-(bisaminooxy)ethane hydrochloride **94** (0.23 mg, 2.5 μmol) that had been dissolved in H_2O (100 μL) and pH adjusted to 5.0 with 1 M NaOH. The resulting oxime product was purified using a SepPak C18 column (500 mg, 100% H_2O) and Sephadex G-10 (100% H_2O, 10 mL resin, 1 cm x 10 cm column) to afford a white solid (1.3 mg, 41%). For complete assignment of the ^{1}H NMR spectra of this compound, ^{1}H decoupling experiments were performed. ^{1}H NMR (600 MHz, D_2O): δ = 7.59 (m, 1H, ON=C*H*), 7.04 (m, 1H, ON=C*H*), 4.85 (s, 2H, H-4 GalNAc, H-4 GalNAc), 4.64 – 4.58 (m, 2H, H-1 GalNAc, H-1 GalNAc), 4.50 – 4.49 (m, 2H, H-1 GlcA, H-1 GlcA), 4.45 (dd, *J* = 5.6, 13.5 Hz, 2H, OC*H*$_2$CH=NO), 4.37 – 4.30 (m, 8H, OC*H*$_2$CH=NO, H-3 GalNAc, H-3 GalNAc, OC*H*$_2$, OC*H*$_2$), 4.21 (dd, *J* = 9.0, 10.8 Hz, 2H, H-2 GalNAc, H-2 GalNAc), 4.12 – 4.09 (m, 6H, H-5 GalNAc, H-5 GalNAc, H-6 GalNAc, H-6 GalNAc, H-6 GalNAc, H-6 GalNAc), 3.68 (d, *J* = 9.0 Hz, 2H, H-5 GlcA, H-5 GlcA), 3.54 (dd, *J* = 9.0, 9.6 Hz, 2H, H-4 GlcA, H-4 GlcA), 3.48 (dd, *J* = 9.0, 9.6 Hz, 2H, H-3 GlcA, H-3 GlcA), 3.37 (dd, *J* = 7.2, 9.0 Hz, 2H, H-2 GlcA, H-2 GlcA), 2.04 (s, 6H, HNC(O)C*H*$_3$). ESI MS: *m/z*: calcd for $C_{34}H_{49}N_4Na_4O_{38}S_4$: 1341.1; found 1341.4 $[M - H]^-$.

Carbohydrate microarray competition studies

Recombinant human midkine (Peprotech, 2 μM) and either an anti-midkine goat IgG (Santa Cruz, 5 μM) or a goat anti-mouse IgG (Pierce, 5μM) in 200 μL 0.1% Triton X-100 in PBS were incubated at room temperature for 2 h. In a similar manner, recombinant human BDNF (Peprotech, 2 μM) and either an anti-BDNF rabbit IgG (Santa Cruz, 5 μM) or a rabbit anti-mouse IgG (Pierce, 5 μM) in 200 μL 0.1% Triton X-100 in PBS were incubated. Carbohydrate microarrays (see Chapter 5) were then treated with these solutions.

Prior to use, the arrays were outlined with a hydrophobic pen (Super Pap Pen, Research Products International) to create a boundary for the protein treatments and rinsed three times with H_2O. The slides were then blocked by treatment with $NaBH_4$ (125 mg) in phosphate buffered saline (PBS, 50 mL) at room temperature for 5 min and washed five times with PBS. The midkine/antibody or BDNF/antibody mixtures were added to the slides in 200 μL quantities, and incubated at room temperature for 2 h. The slides were then washed with PBS and incubated with the appropriate primary antibody [anti-midkine (Peprotech) or anti-BDNF (Santa Cruz); 1:1000 in 0.1% Triton X-100 in PBS] for 2 h at room temperature. Following the incubation, the slides were washed with PBS and treated in the dark at room temperature with a secondary IgG antibody conjugated to Cy3 (Amersham; 1:5000 in 0.1% Triton X-100 in PBS) for 1 h. Slides were washed with PBS followed by H_2O and then dried under a gentle stream of N_2. Microarrays were analyzed at 532 nm using a GenePix 5000a scanner, and fluorescence quantification was performed using GenePix 6.0 software after correction for local

background. Each protein was analyzed in triplicate, and the data represent an average of 5-10 spots for a given carbohydrate concentration.

References

1. Sugahara, K. & Yamada, S. (2000). Structure and function of oversulfated chondroitin sulfate variants: unique sulfation patterns and neuroregulatory activities. *Trends Glycosci. Glycotech.* **12**, 321-349.
2. Kinoshita, A., Yamada, S., Haslam, S.M., Morris, H.R., Dell, A. & Sugahara, K. (2001). Isolation and structural determination of novel sulfated hexasaccharides from squid cartilage chondroitin sulfate E that exhibits neuroregulatory activities. *Biochemistry* **40**, 12654-12665.
3. Kantor, D.B., Chivatakarn, O., Peer, K.L., Oster, S.F., Inatani, M., Hansen, M.J., Flanagan, J.G., Yamaguchi, Y., Sretavan, D.W., Giger, R.J. & Kolodkin, A.L. (2004). Semaphorin 5A is a bifunctional axon guidance cue regulated by heparan and chondroitin sulfate proteoglycans. *Neuron* **44**, 961-975.
4. Bradbury, E.J., Moon, L.D., Popat, R.J., King, V.R., Bennett, G.S., Patel, P.N., Fawcett, J.W. & McMahon, S.B. (2002). Chondroitinase ABC promotes functional recovery after spinal cord injury. *Nature* **416**, 636-640.
5. Henderson, D.J. & Copp, A.J. (1997). Role of the extracellular matrix in neural crest migration. *J. Anat.* **191**, 507-515.
6. Bicknese, A.R., Sheppard, A.M., O'Leary, D.D. & Pearlman, A.L. (1994). Thalamocortical axons extend along a chondroitin sulfate proteoglycan-enriched pathway coincident with the neocortical subplate and distinct from the efferent path. *J. Neurosci.* **14**, 3500-3510.
7. Clement, A.M., Nadanaka, S., Masayama, K., Mandl, C., Sugahara, K. & Faissner, A. (1998). The DSD-1 carbohydrate epitope depends on sulfation,

correlates with chondroitin sulfate D motifs, and is sufficient to promote neurite outgrowth. *J. Biol. Chem.* **273**, 28444-28453.

8. Clarris, H.J., Rauch, U. & Key, B. (2000). Dynamic spatiotemporal expression patterns of neurocan and phosphacan indicate diverse roles in the developing and adult mouse olfactory system. *J. Comp. Neurol.* **423**, 99-111.
9. Clement, A.M., Sugahara, K. & Faissner, A. (1999). Chondroitin sulfate E promotes neurite outgrowth of rat embryonic day 18 hippocampal neurons. *Neurosci. Lett.* **269**, 125-128.
10. Hacker, U., Nybakken, K. & Perrimon, N. (2005). Heparan sulphate proteoglycans: the sweet side of development. *Nat. Rev. Mol. Cell Biol.* **6**, 530-541.
11. Brickman, Y.G., Ford, M.D., Gallagher, J.T., Nurcombe, V., Bartlett, P.F. & Turnbull, J.E. (1998). Structural modification of fibroblast growth factor-binding heparan sulfate at a determinative stage of neural development. *J. Biol. Chem.* **273**, 4350-4359.
12. Deepa, S.S., Umehara, Y., Higashiyama, S., Itoh, N. & Sugahara, K. (2002). Specific molecular interactions of oversulfated chondroitin sulfate E with various heparin-binding growth factors. Implications as a physiological binding partner in the brain and other tissues. *J. Biol. Chem.* **277**, 43707-43716.
13. Tully, S.E., Mabon, R., Gama, C.I., Tsai, S.M., Liu, X. & Hsieh-Wilson, L.C. (2004). A chondroitin sulfate small molecule that stimulates neuronal growth. *J. Am. Chem. Soc.* **126**, 7736-7737.

14. Kursche-Gullberg, M. & Kjellen, L. (2003). Sulfotransferases in glycosaminoglycan biosynthesis. *Curr. Opin. Struct. Biol.* **5**, 605-611.

15. Jacquinet, J.C., Rochepeau-Jobron, L. & Combal, J.P. (1998). Multigram syntheses of the disaccharide repeating units of chondroitin 4- and 6-sulfates. *Carbohydr. Res.* **314**, 283-288.

16. Lucas, H., Basten, J.E.M., van Dinther, T.G., Meuleman, J.G., van Aelst, S.F. & van Boeckel, C.A.A. (1990). Syntheses of heparin-like pentamers containing opened uronic-acid moieties. *Tetrahedron* **46**, 8207-8228.

17. Gilbert, E.E. (1962). Reactions of sulfur trioxide, and of its adducts, with organic compounds. *Chem. Rev.* **62**, 549-589.

18. Mikhailov, D., Mayo, K.H., Vlahov, I.R., Toida, T., Pervin, A. & Linhardt, R.J. (1996). NMR solution conformation of heparin-derived tetrasaccharide. *Biochem. J.* **318**, 93-102.

19. Shirayev, A., Thoo lin, P.K. & Moiseev, I.K. (1997). Synthesis of novel adamantylalkoxyurea derivatives from 2-(1-adamantylimino)-1,3-oxathiolane. *Synthesis* **1**, 38-40.

20. Gama, C.I., Tully, S.E, Sotogaku, N., Clark, P.M. Rawat, M., Vaidehi, N., Goddard III, W.A., Nishi, A. & Hsieh-Wilson, L.C. (2006). Sulfation patterns of glycosaminoglycans encode molecular recognition and activity. *Nat. Chem. Biol.* accepted.

21. Mayo, S.L., Olafson, B.D. & Goddard III, W.A. (1990). DREIDING: a generic force field for molecular simulations. *J. Phys. Chem.* **94**, 8897-8909.

22. Rappe, A.K. & Goddard III, W.A. (1991). Charge equilibration for molecular dynamics simulations. *J. Phys. Chem.* **95**, 3358-3363.

23. Lim, K.T., Brunett, S., Iotov, M., McClurg, R.B., Vaidehi, N., Dasgupta, S., Taylor, S. & Goddard III, W.A. (1997). Molecular dynamics for very large systems on massively parallel computers: the MPSim program. *J. Comp. Chem.* **18**, 501-521.

24. Capila, I. & Linhardt, R.J. (2002). Heparin-protein interactions. *Angew. Chem. Int. Ed.* **41**, 391-412.

25. Nandini, C.D., Mikami, T., Ohta, M., Itoh, N., Akiyama-Nambu, F. & Sugahara, K. (2004). Structural and functional characterization of oversulfated chondroitin sulfate/dermatan sulfate hybrid chains from the notochord of hagfish. Neuritogenic and binding activities for growth factors and neurotrophic factors. *J. Biol. Chem.* **279**, 50799-50809.

26. Jenner, P. & Olanow, C.W. (2006). The pathogenesis of cell death in Parkinson's disease. *Neurology* **66**, S24-36.

27. Muramatsu, T. (2002). Midkine and pleiotrophin: two related proteins involved in development, survival, inflammation and tumorigenesis. *J. Biochem.* **132**, 359-371.

28. Huang, E.J. & Reichardt, L.F. (2001). Neurotrophins: roles in neuronal development and function. *Annu. Rev. Neurosci.* **24**, 677-736.

29. Holt, C.E. & Dickson, B.J. (2005). Sugar codes for axons? *Neuron* **46**, 169-172.

30. Bellaiche, Y., The, I. & Perrimon, N. (1998). Tout-velu is a *Drosophila* homologue of the putative tumour suppressor EXT-1 and is needed for Hh diffusion. *Nature* **394**, 85-88.

31. Fernaud-Espinosa, I., Nieto-Sampedro, M. & Bovolenta, P. (1996). Developmental distribution of glycosaminoglycans in embryonic rat brain: relationship to axonal tract formation. *J. Neurobiol.* **30**, 410-424.

32. Thanawiroon, C., Rice, K.G., Toida, T. & Linhardt, R.J. (2004). Liquid chromatography/mass spectrometry sequencing approach for highly sulfated heparin-derived oligosaccharides. *J. Biol. Chem.* **279**, 2608-2615.

Appendix for Chapter 4: Relevant Spectral Data for Compounds of Chapter 4

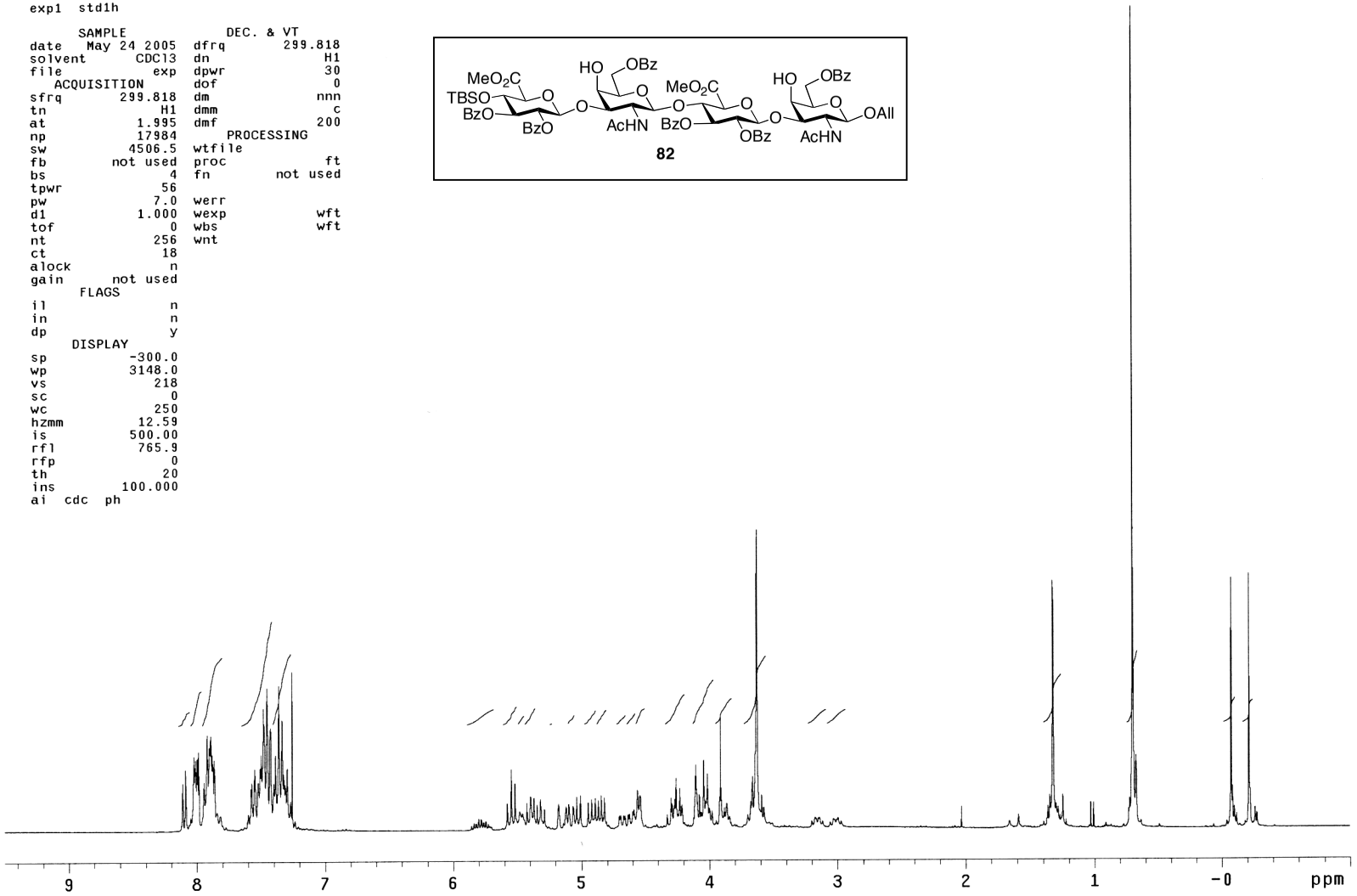

Figure A4.1: ^{1}H NMR (300 MHz, $CDCl_3$) of compound **82**.

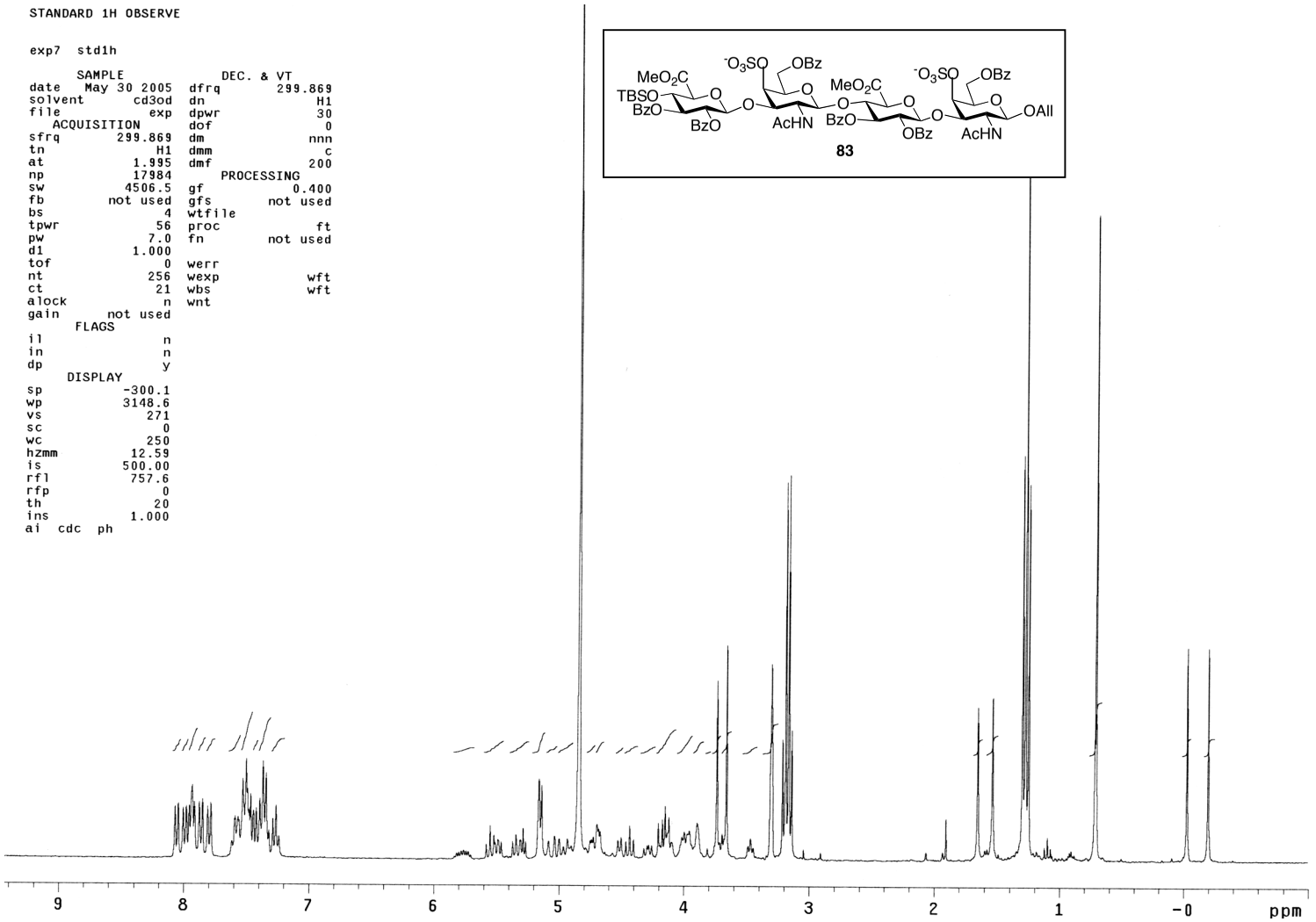

Figure A4.2: ^{1}H NMR (300 MHz, CD_3OD) of compound **83**.

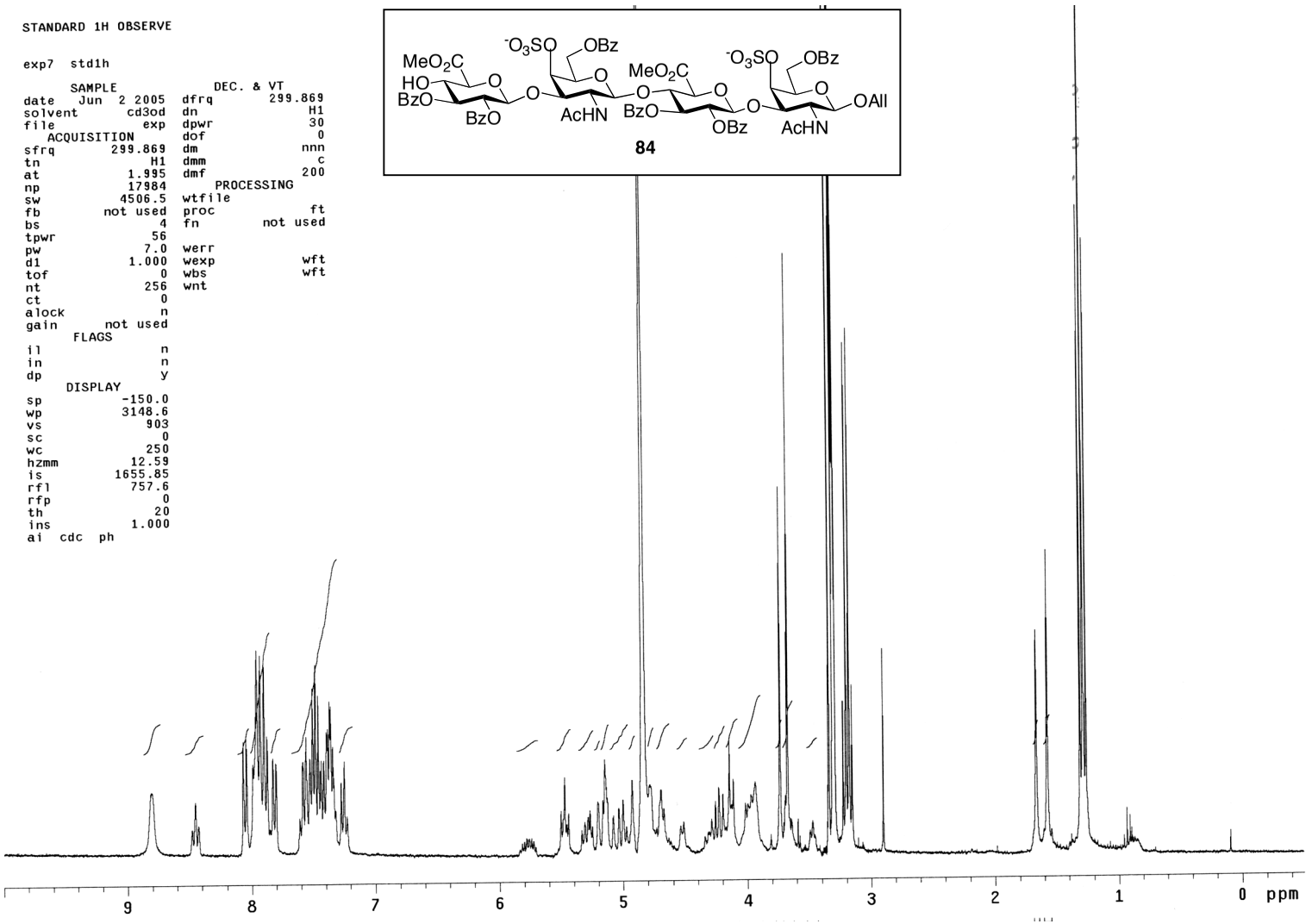

Figure A4.3: ^{1}H NMR (300 MHz, CD_3OD) of compound **84**.

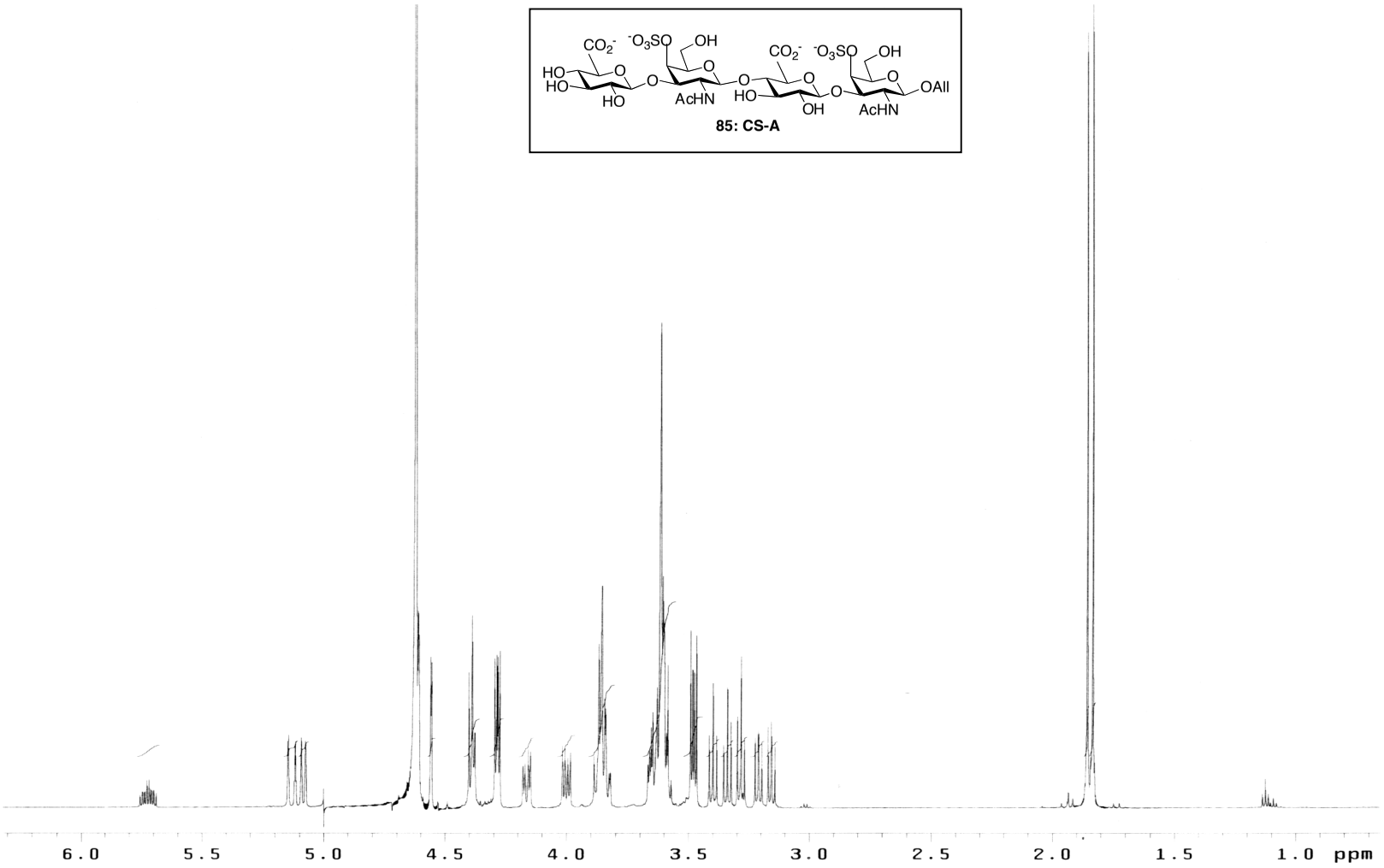

Figure A4.4: ^{1}H NMR (600 MHz, D_2O) of compound **85: CS-A**.

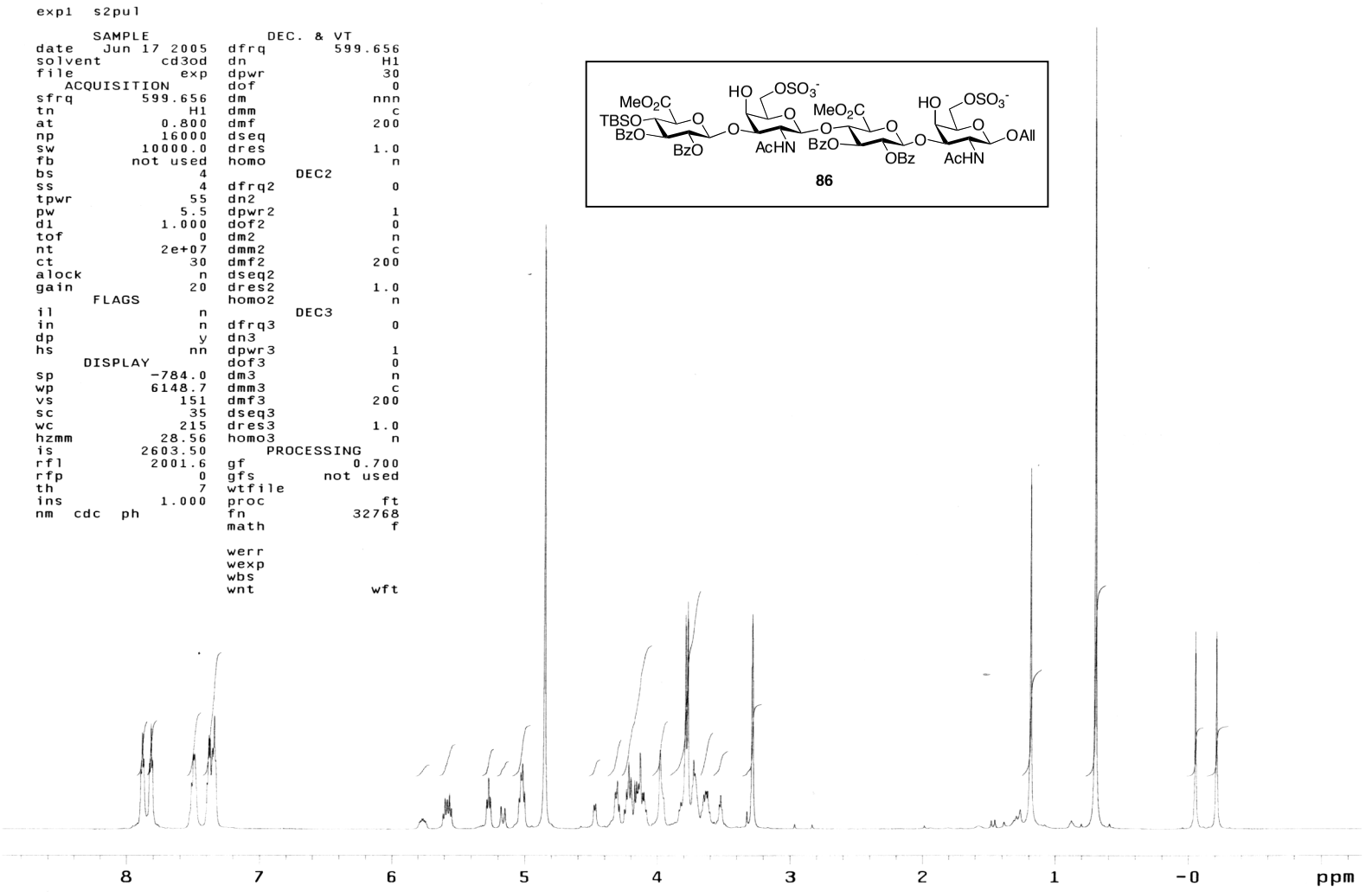

Figure A4.5: ^{1}H NMR (600 MHz, CD_3OD) of compound **86**.

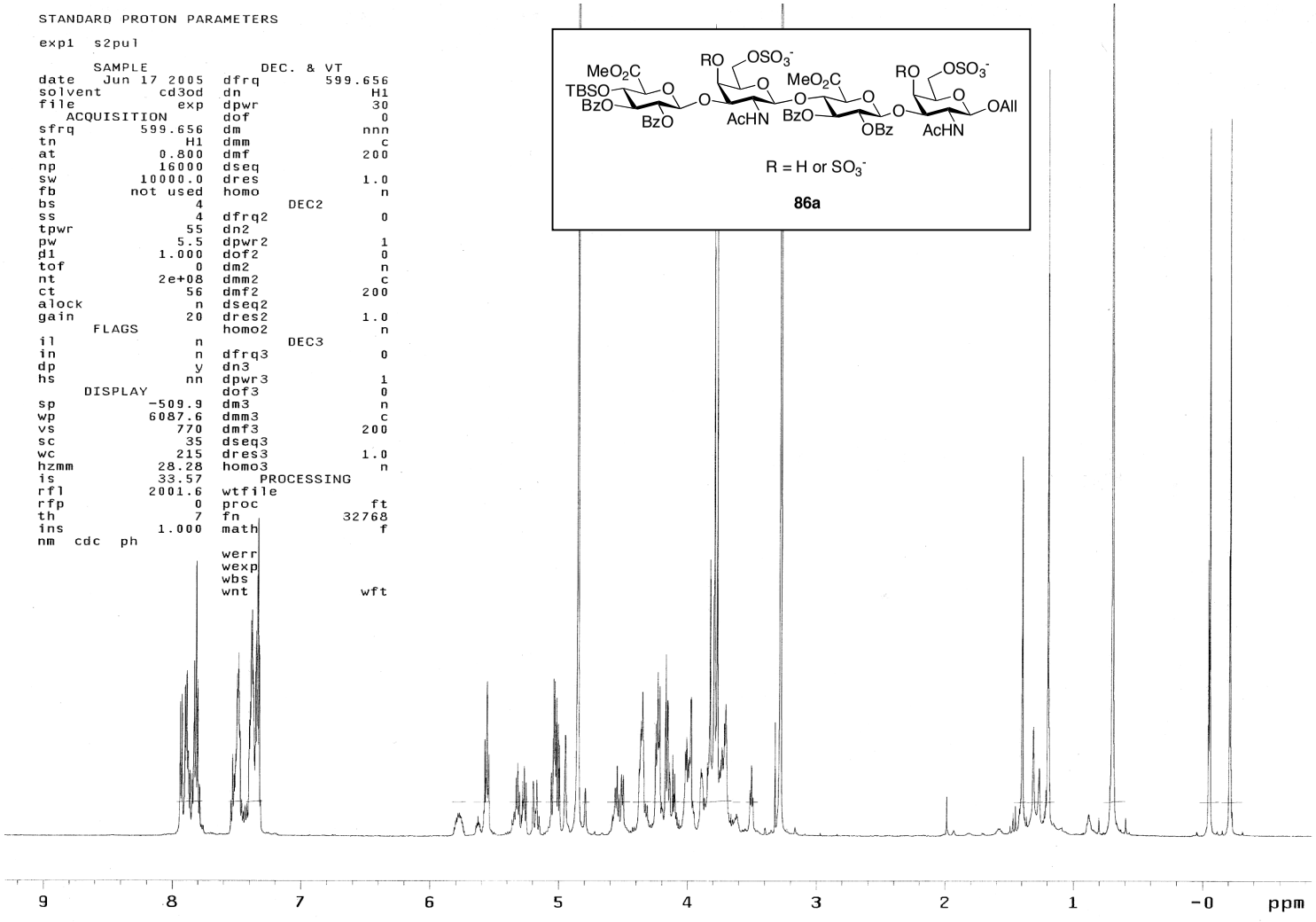

Figure A4.6: ^{1}H NMR (600 MHz, CD_3OD) of compound **86a**.
The peaks at 4.81 and 4.95 Hz are due to sulfation at the C-4 hydroxyls.

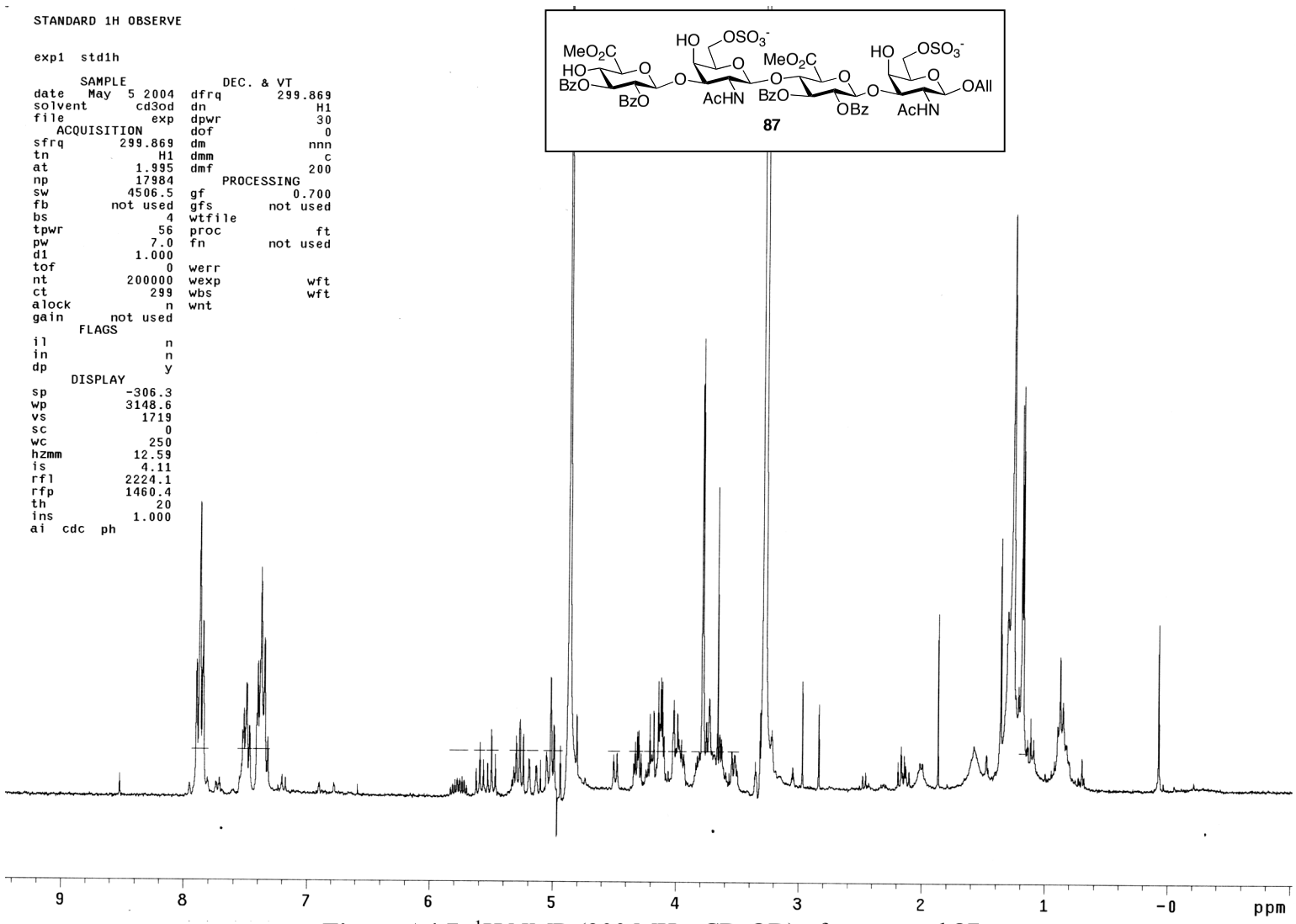

Figure A4.7: ^{1}H NMR (300 MHz, CD_3OD) of compound **87**.

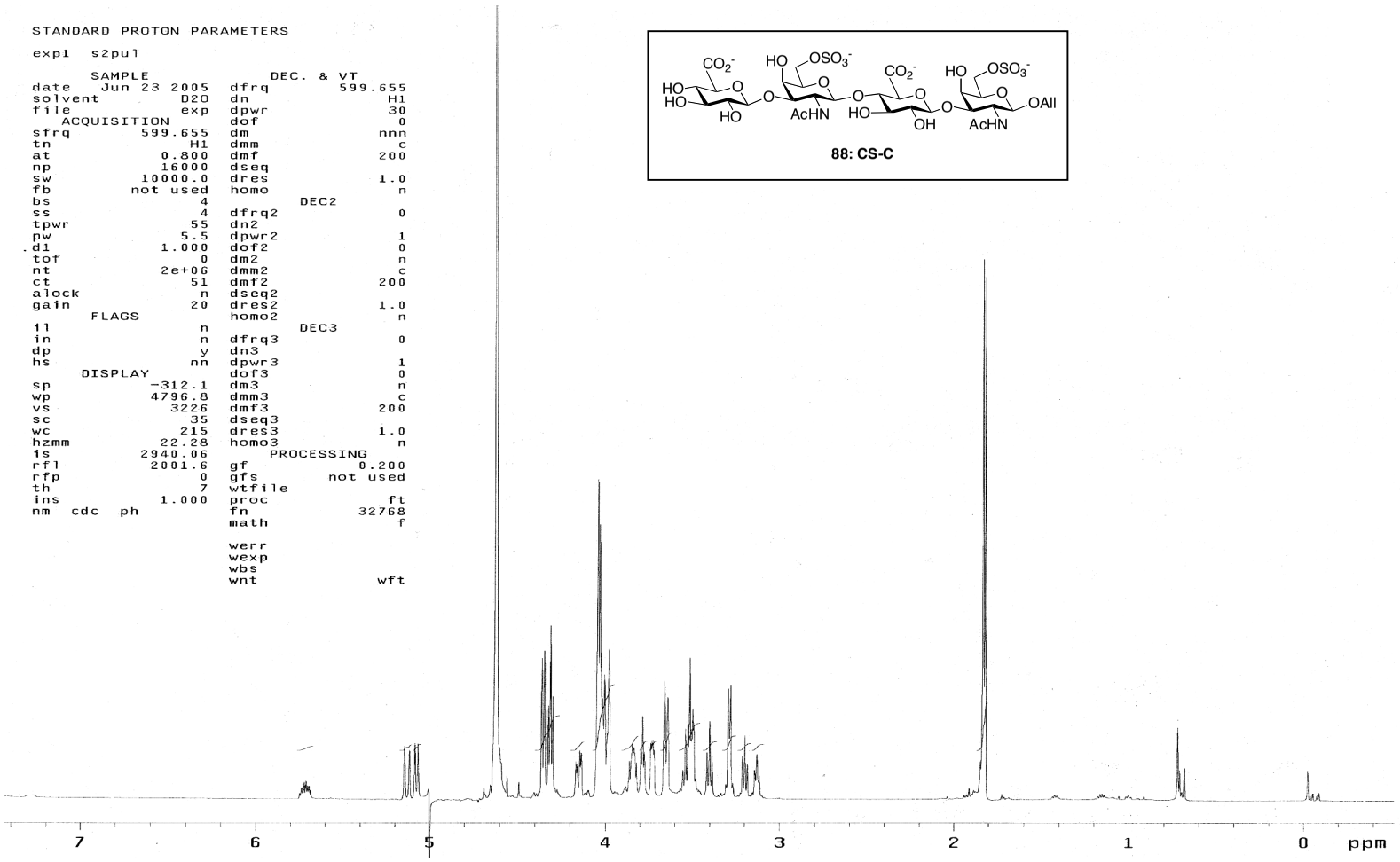

Figure A4.8: ^{1}H NMR (600 MHz, D_2O) of compound **88: CS-C**.

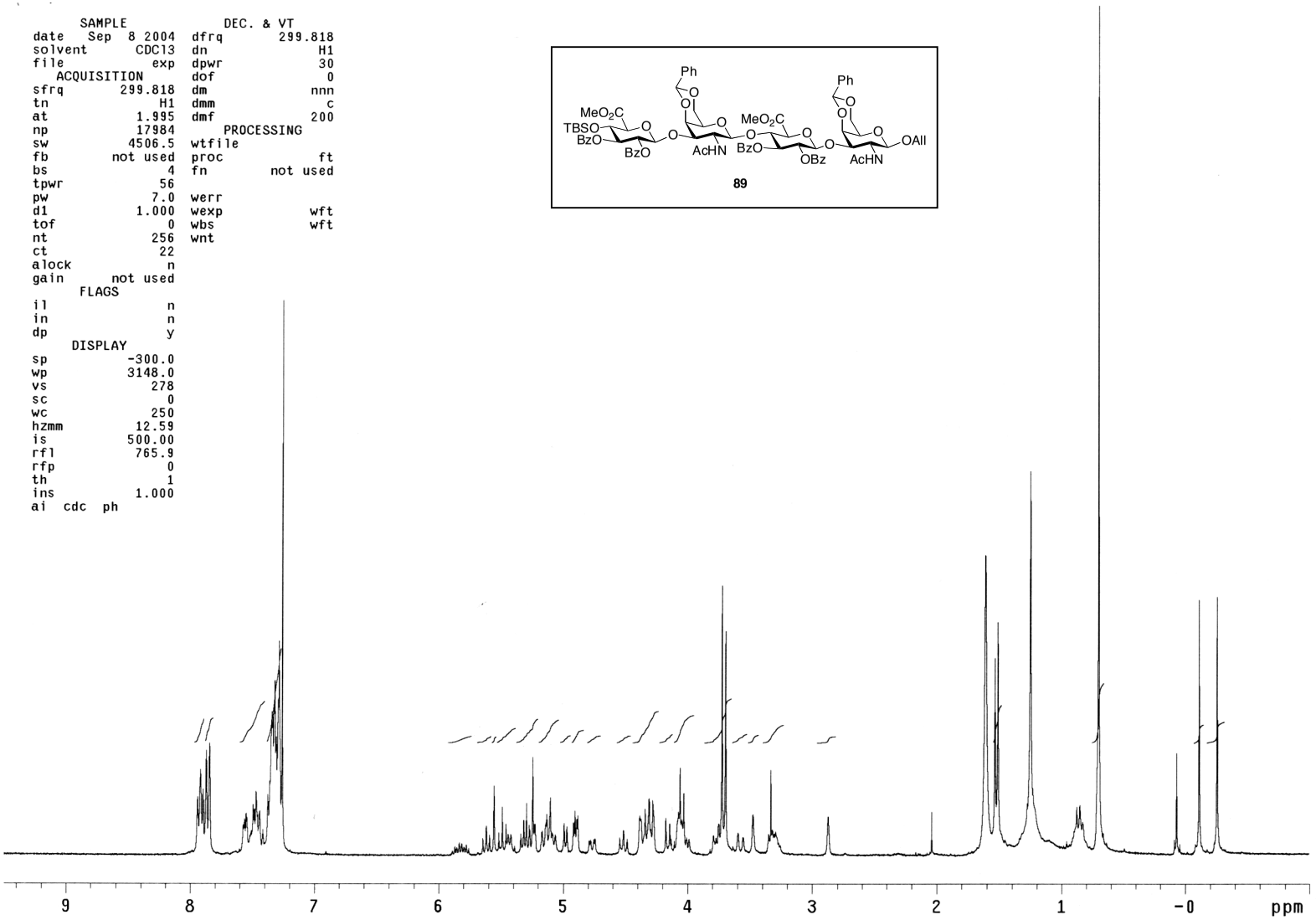

Figure A4.9: ^{1}H NMR (300 MHz, $CDCl_3$) of compound **89**.

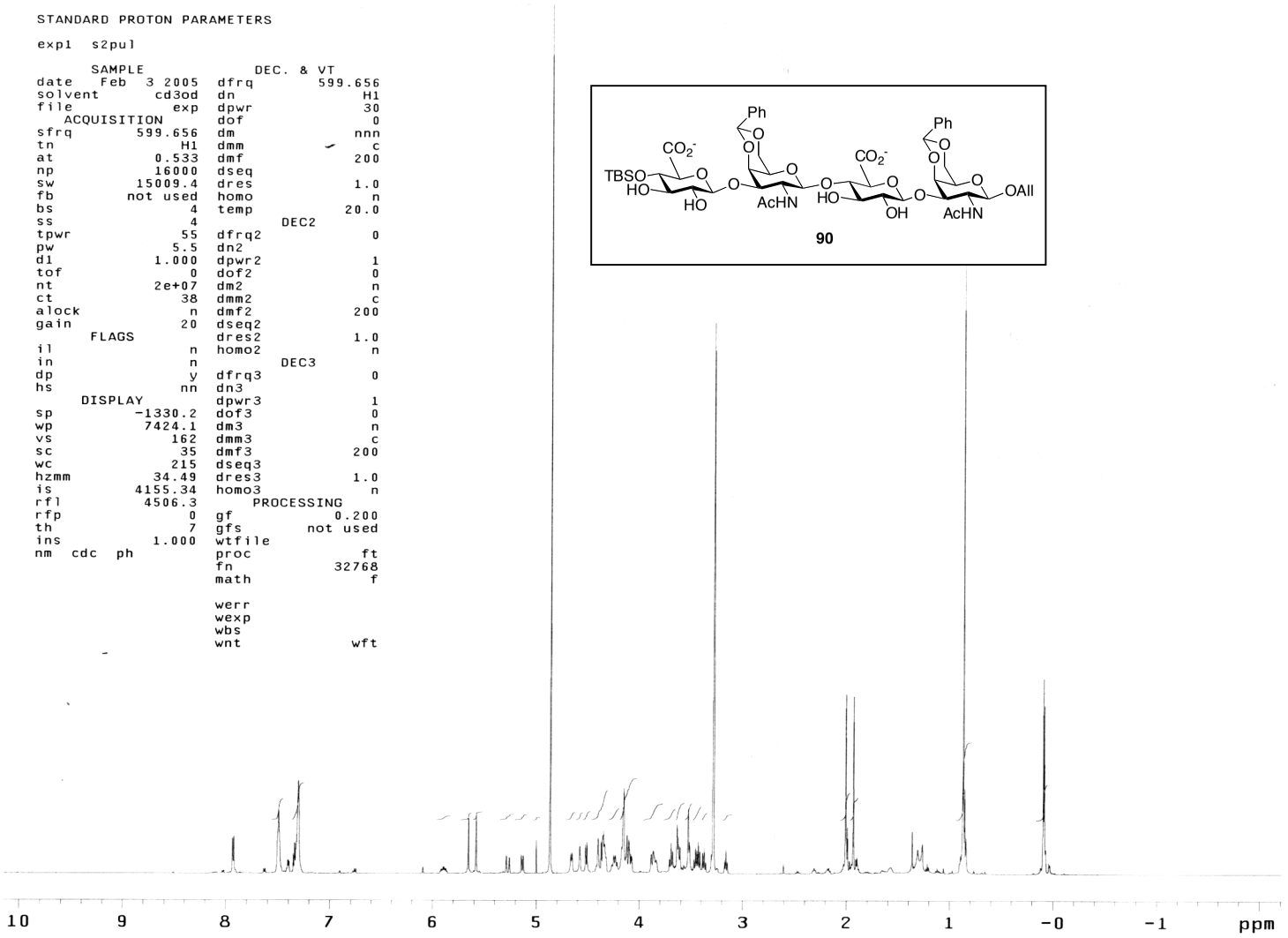

Figure A4.10: ^{1}H NMR (600 MHz, CD_3OD) of compound **90**.

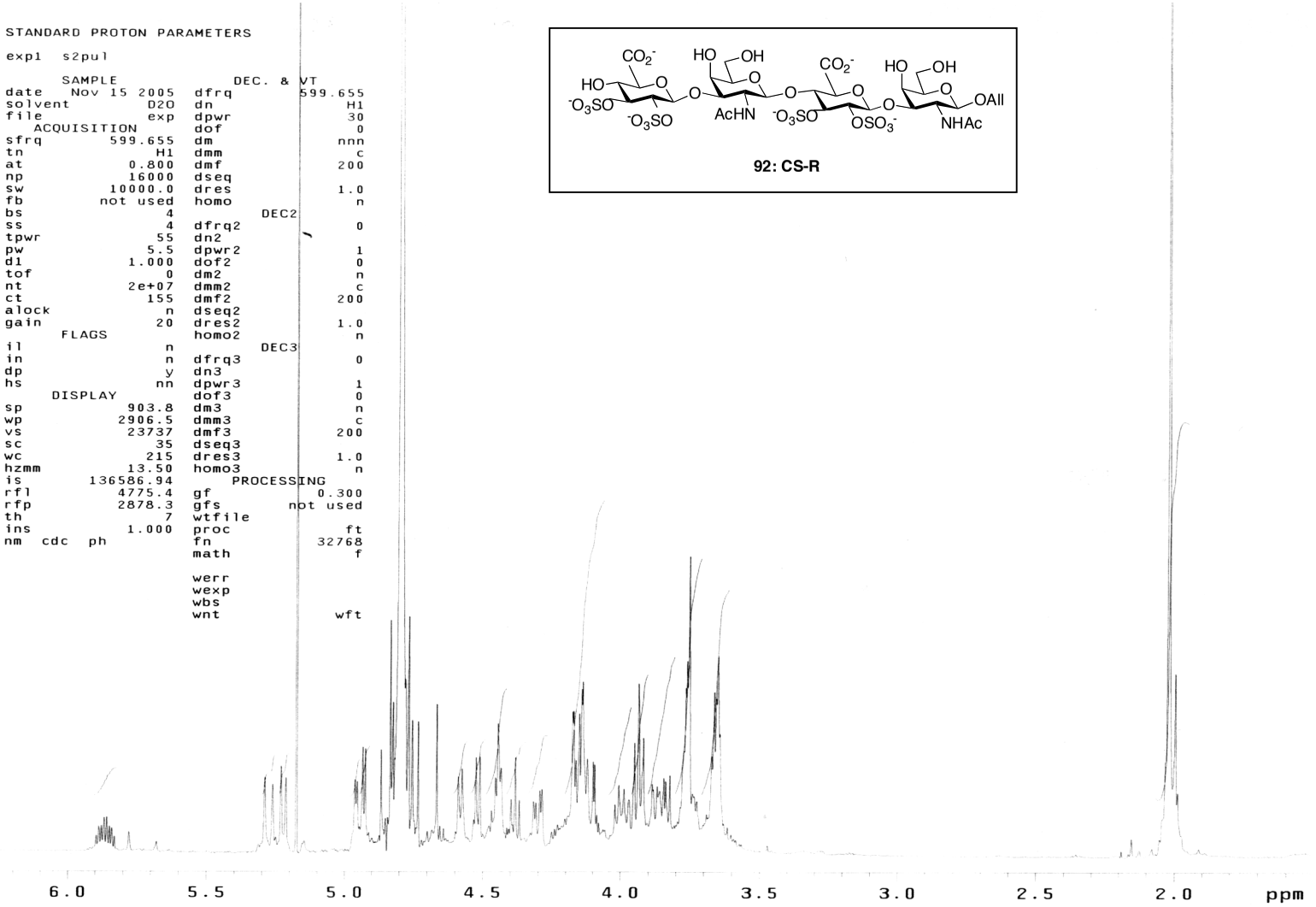

Figure A4.11: ^{1}H NMR (600 MHz, D_2O) of compound **92: CS-R**.

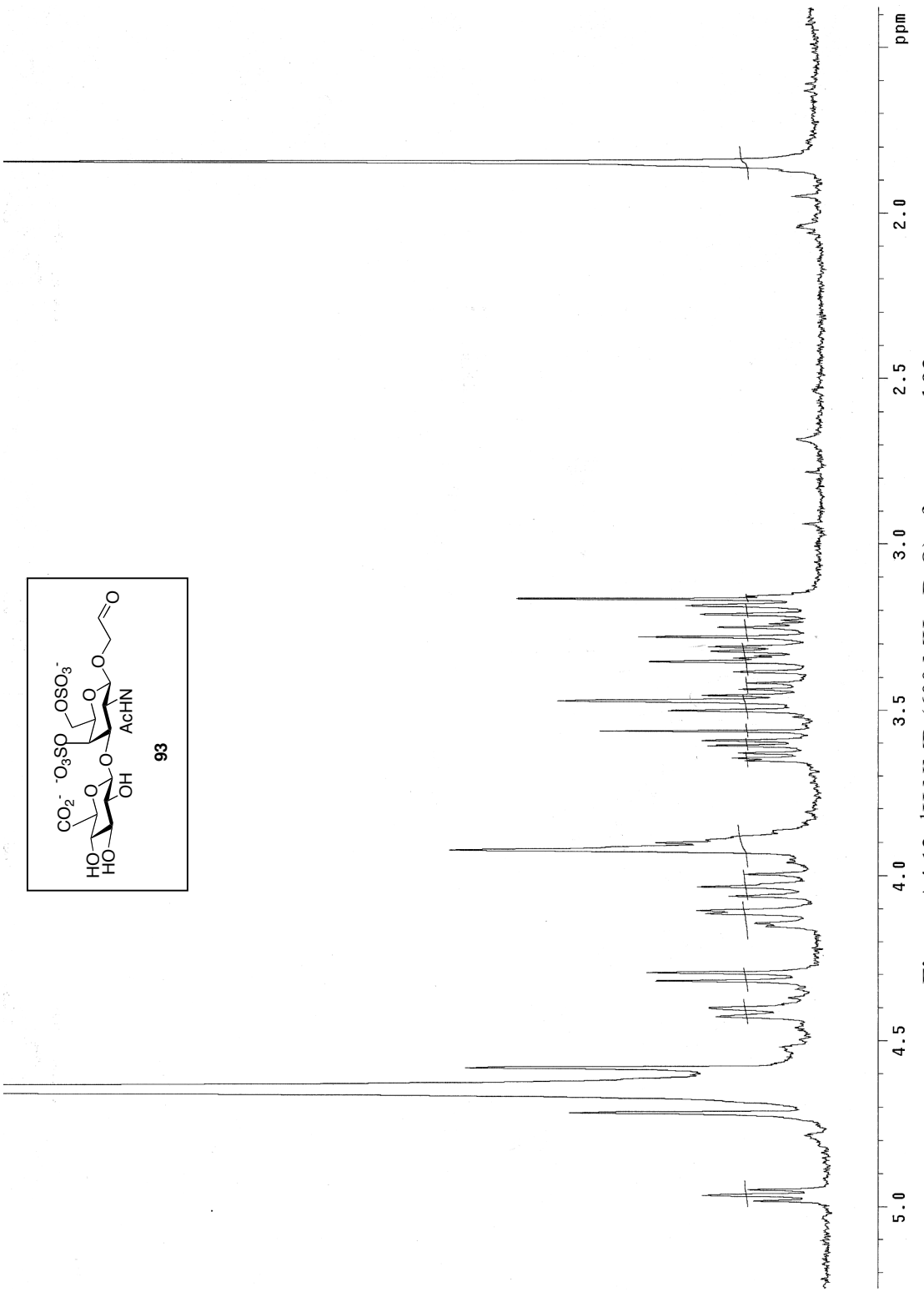

Figure A4.12: ^{1}H NMR (600 MHz, D_2O) of compound **93**.

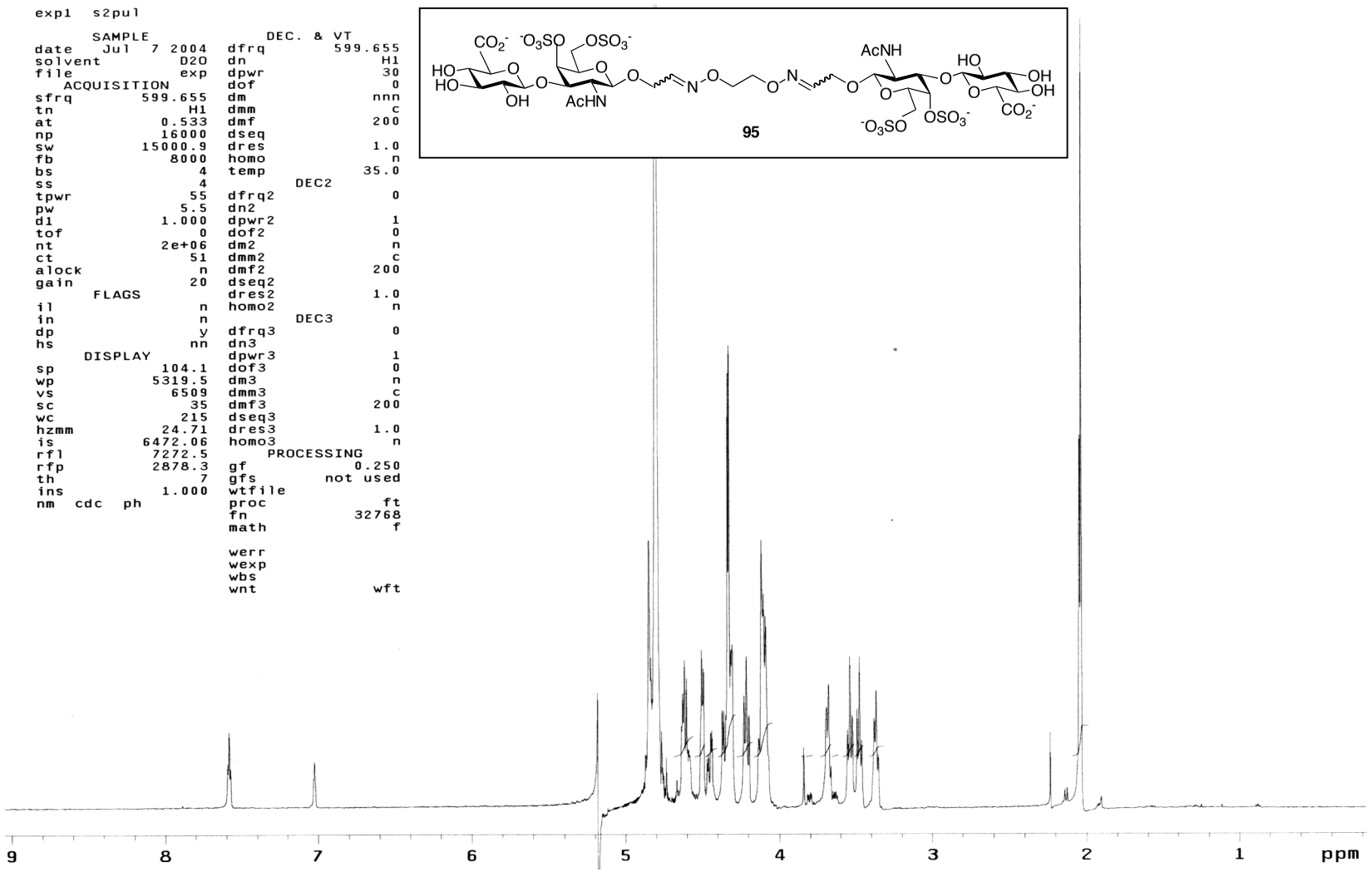

Figure A4.13: ^{1}H NMR (600 MHz, D_2O) of compound **95**.

Chapter 5: Development of Chondroitin Sulfate Microarrays*

Background

Interest in the functions and significance of carbohydrates and glycoconjugates has grown rapidly in recent years. Carbohydrates are involved in diverse processes such as transcriptional regulation, cell-cell interactions, inflammation, viral and bacterial infections, tumor metastasis, development, and signal transduction.[1-11] To understand how carbohydrates modulate these activities, it is necessary to know the proteins and ligands that interact with oligosaccharides. Current biochemical approaches to understand carbohydrate-protein interactions are cumbersome,[12] and methods are needed for sensitive, high-throughput screening of such interactions.

As shown in Chapters 3 and 4, chemical synthesis can provide access to sugars with defined length and structure, and oligosaccharides can also be obtained utilizing chemoenzymatic synthesis[13] or isolated from natural sources.[14] Typically, small amounts of material are generated, making crucial the development of a miniature assay for studying oligosaccharide interactions with proteins. Inspired by DNA and protein microarrays, glycobiologists and carbohydrate chemists have fabricated carbohydrate microarrays for analysis of protein binding to carbohydrate ligands.[15,16] Microarrays allow for analysis of thousands of sugar-proteins interactions in one experiment and require only nanogram to microgram amounts of both protein and oligosaccharides.

---

* Polylysine heparan sulfate microarrays were done in collaboration with Eric L. Shipp, a postdoctoral scholar in the Hsieh-Wilson laboratory. Aldehyde-coated microarrays were done in collaboration with Claude J. Rogers, a graduate student in the Hsieh-Wilson laboratory. Dr. Jose Luis Riechmann, Director of the Millard and Muriel Jacobs Genetics and Genomics Laboratory at Caltech, assisted with printing the microarrays.

DNA-DNA, DNA-RNA, and protein-protein interactions tend to be strong and are readily detectable through use of microarrays.[17,18] In contrast, protein-carbohydrate interactions are relatively weak, and this fact must be considered when performing microarray analysis. To achieve maximum binding, the carbohydrates must be immobilized in such a manner that they are fully exposed and are not blocked by the slide surface. Multiple carbohydrate microarray methods have been developed and will be discussed in the following sections.

Noncovalent attachment strategies to microarray surfaces

An early strategy to understand the interactions of proteins with carbohydrates was through binding analysis of six common lectins to biotinylated sugars immobilized to streptavidin-coated microtiter plates.[19] Later investigations added a chromophore in the carbohydrate linker region to simplify analysis, and binding was monitored by surface plasmon resonance (SPR) spectroscopy (Figure 5.1).[20,21] These methods did display some drawbacks. The linker length was an important component in the study, and shorter linkers resulted in more nonspecific ligand-surface interactions and reduced signal due to higher background. Additionally, while SPR does provide valuable kinetic information, it does not allow high-throughput screening, and microtiter plates require greater amounts of both proteins and carbohydrates than microarrays.

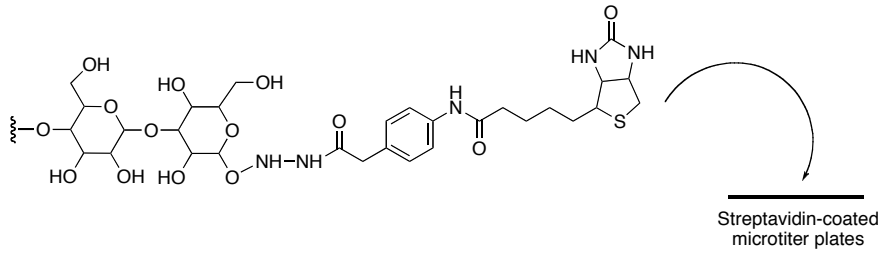

Figure 5.1: Surface display of oligosaccharides for SPR analysis using the biotin-streptavidin interaction.

In 2002, Wang *et al*., developed nitrocellulose-coated microarrays of glycoproteins and polysaccharides (Figure 5.2).[22] The arrays were spotted with a standard robotic printer used for the fabrication of DNA microarrays, the spots were immobilized by air-drying on the hydrophobic surface, and a large repertoire of microbial antigens were analyzed. While the arrays successfully bound to the antibodies of interest, the efficiency of immobilization was dependent on molecular mass, and larger molecules bound better than smaller molecules.

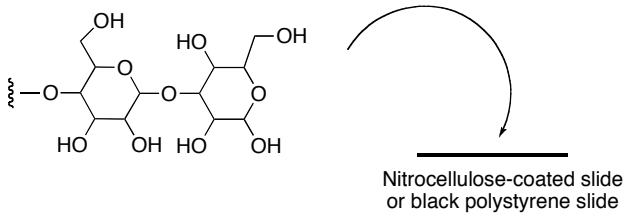

Figure 5.2: Non-covalent display of isolated polysaccharides.

Hydrophobic black polystyrene-coated slides were utilized by Willats *et al*. (Figure 5.2) for noncovalent adsorption of polysaccharides, and arrays of neoglycoproteins and proteoglycans were generated.[23] The arrays were probed with characterized dye-labeled antibodies, but due to the black hydrophobic resin, a high signal-to-noise ratio was observed.

To allow for immobilization of small oligosaccharides to the microarray surface, Fukui *et al*. generated arrays of oligosaccharides as neoglycolipids and displayed them on nitrocellulose (Figure 5.3).[24] The size of the oligosaccharides ranged from two to twenty monosaccharides, and they were linked via reductive amination to amino phospholipid 1,2-dihexadecyl-*sn*-glycerol-3-phosphoethanolamine. Known antibodies, a chemokine, and a cytokine were tested, and binding detected by ELISA-type methods. One limitation

of this method is potential loss of the ring-form of the reducing-end sugar during conjugation to the lipid, a significant problem when studying small oligosaccharides. In addition, each array contained 30-50 spots, so only a limited number of interactions were studied, lipid-derivatized oligosaccharides are difficult to purify, nitrocellulose membranes are less robust than coated-glass slides, and it is difficult to know precisely how much oligosaccharide is adhered to the surface.

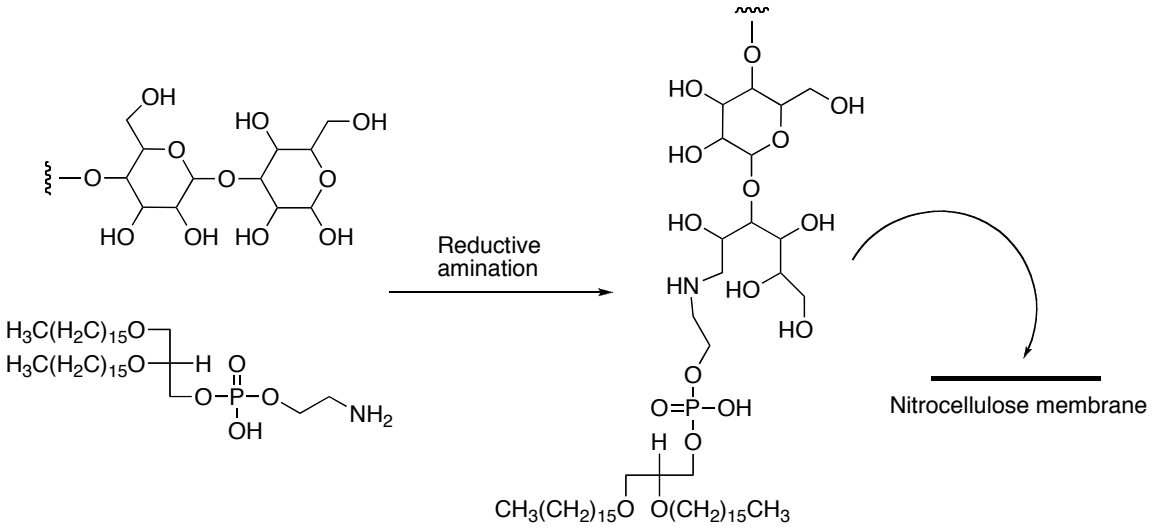

Figure 5.3: Immobilization of neoglycolipids to nitrocellulose arrays.

In 2005, Pohl's laboratory developed fluorous-based carbohydrate microarrays, starting with the placement of C_8H_{17} fluorous tags on monosaccharides of interest (Figure 5.4).[25] Fluorous tags can simply purification of oligosaccharides after solution or solid-phase synthesis. Monosaccharides were robotically printed onto fluoroalkylsilane-coated slides, and the slides were probed with lectins of interest. However, a drawback of this approach is the hydrophobic surface causes beading of the protein treatment solution on the slide, possibly making complete coverage of the array difficult. Additionally,

methanol is used in the spotting buffer and due to evaporation, the concentrations of the sugars could change during long print runs, and the slide surface is sometimes fluorescent at wavelengths used for detecting protein interactions.

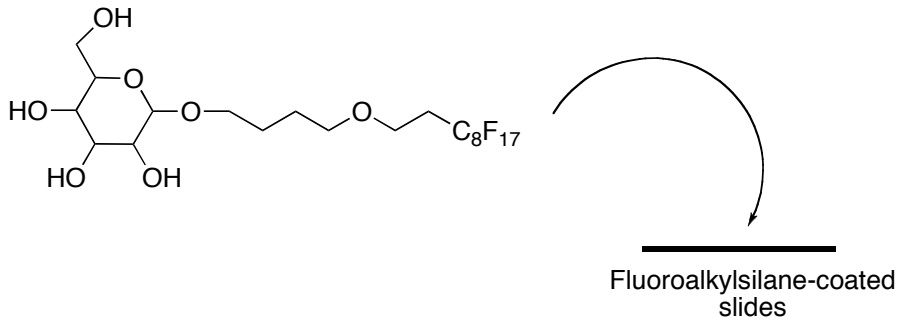

Figure 5.4: Pohl's approach to fluorous-based microarrays.

Wong and co-workers created an approach that was a combination of noncovalent and covalent attachment (Figure 5.5).[26] Sugars derivatized with azide linkers were conjugated to alkynylated lipids noncovalently attached to microtiter plates by a cycloaddition reaction. Several di- and tetrasaccharides were tested, and the noncovalent attachment strategy allows convenient characterization of the lipid-linked products by mass spectrometry. The method does require multiple chemical manipulations to link the sugars to the plate surface, and the use of microtiter plates requires greater amounts of material than microarrays.

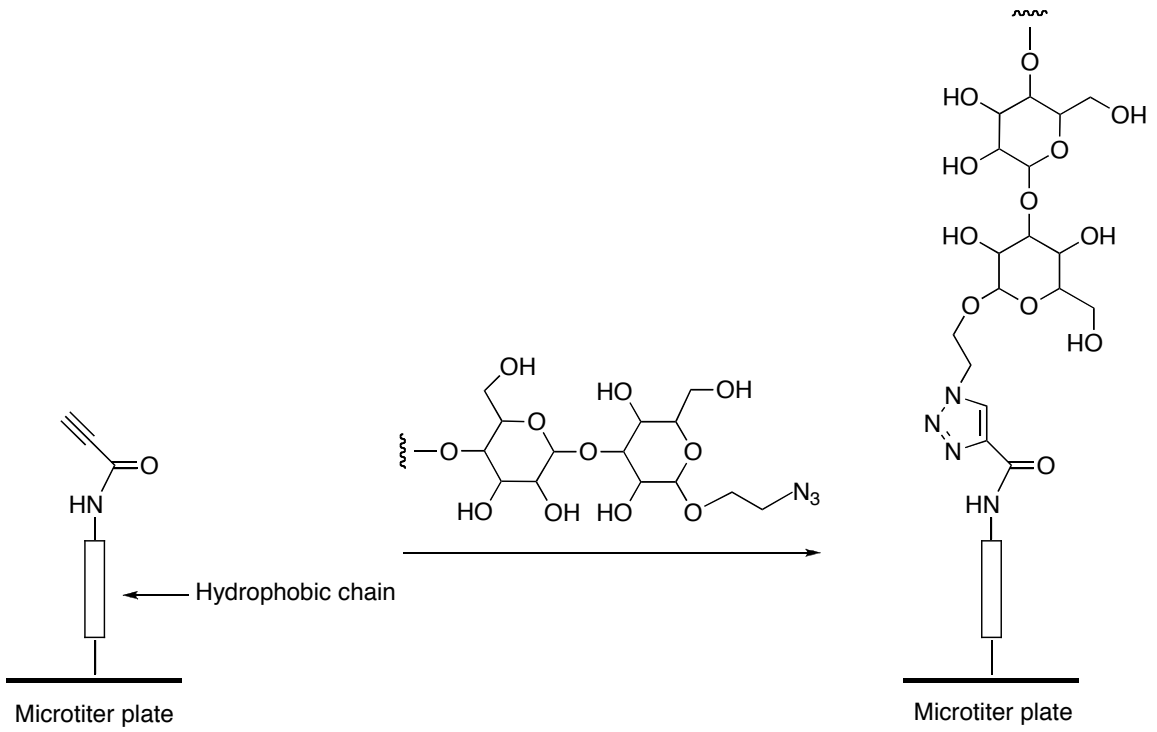

Figure 5.5: Wong's generation of lipid-linked oligosaccharide microtiter plates.

Covalent attachment strategies to microarray surfaces

Limitations exist in non-covalent attachment strategies for the preparation of carbohydrate microarrays. Nitrocellulose-coated arrays can only be used to analyze large oligosaccharides or lipid-linked oligosaccharides. Relying on hydrophobic interactions to affix oligosaccharides to the slides limits the washes and detergents one can use to reduce nonspecific interactions and inevitably, loss of the carbohydrates from the surface occurs during treatment. Additionally, with non-covalent attachment, the precise carbohydrate amount on the array is not defined. In 2002, Mrksich reported development of benzoquinone-coated gold surfaces and covalent conjugation of cyclopentadiene-containing carbohydrates through use of the Diels-Alder reaction (Figure 5.6).[27] The reaction was efficient and selective, ten monosaccharides were linked to the slide surface,

and lectins that bind these carbohydrates were screened. This method is relatively expensive due to the use of gold-coated slides, and the linker synthesis and surface chemistry technologies are fairly complicated and require many steps to complete.

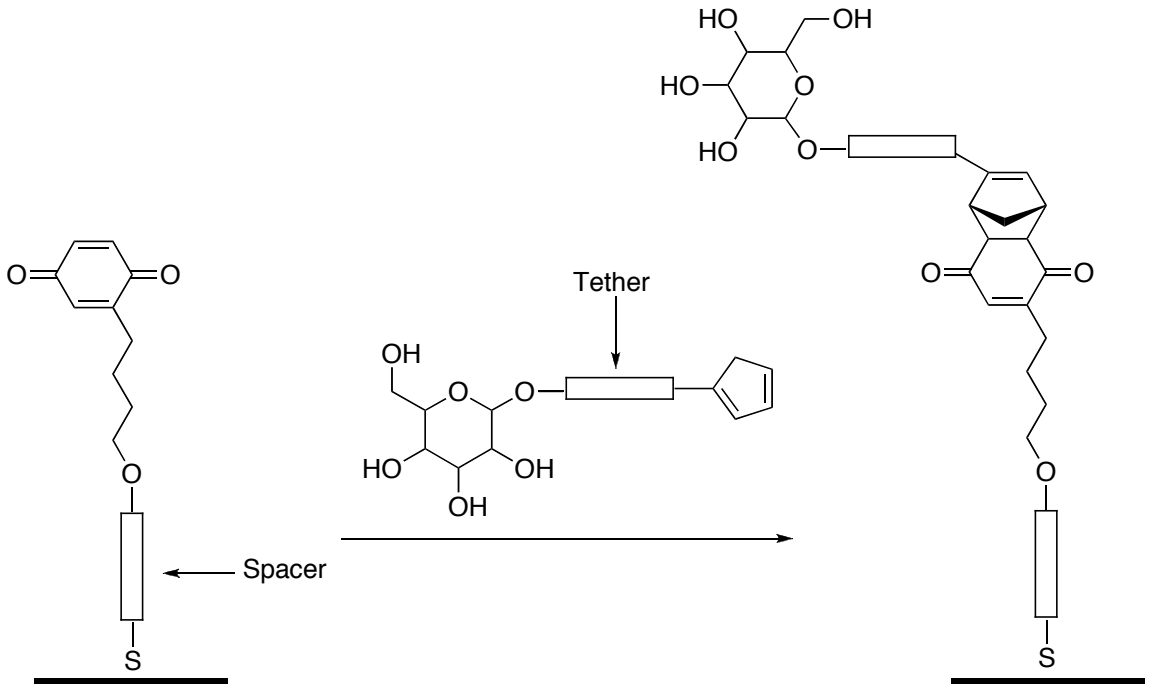

Figure 5.6: Formation of covalently attached carbohydrate microarrays through use of a Diels-Alder reaction.

Shin's group generated covalently linked arrays through use of thiol-coated glass slides and carbohydrates containing maleimide linkers (Figure 5.7).[28] Monosaccharides and disaccharides were printed robotically and linked to the slide surface by a hetero-Michael addition between the thiol group and the maleimide. A set of known lectins was screened and binding was observed as expected. As in the previous example, the linker chemistry is complicated and requires multiple derivatization steps.

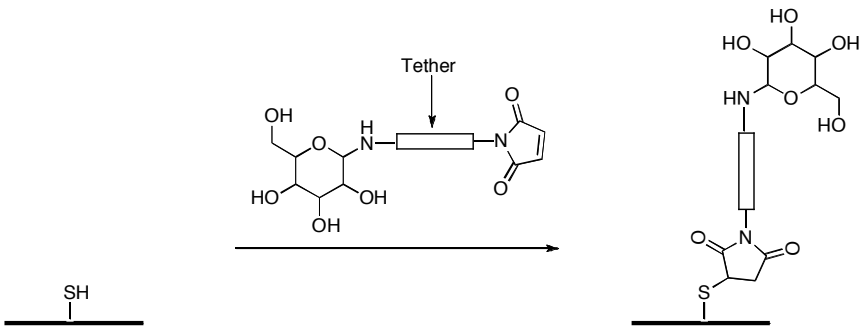

Figure 5.7: Shin's approach to covalent attachment of oligosaccharides.

Seeberger and co-workers developed a similar methodology to the Shin laboratory, but the carbohydrates contained a linker with a thiol at the terminus and the slides were coated with maleimide functionalities (Figure 5.8).[29] Several high-mannose derivatives were conjugated to the slide surface and HIV-binding proteins were screened. Similar to other covalent strategies, preparation of the slide surface and the linker chemistry to attach the oligosaccharide required several synthetic manipulations.

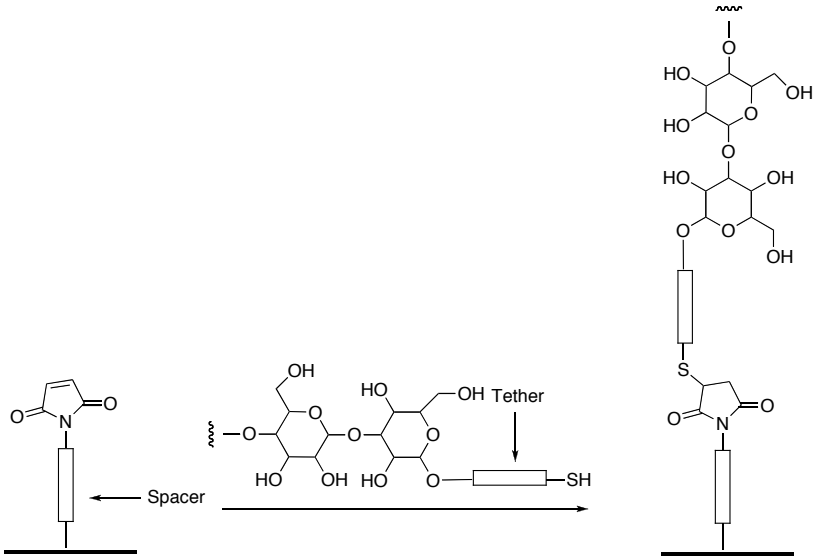

Figure 5.8: Seeberger's approach to covalent conjugation of oligosaccharides to microarrays.

Through the use of microarrays coated with hydrazide- or aminooxy-derviatized glass slides, Shin *et al*. conjugated free carbohydrates including mono-, di-, oligo-, and polysaccharides to slide surfaces (Figure 5.9).[30] With these methods, the sugars do not require linker chemistry strategies, and high-throughput analysis of carbohydrate-protein interactions has been performed. Closure of the ring after conjugation to the hydrazide-coated slides was the predominant product observed, but the acyclic form was the major product of conjugation to the aminooxy slides. For this reason, greater protein binding to the carbohydrates occurred on the hydrazide-coated microarrays. High concentrations of carbohydrate are necessary for conjugation to either slide surface because the reaction is dependent on the presence of the ring-opened form of the carbohydrate, making it difficult to determine the amount of carbohydrate linked to the surface.

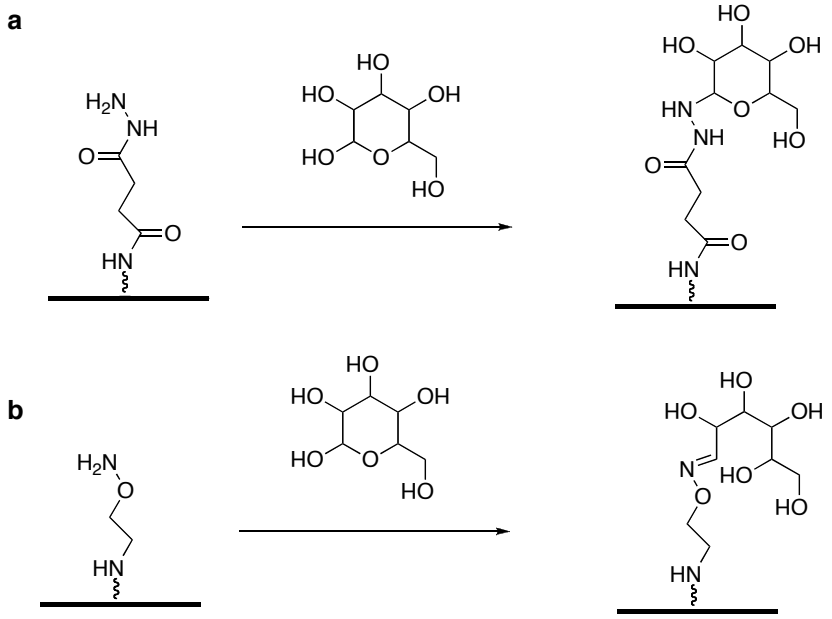

Figure 5.9: Covalent attachment of unmodified oligosaccharides to (**a**) hydrazide- or (**b**) aminooxy-coated slides.

In 2004, the laboratories of Wong and Paulson conjugated amine-derivatized oligosaccharides to *N*-hydroxysuccinimide (NHS)-activated slides (Figure 5.10).[31] Two hundred synthetic and natural glycans were screened and tested for binding to lectins, antibodies, siglecs, galectins, and viruses. The approach is one of the most direct methods to create microarrays as the slides are commercially available and require no modification. Seeberger and co-workers generated heparan sulfate (HS) microarrays in a similar manner, but with a more complicated linker strategy, involving reaction of a pentenyl glycoside with an amine-terminated thiol followed by conjugation to the NHS esters.[32] HS molecules of 4 different lengths, but only one sulfation pattern, were analyzed for their abilities to bind fibroblast growth factor-1 (FGF-1) and fibroblast growth factor-2 (FGF-2), two proteins known to interact with HS.

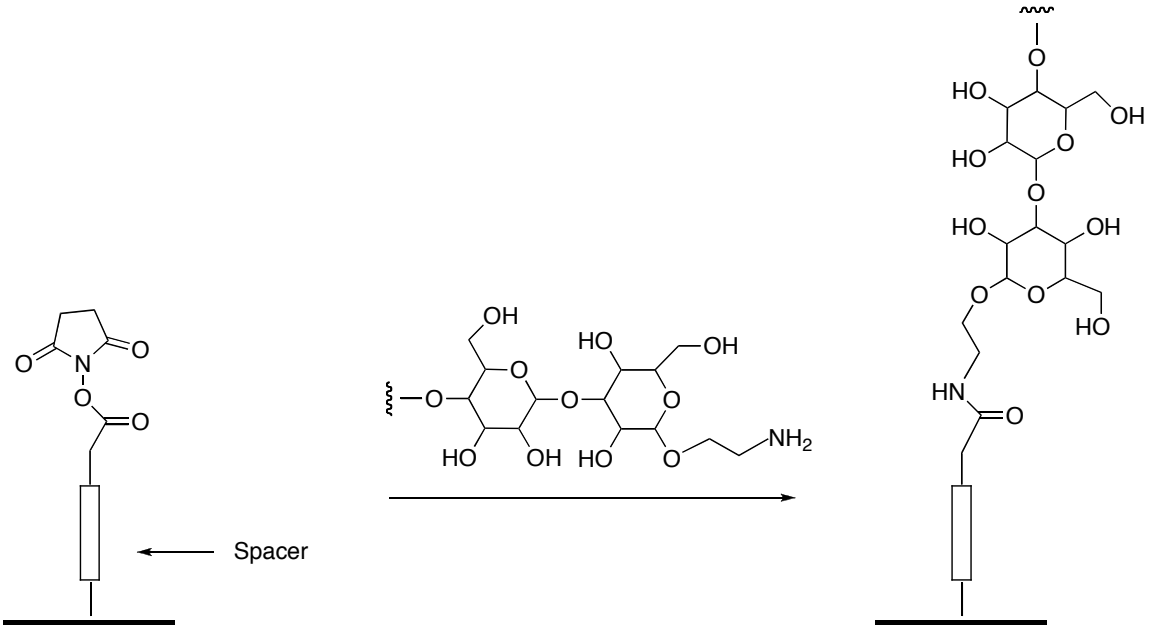

Figure 5.10: Wong and Paulson's approach to NHS-activated microarrays.

Creation of chondroitin sulfate microarrays

As described in the previous two sections, carbohydrate microarrays have been used extensively to characterize glycan-protein interactions, but they have not been exploited for detailed structure-function studies of glycosaminoglycans (GAGs). Moreover, application of carbohydrate microarrays has been limited largely to confirming known interactions with well-characterized lectins, proteins and antibodies.[19-31] We envisioned that carbohydrate microarrays should provide a powerful approach to evaluate the importance of sulfation in modulating protein recognition and provide insight into the mechanisms through which synthetic chondroitin sulfate (CS) small molecules stimulate neuronal outgrowth (see Chapters 3 and 4).

The three major sulfation motifs found *in vivo*, CS-A, CS-C and CS-E,[32] and the unnatural motif, CS-R (Figure 5.11), differ only subtly in their sulfation patterns and are identical in terms of stereochemistry and sugar composition. The potential of microarrays to distinguish such closely related structures was unclear, as most studies have utilized carbohydrates of very different composition, such as mannose versus galactose or tetrasaccharides versus hexasaccharides.[30-32] We decided to test two commercially available microarray platforms for the fabrication of CS arrays, polylysine-coated slides and aldehyde-coated slides, investigating both noncovalent and covalent attachment strategies. We also hoped to develop a simpler, more direct route to carbohydrate microarray formation than those used in previous studies, and one that was more amenable to our synthesis.

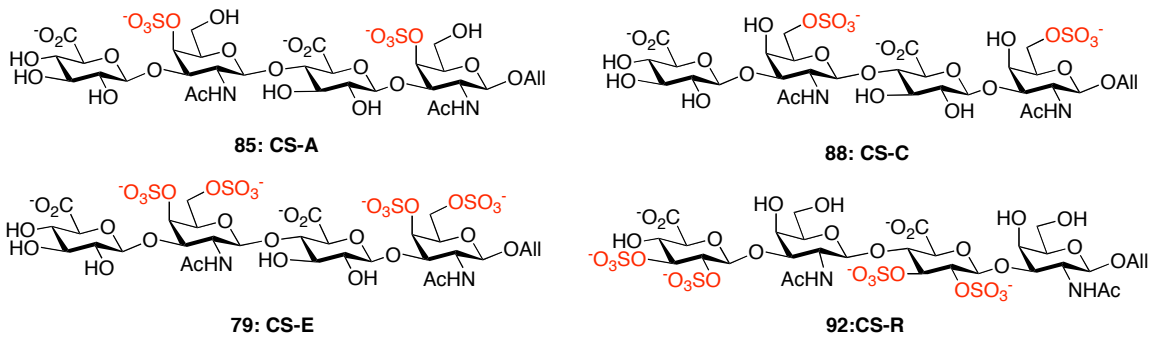

Figure 5.11: Synthetic chondroitin sulfate library for microarray analysis.

Results and Discussion

Polylysine-coated microarrays

Polylysine-coated microarrays are often used as the platform for DNA and RNA arrays, as these large, negatively-charged molecules interact with the positively-charged slide surface.[17] Due to the highly anionic nature of CS oligosaccharides, we expected strong interactions with polylysine slides. Solutions of the tetrasaccharides in water were spotted onto the slides in 1 μL quantities, and the sugars were allowed to bind to the slide surface for 12 hours in a 70% humidity chamber. The slides were blocked with bovine serum albumin (BSA) in phosphate buffered saline (PBS) at 37 °C for 1 hour. Concentrations of BSA tried were between 1 and 10%, and through use of HS polysaccharide microarrays, Eric L. Shipp established 5% BSA in PBS as the best blocking condition.

The slides were then treated with solutions of proteins of interest in 1% BSA in PBS. To reduce nonspecific binding, detergents such as Tween-20 and Triton X-100, were added to the protein treatment solution but led to the appearance of streaks during slide analysis, and subsequently, use of these detergents was avoided. Arrays of CS tetrasaccharides were incubated with the proteins midkine and nerve growth factor

(NGF). Midkine (MK), as described in Chapter 4, is a known CS binder and participates in the development and repair of neural and other tissues.[34] NGF was not known to interact with CS GAGs prior to our work, and is a neurotrophic factor belonging to a family of cysteine-knot growth factors which exist as stable dimers and includes brain-derived neurotrophic factor (BDNF, see Chapter 4).[35] The slides were then treated with appropriate primary antibodies in 1% BSA in PBS followed by secondary antibodies conjugated to Cy3 or Cy5 dyes, and visualized at 532 or 635 nm using a GenePix 5000a scanner. While binding to both MK and NGF to the CS tetrasaccharides was observed, with the highest binding being to the CS-E tetrasaccharide, the slides consistently had high backgrounds. Robotic printing of the slides improved their quality, but the signal-to-noise ratio could never be fully optimized. This is presumably due to nonspecific binding of the proteins and antibodies to the slide surface, and the inability of the CS tetrasaccharides to be fully displayed on the array due to their interactions with polylysine. Eric Shipp has successfully analyzed HS-protein interactions using these arrays, although his studies were performed with naturally derived polysaccharides, molecules that are hundreds of monosaccharides longer than the synthetic CS tetrasaccharides. The length of the polysaccharides presumably allows for greater display on the slide surface and protein binding can more readily occur, increasing the signal-to-noise ratio.

Aldehyde-coated microarrays

Due to the difficulty in observing good protein binding with a noncovalent attachment strategy, we decided to develop a method to covalently link our synthetic tetrasaccharides to commercially available aldehyde-coated slides. With the allyl moiety on the reducing end of the sugar (Figure 5.11), we sought to functionalize it for surface conjugation. Ozonolysis of the synthetic tetrasaccharides followed by treatment with 1,2-(bisaminooxy)ethane **94**[36] (see Scheme 4.4, Chapter 4) furnished CS oligosaccharides with a convenient aminooxy handle for covalent attachment to aldehyde-coated glass slides. Importantly, this strategy requires minimal manipulation of the sulfated oligosaccharides, enabling their direct conjugation in three short, high-yielding steps and avoiding lengthy linker chemistries typically used in carbohydrate microarray fabrication (Scheme 5.1).[19-30]

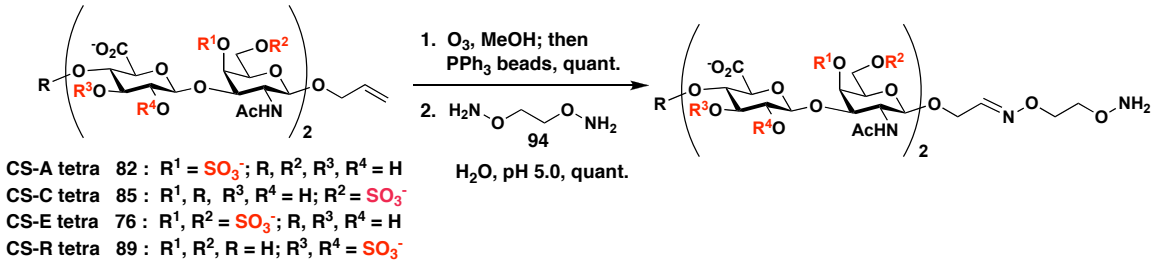

Scheme 5.1: Attachment of an aminooxy linker to chondrotin sulfate tetrasaccharides.

We began to optimize reaction conditions for the conjugation of the oligosaccharides to the slide surface (Table 5.1). The reaction of aminooxy moieties and aldehydes to form oximes has an optimal pH of 4.0 to 5.0.[37] We tried numerous buffers in that pH range and found 300 mM sodium phosphate, pH 5.0 to be the ideal buffer. The high concentration of salt yielded better spot morphology with both hand-printed and

robotically printed microarrays. Attempts to improve spot morphology using glycerol led to streaky spots and high background. To confirm that pH 5.0 afforded the highest amount of linkage to the slides, we performed a pH screen with 300 mM sodium phosphate buffer ranging in pH from 4.0 – 9.0 (Figure 5.12) and analyzed the slides with an anti-CS-A antibody (see Chapter 6 for a description of the antibody). Optimal binding was observed at pH 4.0 and pH 5.0. To ensure the stability of the carbohydrates during the print run, we selected pH 5.0 for the spotting buffer.

Spotting Conditions
250 mM NaOAc, 300 mM NaCl, pH 5.2
150 mM Sodium phosphate, pH 8.5
250 mM NaOAc, 300 mM NaCl, 30% glycerol, pH 5.2
100 mM Sodium phosphate, pH 5.0
100 mM Sodium phosphate, 30% glycerol, pH 5.0
H_2O, pH 5.0
0.9% NaCl, pH 5.0
200 mM Sodium phosphate, pH 5.0
300 mM Sodium phophate, pH 5.0
300 mM Sodium phosphate, pH 4.0
300 mM Sodium phosphate, pH 6.0
300 mM Sodium phosphate, pH 7.0
300 mM Sodium phosphate, pH 8.0
300 mM Sodium phosphate, pH 9.0

Table 5.1: Conditions tested for the conjugation of aminooxy oligosaccharides to aldehyde-coated slides.

The next step in the microarray methodology was development of blocking conditions (Table 5.2). Initially, methoxyamine was used to quench the reactive aldehydes, an approach previously employed by the Ellman laboratory to block aldehyde-coated protein microarrays,[38] but the observed background was rather high. The aldehyde-coated slides were purchased from NoAb Biodiscoveries, and the company recommends use of a blocking buffer containing a mixture of primary and secondary

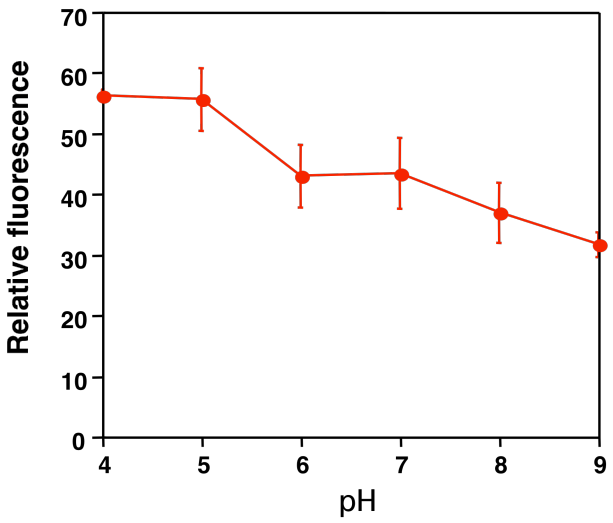

Figure 5.12: pH-dependence of aminooxy oligosaccharide conjugation to aldehyde-coated slides, as determined by relative binding of an antibody to the CS-A tetrasaccharide on the array.

amines, but again, the signal-to-noise ratio was low. Odyssey system blocking buffer and 5% BSA in PBS resulted in high backgrounds, and the use of a C_6F_{13} aminooxy tag led to beading of the protein treatment solution on the slide surface, incomplete coverage of the slide, and a high background. The optimal blocking condition was treatment with sodium borohydride in PBS for 5 minutes at room temperature; an efficient blocking strategy, considering attempts using other conditions took 1 to 3 hours. This method successfully quenched all of the aldehydes to prevent nonspecific protein binding, and the slides had a very high signal-to-noise ratio.

Blocking Conditions
0.5 M MeO-NH_2, 0.5 M NaOAc, pH 5.5
0.5 M MeO-NH_2, 0.5 M NaH_2PO_4, pH 7.4
NoAb 1X Pre-hybridization buffer
5 mM Aminooxy-fluorous tag, 5 mM NaOAc, pH 5.2
Odyssey system blocking buffer
5% BSA in PBS, pH 7.4
$NaBH_4$ in PBS, pH 7.4

Table 5.2: Conditions tested for the blocking of aldehyde-coated slides.

Finally, the buffer exploited for the protein treatment solutions was optimized (Table 5.3). As detergents and BSA are frequently used to prevent nonspecific binding, PBS solutions containing Tween-20, Triton X-100 and BSA were tested. Attempts with BSA resulted in high backgrounds, and Tween-20-treated slides were streaky and difficult to analyze. Ultimately, 0.1% Triton X-100 in PBS afforded the lowest backgrounds and cleanest arrays. The washes employed in between protein treatments were performed with PBS.

Protein Treatment Conditions Attempted
1% BSA, 0.05% Tween-20 in PBS, pH 7.4
0.05% Tween-20 in PBS, pH 7.4
0.1% Tween-20 in PBS, pH 7.4
0.1% Triton X-100 in PBS, pH 7.4
0.5% BSA, 0.1% Tween-20 in PBS, pH 7.4
0.5% BSA, 0.1% Triton X-100 in PBS, pH 7.4

Table 5.3: Conditions tested for protein incubations on aldehyde microarrays.

We validated our microarray approach using antibodies selective for specific CS sulfation motifs (see Chapter 6). A high-precision, contact-printing robot was used to deliver nanoliter volumes of the compounds to the slides, yielding spots approximately 200 μm in diameter. After blocking, the microarrays were then incubated with monoclonal antibodies raised against CS-A tetrasaccharide **85**, CS-C tetrasaccharide **88** or CS-E tetrasaccharide **79** conjugated to keyhole limpet hemocyanin (Scheme 5.1 and Chapter 6), and antibody binding was visualized using a secondary Cy3-conjugated goat anti-mouse antibody. The anti-CS-A antibody **(**10G9-2B5) bound to the CS-A tetrasaccharide in a concentration-dependent manner, and strong selectivity for the CS-A motif was observed, with little detectable binding to the CS-C or CS-E sulfation motifs (Figure 5.13a). The anti-CS-C antibody (2D5-1D2) was also extremely specific for the

CS-C tetrasaccharide and did not recognize the other patterns (Figure 5.13b). Similarly, the anti-CS-E antibody (2D11-2A10) selectively recognized the CS-E tetrasaccharide and displayed only weak binding to the CS-C motif at high tetrasaccharide concentrations (Figure 5.13c).

Having shown that microarrays can be exploited to identify specific sulfation motifs involved in protein recognition, we turned to the identification of novel CS binding proteins and characterization of the sulfation patterns required for interaction with known CS binding proteins (Table 5.4). Proteins were tested for their abilities to bind to the CS tetrasaccharides conjugated on aldehyde-coated slides, and Eric Shipp tested binding to HS polysaccharides immobilized on polylysine arrays.

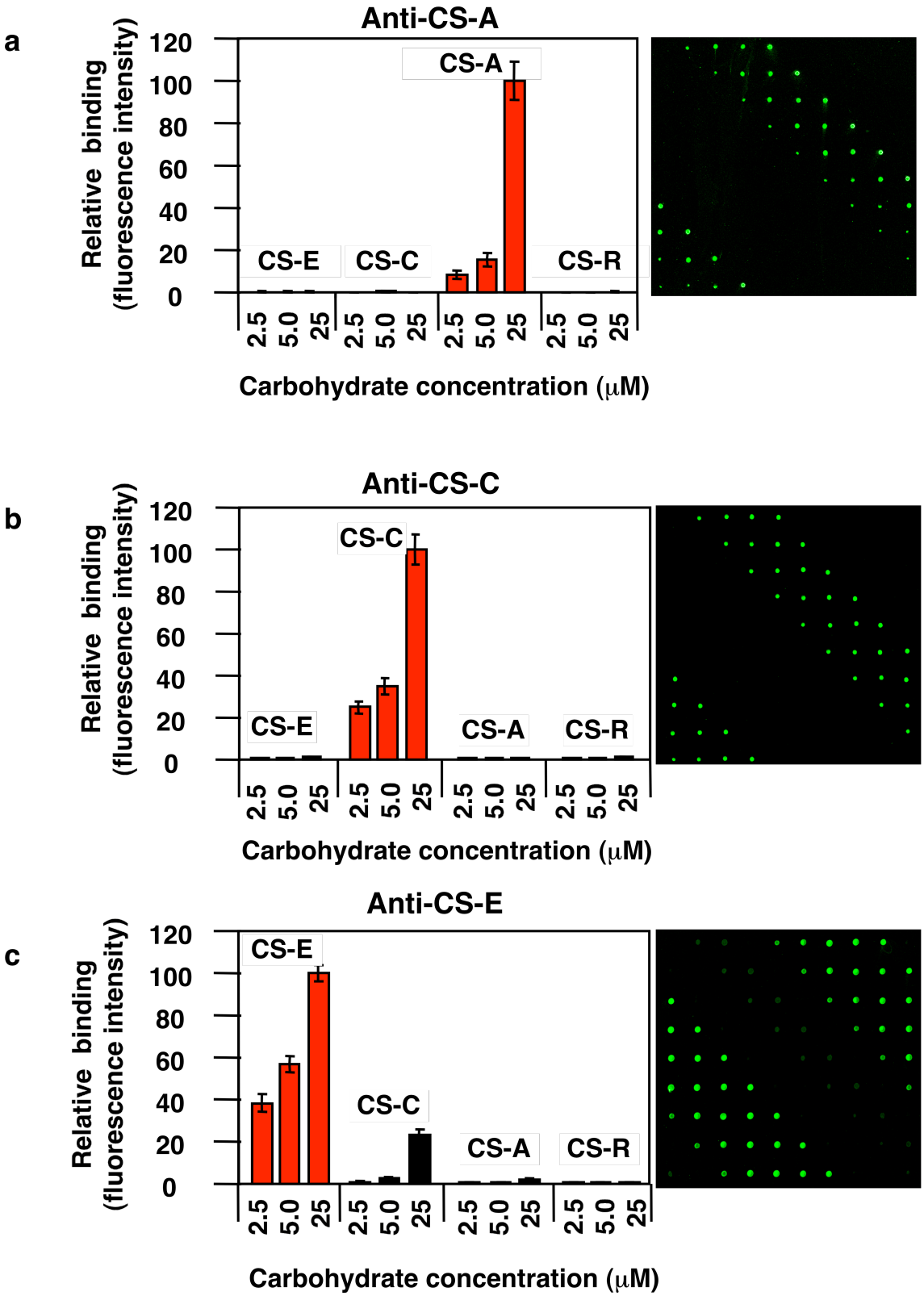

Figure 5.13: Binding analysis of the (**a**) anti-CS-A, (**b**) anti-CS-C or (**c**) anti-CS-E antibodies to the microarrays. The left panels show bar graphs depicting the data, and the right panels are selected grids of the microarrays. Keys for the grids are shown in the Appendix for Chapter 5.

Protein	Heparan Sulfate Binding	Chondroitin Sulfate Binding
Adam-10 ECD-Fc*	No	Weak
BDNF	Yes	Yes
CXCL-16 ECD-Fc*	Yes	No
DCC (aa 423-807)*	No	No
DLAR-3 IgG-like domains-Fc*	Yes	No
EGF	Yes	No
EphA3-ECD-Fc*	No	No
EphB2-ECD-Fc*	No	No
EphB4-ECD-Fc*	No	No
Ephrin A1	Yes	Weak
Ephrin A5	Yes	No
FGF-1	Yes	No
FGF-2	Yes	Yes
FGF-4	Yes	No
FGF-16	Yes	Yes
FGF-17	Yes	Yes
GDNF	Yes	Yes
HB-EGF	Not tested	Yes
MAG-Fc (5 domains)*	No	No
Midkine	Not tested	Yes
Netrin VI-V domains	Yes	No
NGF	Yes	Yes
Nogo-A-Fc	Yes	Yes
Nogo-R-Fc (aa 1-131)*	Weak	Weak
Pleiotrophin	Yes	Yes
Tie2-Fc (aa 1-450)*	No	No
TNF-α	Yes	Yes
TrkB	Not tested	Weak
Unc-5 (aa 49-356)*	No	No

Table 5.4: Binding of proteins to heparan sulfate polysaccharides on polylysine microarrays and chondroitin sulfate tetrasaccharides on aldehyde microarrays. ECD = extracellular domain. * Proteins were kindly provided by Prof. Dimitar Nikolov, Memorial Sloan-Kettering Cancer Center.

Previously characterized chondroitin sulfate binding proteins

MK, pleiotrophin (PTN), and fibroblast growth factor-16 (FGF-16) are known CS polysaccharide binders,[34] and we confirmed this through use of our tetrasaccharide microarrays. Additionally, we demonstrated that the tetrasaccharide must be a large enough motif to bind these proteins (Figure 5.14). MK and PTN are members of a family of heparin-binding proteins, have a 45% amino acid sequence homology, and share many neuroregulatory activities.[39,40] MK has been shown to bind the CS proteoglycan (CSPG) versican[41] and PTN binds the CSPGs neurocan and phosphacan, common proteoglycans in the brain.[42,43] According to our microarrays, MK binding was selective for the CS-E motif at CS concentrations within the approximate physiological value of 5 μM,[6,44,45] and it did not interact as strongly with CS-R, indicating that the midkine-CS association requires a specific arrangement of sulfate groups and is not governed by non-specific, electrostatic interactions. PTN bound all of the sulfation patterns, with only a small amount of preferential binding to CS-E. Perhaps lower concentrations of carbohydrate on the slide surface are necessary to observe selectivity, or CS-A and CS-C are low-affinity motifs that act to capture this growth factor, direct it to high affinity binding sites and then to its cell surface receptor.[46]

FGF-16 is a member of a large family of growth factors involved in cell proliferation, development, and angiogenesis.[47] Hepatocyte proliferation is modulated by FGF-16, and a truncated version of FGF-16 induces proliferation of oligodendrocytes isolated from the rat brain.[48] FGF-16 displayed a slight preference for the CS-E motif over CS-R, and did not bind CS-A or CS-C.

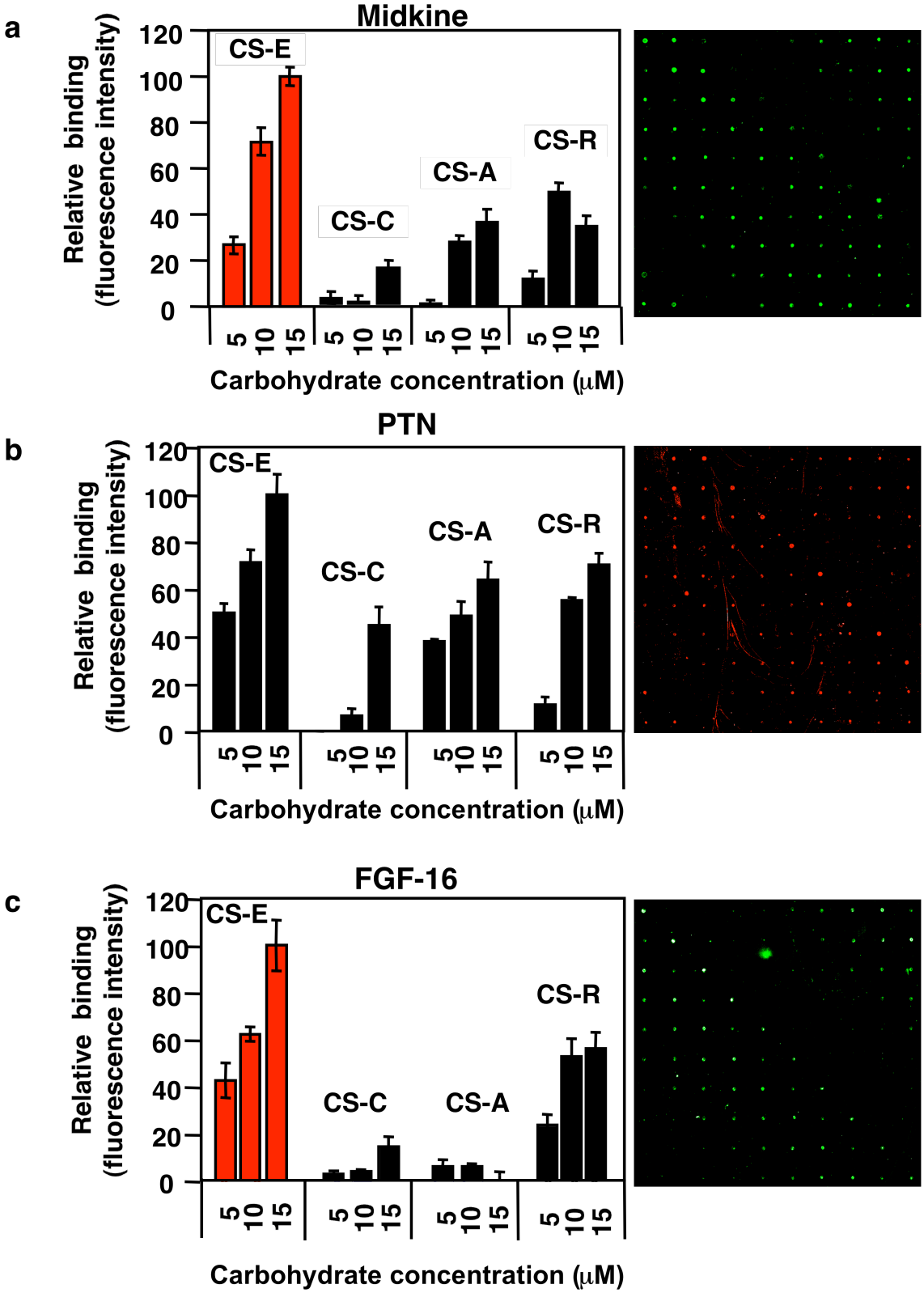

Figure 5.14: Binding analysis of (**a**) MK, (**b**) PTN or (**c**) FGF-16 to the microarrays. The left panels show bar graphs depicting the data and the right panels are selected grids of the microarrays. Keys for the grids and full midkine binding curves are shown in the Appendix for Chapter 5.

The known CS binding proteins FGF-2, FGF-17, and heparin-binding epidermal growth factor (HB-EGF) were also tested, and preliminary results indicate selective binding for the CS-E tetrasaccharide. FGF-2 binds to phosphacan through its CS side chains to promote mitogenic activity,[43] and this interaction may be due to CS-E motifs on the oligosaccharide. FGF-17 regulates patterning in the embryonic brain.[47] HB-EGF is an EGF family member involved in the regulation of midbrain dopaminergic neuron survival and stimulates migration and differentiation of neuronal precursor cells.[49,50] Our microarray results and previous SPR studies[34] suggest that CS-E and HS may direct these processes.

Newly characterized chondroitin sulfate binding proteins

With the CS microarrays, we discovered novel binding interactions with BDNF, glial-derived neurotrophic factor (GDNF), NGF, Nogo-A, tumor necrosis factor-alpha (TNF-α, see Chapter 7), and weak binding to TrkB and NogoR (Figures 5.15 and 5.16). As described in Chapter 4, BDNF contributes to synaptic plasticity, neurotransmission and neurodegenerative disease, and controls many aspects of mammalian nervous system development.[51] It is related to NGF, a protein that can protect neurons from degeneration and promote cell growth,[35] and both proteins exhibit selective binding to the CS-E tetrasaccharide. We found that BDNF exhibited a 20-fold preference for the CS-E motif relative to CS-C, -A, and -R at the 5 μM CS concentration, which approximates the estimated concentration of CS-E present in physiological samples.[6] TrkB, the cell-surface receptor for BDNF,[51] weakly bound to the CS tetrasaccharides but showed no preferential binding to any specific sulfation pattern. This result may indicate that CS forms a

complex with BDNF and TrkB to initiate signal transduction cascades in the cell. Such ternary complexes have been observed between heparin, FGF, and FGF receptor, and cause induction of mitogenic activity in BaF3 cells.[52-54] Claude Rogers is currently investigating the possibility of CS-modulated ligand/receptor complex formation.

GDNF is a powerful factor in the survival of neurons injured in Parkinson's, for example, nigrostriatal and dopaminergic neurons.[55] Recently, this factor has been shown to promote the growth of embryonic stem cell-derived neurons in the spinal cord and cause these neurons to connect with muscles to restore partial movement in paralyzed mice.[56] The binding of GDNF to CS-E implicates this motif in modulating the functions of GDNF.

Nogo-A demonstrated selective binding to the CS-E tetrasaccharide, and its receptor, Nogo-R had a relatively weak interaction with the tetrasaccharide. Secreted by supporting glial cells called oligodendrocytes, Nogo-A is typically a growth inhibitory protein that is released in areas of brain or spinal cord injury.[57] Myelin-associated glycoprotein (MAG) is another growth inhibitory protein produced by oligodendrocytes,[57] but it displayed no binding to the CS tetrasaccharides or heparan sulfate. According to neurite inhibition assays performed by Cristal Gama, the MAG we tested was not functional and perhaps this is why binding was not observed. New research has demonstrated the presence of Nogo-A in areas of development, especially in the developing rat olfactory system.[58] As shown in Western blots of embryonic rat brain lysates probed with a CS-E specific antibody, CS-E is a prevalent sulfation motif in the olfactory bulb (see Chapter 6), and perhaps Nogo-A and CS-E-containing proteoglycans cooperate to modulate development of this brain region.

Previous studies have shown that CS plays a role in inflammation and injury.[7,9,11] Thus, we examined whether CS could bind to TNF-α, a proinflammatory cytokine involved in numerous diseases, including rheumatoid arthritis, Crohn's disease and psoriasis.[59-61] TNF-α is a known heparin binder[62] and our microarrays established it as a CS-E selective binder as well. This interaction will be discussed in greater detail in Chapter 7.

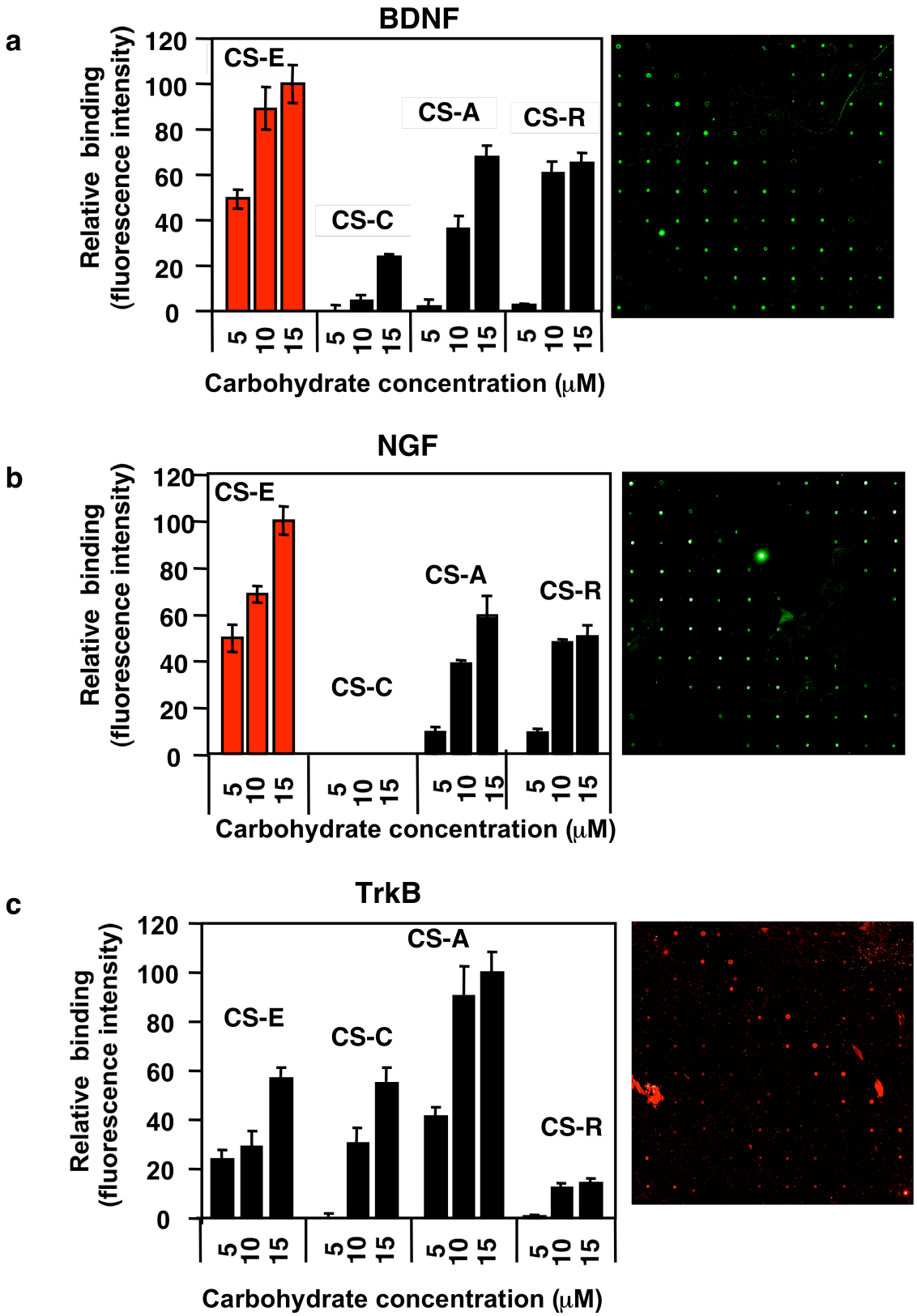

Figure 5.15: Binding analysis of (**a**) BDNF, (**b**) NGF, or (**c**) TrkB to the microarrays. The left panels show bar graphs depicting the data and the right panels are selected grids of the microarrays. Keys for the grids and full BDNF binding curves are shown in the Appendix for Chapter 5.

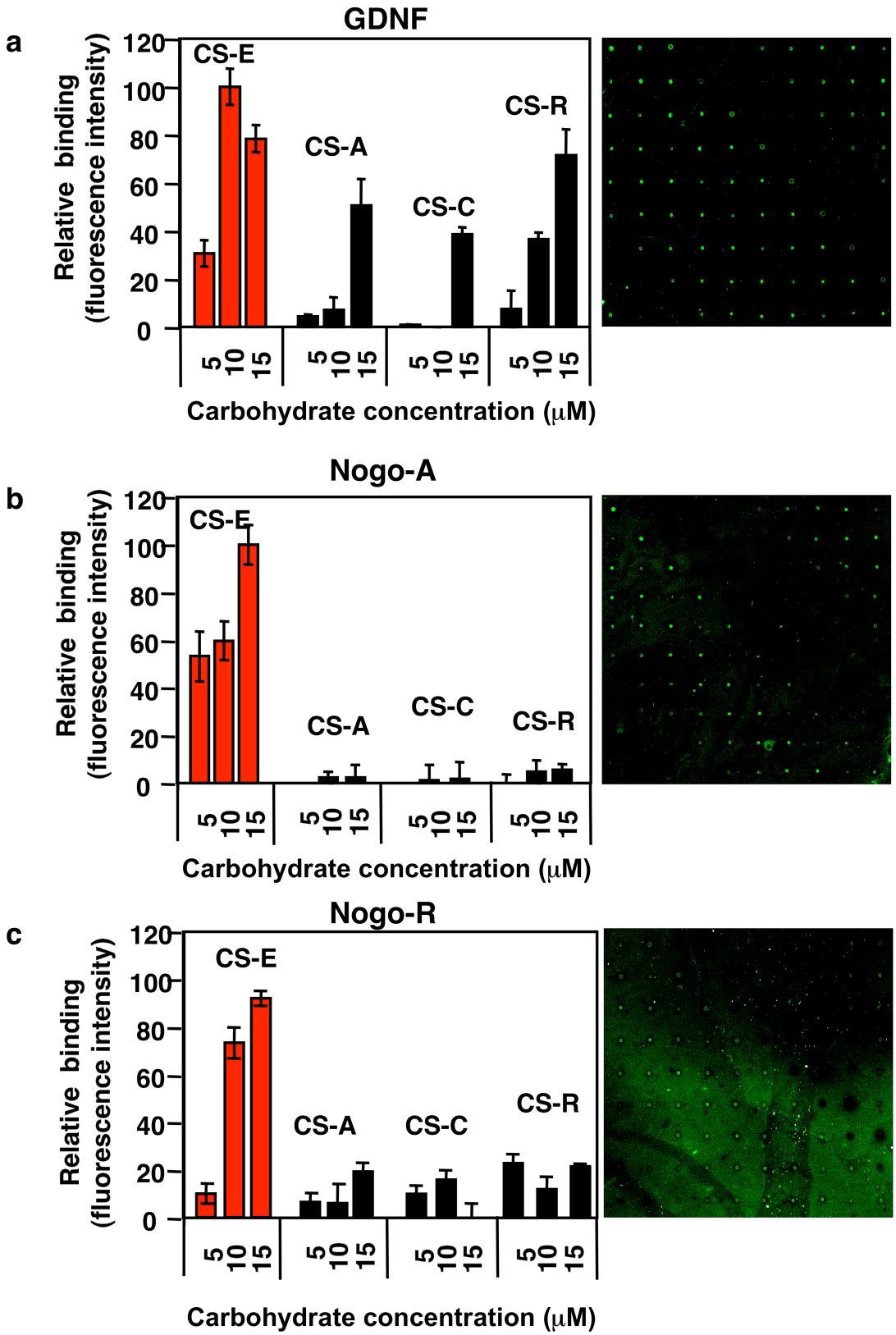

Figure 5.16: Binding analysis of (**a**) GDNF, (**b**) Nogo-A or (**c**) Nogo-R to the microarrays. The left panels show bar graphs depicting the data and the right panels are selected grids of the microarrays. Keys for the grids are shown in the Appendix for Chapter 5.

Heparan sulfate binding proteins

Interestingly, through our microarray studies we found proteins that interacted with both CS and HS, and some that recognized only HS, suggesting that these two GAG families may have some common binding mechanisms and biological functions but they have distinct roles as well. It also demonstrates how subtle stereochemical and sulfation differences can influence protein binding. Epidermal growth factor (EGF), FGF-1, and -4, netrin, ephrins A1 and A5, CXC-chemokine ligand-16 (CXCL-16), and *Drosophila* LAR receptor (DLAR) only bound to HS polysaccharides. The lack of binding to EGF was unexpected, as CS-E did interact with a related protein, HB-EGF. EGF typically regulates cell growth, proliferation, and differentiation,[50] but activation of the EGF receptor (EGFR) mediates inhibition of axon regeneration by MAG and CSPGs.[63] Perhaps CS does not bind to EGF in order to potentiate this effect. It is also possible that EGF binding requires a structural motif longer than a tetrasaccharide.

While FGF-2 and FGF-16 strongly bound to the CS-E tetrasaccharide, FGF-1, and FGF-4 did not. FGF-1 had been previously reported to not bind CS-E polysaccharides, despite its strong interaction with heparin.[34]

Netrins and ephrins are families of important axonal guidance cues that can act as repellents or attractants to developing axons. Neuronal cell movements are affected by netrins, and ephrins direct neural crest migration.[64] Both families of proteins appear to be modulated by HSPGs, but the receptors for these proteins, deleted in colorectal cancer (DCC) for netrins and the Ephs for ephrins, did not bind to HS polysaccharides.

The proteins CXCL-16 and DLAR interacted strongly with HS polysaccharides displayed on polylysine microarrays. Cell surface-expressed HS GAGs are thought to

immobilize CXCL-16 and bring it to the cell surface to interact with its receptor. CXCL-16 has an important role in inflammation and its activity is regulated by Adam-10 (*a* *d*isintegrin *a*nd *m*etalloproteinase),[65] which we found did not bind to CS or HS. DLAR, a receptor tyrosine phosphatase essential for axonal guidance and synaptogenesis in *Drosophila* that binds to the HS proteoglycan syndecan,[66] recognized HS polysaccharides as expected.

While not characterized in these studies, angiopoietin-3, a member of a family of proteins known to be important in angiogenesis, is tethered to the cell surface by the proteoglycan perlecan via the HS chains.[67] The receptor for angiopoietin-3 is Tie-2, a tyrosine kinase, and microarray analysis of this protein showed no binding to either CS or HS.

Conclusion

In conclusion, we report the first example of carbohydrate microarrays to rapidly identify GAG-protein interactions and probe the specificity of proteins for distinct sulfation sequences. Using a library of synthetic CS oligosaccharides modified at the reducing end with an allyl group, we were able to conjugate the molecules to commercially available aldehyde-coated slides via a 1,2-(bisaminooxy)ethane **94** in three high-yielding steps, an improvement over existing carbohydrate microarray methodologies. We also demonstrated the power of the arrays to rapidly afford information, identify new CS binding proteins, and understand CS-protein interactions.

Through comparison of CS-E and CS-R, we found binding to be determined by the specific orientation of the sulfate groups, not simply based on random electrostatic

interactions. This provides further evidence that CS and HS bind to proteins through a "sulfation code," and the regulation of sulfation patterns *in vivo* is crucial in dictating the extracellular matrix cues a cell receives.

The range of growth factors and cytokines recognized by both CS and HS suggests that these GAGs are involved in many processes that have yet to be elucidated. We anticipate that CS microarrays will accelerate our understanding of GAG-protein interactions and the role of sulfation in modulating physiological and disease states.

Experimental Procedures for Chapter 5

Conjugation of CS oligosaccharides to 1,2-(bisaminooxy)ethane for microarray production

Ozonolysis of the anomeric allyl group and linkage of CS compounds **73**, **79**, **85**, **88** and **92** to 1,2-(bisaminooxy)ethane **94**[36] proceeded as follows: oligosaccharide (0.51 μmol) was dissolved in MeOH (500 μL) and cooled to –78 °C. O_3 was bubbled through the reaction until a blue color persisted (1 min). The reaction was then purged with N_2 until colorless, quenched with Ph_3P beads (3 mg), and gradually warmed to rt over 12 h. Following filtration, the product was concentrated to afford the desired aldehyde as a white solid. The aldehyde (0.51 μmol) was then reacted for 14 h at rt with 1,2-(bisaminooxy)ethane hydrochloride (1.4 mg, 15 μmol) that had been dissolved in H_2O (100 μL) and pH adjusted to 5.0 with 1 M NaOH. The resulting oxime product was purified using a SepPak C18 column (500 mg, H_2O) and Sephadex G-10 (CS-E disaccharide, 5 g resin, H_2O) or Sephadex G-25 (tetrasaccharides, 5 g, resin, H_2O) to afford a white solid in quantitative yield (0.51 μmol). **CS-A aminooxy:** ESI MS: *m/z*: calcd for $C_{32}H_{48}N_4Na_3O_{31}S_2$: 1117.1; found 1117.0. **CS-C aminooxy:** ESI MS: *m/z*: calcd for $C_{32}H_{48}N_4Na_3O_{31}S_2$: 1117.1; found 1117.0. **CS-E aminooxy:** ESI MS: *m/z*: calcd for $C_{32}H_{46}N_4Na_5O_{37}S_4$: 1321.0; found 1321.0. **CS-E di amminooxy:** ESI MS: *m/z*: calcd for $C_{18}H_{28}N_3Na_2O_{20}S_2$: 716.1; found 716.0. **CS-R amminooxy:** ESI MS: *m/z*: calcd for $C_{32}H_{46}N_4Na_5O_{37}S_4$: 1321.0; found 1321.0. Mass spectra were obtained on a PerkinElmer/Sciex API 365 triple quadrupole/electrospray tandem mass spectrometer in the Protein/Peptide MicroAnalytical Laboratory at the California Institute of Technology.

The relative concentrations of the aminooxy oligosaccharides were calibrated to one another using the carbazole assay for uronic acid residues.[68] Briefly, the acid borate reagent (1.5 mL of 0.80 g sodium tetraborate, 16.6 mL H_2O, and 83.3 mL H_2SO_4) was added to 20-mL glass vials with Teflon caps. The aminooxy oligosaccharides (50 μL of a 0.2 mg/mL stock in H_2O) were added and the solution placed in a boiling H_2O bath for 10 min. Following addition of the carbazole reagent (50 μL of 0.1% *w/v* carbazole in 100% EtOH), the solution was boiled for 15 min. The absorbance was read at 530 nm and compared to a D-glucuronolactone standard in H_2O.

Aldehyde-coated carbohydrate microarrays

Solutions of the aminooxy oligosaccharides (in 300 mM NaH_2PO_4, pH 5.0, 10 μL/well in a 384-well plate) were arrayed on Hydrogel Aldehyde slides (NoAb Biodiscoveries) by using a Microgrid II arrayer (Biorobotics) to deliver sub-nanoliter volumes at rt and 50% humidity. Concentrations of carbohydrates ranged from 0 – 500 μM. The resulting arrays were incubated in a 70% humidity chamber at rt for 12 h and then stored in a low humidity, dust-free desiccator. The pH and reaction time were optimized to provide maximum immobilization of the compound. A pH screen with values between 4.0 and 9.0 (0.5 unit increments) showed that pH 5.0 yielded maximal binding to the slide and a time screen with values between 0 and 16 hours (4 h increments) showed that 12 h provided maximal immobilization. Non-specific attachment of CS oligosaccharides lacking the aminooxy linker (e.g., compounds **73**, **79**, **85**, **88** and **92**) was not observed. Prior to use, the arrays were outlined with a hydrophobic pen (Super Pap Pen, Research Products International) to create a boundary

for the protein treatments and rinsed three times with H_2O. The slides were then blocked by treatment with $NaBH_4$ (125 mg) in 140 mM NaCl, 2.7 mM KCl, 5.4 mM Na_2HPO_4, and 1.8 mM KH_2PO_4 (phosphate buffered saline, PBS, 50 mL) at rt for 5 min with gentle rocking and washed five times for 3 min with PBS. For all incubations, the slides were placed in a covered pipette tip box. Human BDNF, human GDNF, human midkine, human NGF, and human TNF-α (Peprotech); human FGF-1, -2, -4, -16, and -17, human EGF, human ephrin A1, human ephrin A5, human HB-EGF, rat Nogo-A-Fc (aa 544 – 725), human pleiotrophin, human TrkB (aa 31 – 397), and chicken netrin VI-V (aa 26 – 606, R&D Systems); human Adam-10 ECD-Fc, CXCL-16 ECD-Fc, DCC, DLAR-3 IgG-like domains-Fc, EphA3 ECD-Fc, EphB2 ECD-Fc, EphB4 ECD-Fc, MAG-Fc, Nogo-R-Fc, and Tie2-Fc (gifts of D.B. Nikolov, Memorial Sloan-Kettering Cancer Center; all reconstituted to 2 μM in 0.1% Triton X-100 in PBS), cell culture supernatant containing monoclonal anti-CS-A antibody (10G9-2B5), cell culture supernatant containing monoclonal anti-CS-C antibody (2D5-1D2) or cell culture supernatant containing monoclonal anti-CS-E antibody (2D11-2A10; all 1:1 in 0.1% Triton X-100 in PBS), were spotted onto the slides in 200 μL quantities, and incubated statically at rt for 2 h. The slides were then washed as previously described and incubated with the appropriate primary antibody [anti-BDNF (Santa Cruz); anti-GDNF, midkine, NGF, and TNF-α (Peprotech) or anti-FGF-1, -2, -4, -16, and -17, EGF, ephrin A1, ephrin A5, HB-EGF, pleiotrophin, TrkB, and netrin VI-V (R&D Systems); 1:1000 in 0.1% Triton X-100 in PBS] for 2 h at rt with gentle rocking. Following the incubation, the slides were washed as previously described and treated in the dark at rt with a secondary IgG antibody conjugated to Cy3 or Cy5 (Amersham; 1:5000 in 0.1% Triton X-100 in PBS) at rt for 1 h

with gentle rocking. The slides were washed three times for 2 min with PBS, two times for 1 min with H_2O, and dried under a gentle stream of N_2. Microarrays were analyzed at 532 nm (Cy3) or 635 nm (Cy5) using a GenePix 5000a scanner, and fluorescence quantification was performed using GenePix 6.0 software after correction for local background. Each protein was analyzed in triplicate, and the data represent an average of at least five spots for a given carbohydrate concentration. All solutions used for the carbohydrate microarrays were sterile-filtered through a 0.2 μm syringe filter prior to use.

Polylysine-coated carbohydrate microarrays

Solutions of oligosaccharides **73**, **79**, **85**, **88** and **92** (in ddH_2O, 10 μL/well in a 384-well plate) were arrayed on polylysine slides (Erie Scientific) by using a Microgrid II arrayer (Biorobotics) to deliver sub-nanoliter volumes at rt and 50% humidity. Concentrations of carbohydrates ranged from 0 – 500 μM. The resulting arrays were incubated in a 70% humidity chamber at rt for 12 h and then stored in a low humidity, dust-free dessicator. Prior to use, the arrays were outlined with a hydrophobic pen (Super Pap Pen, Research Products International) to create a boundary for the protein treatments. The slides were then blocked by treatment with 5% BSA in PBS at 37 °C for 1 h with gentle rocking. For all incubations, the slides were placed in a covered pipette tip box. Human midkine or human NGF (Peprotech; both reconstituted to 2 μM in 1% BSA in PBS) was spotted onto the slides in 200 μL quantities, and incubated statically at rt for 2 h. The slides were then washed 5 times for 3 min with PBS and incubated with the appropriate primary antibody [anti-midkine or anti-NGF (Peprotech); 1:1000 in 1% BSA in PBS] for 2 h at rt with gentle rocking. Following the incubation, the slides were washed as previously described and treated in the dark at rt with a secondary IgG

antibody conjugated to Cy3 (Amersham; 1:5000 in 1% BSA in PBS) at rt for 1 h with gentle rocking. The slides were washed three times for 2 min with PBS, two times for 1 min with H_2O, and dried under a gentle stream of N_2. Microarrays were analyzed at 532 nm using a GenePix 5000a scanner, and fluorescence quantification was performed using GenePix 6.0 software after correction for local background. Each protein was analyzed in triplicate, and the data represent an average of at least five spots for a given carbohydrate concentration. All solutions used for the carbohydrate microarrays were sterile-filtered through a 0.2 μm syringe filter prior to use.

References

1. Lamarre-Vincent, N. & Hsieh-Wilson, L.C. (2003). Dynamic glycosylation of the transcription factor CREB: a potential role in gene regulation. *J. Am. Chem. Soc.* **125**, 6612-6613.
2. Roth, J. (2002). Protein *N*-glycosylation along the secretory pathway: relationship to organelle topography and function, protein quality control, and cell interactions. *Chem. Rev.* **102**, 285-304.
3. Ritchie, G.E., Moffatt, B.E., Sim, R.B., Morgan, B.P., Dwek, R.A. & Rudd, P.M. (2002). Glycosylation and the complement system. *Chem. Rev.* **102**, 305-320.
4. Zachara, N.E. & Hart, G.W. (2002). The emerging significance of *O*-GlcNAc in cellular regulation. *Chem. Rev.* **102**, 431-438.
5. Bertozzi, C.R. & Kiessling, L.L. (2001). Chemical glycobiology. *Science* **291**, 2357-2364.
6. Ueoka, C., Kaneda, N., Okazaki, I., Nadanaka, S., Muramatsu, T. & Sugahara, K. (2000). Neuronal cell adhesion, mediated by the heparin-binding neuroregulatory factor midkine, is specifically inhibited by chondroitin sulfate E. Structural and functional implications of the over-sulfated chondroitin sulfate. *J. Biol. Chem.* **275**, 37407-37413.
7. Sugahara, K., Mikami, T., Uyama, T., Mizuguchi, S., Nomura, K. & Kitagawa, H. (2003). Recent advances in the structural biology of chondroitin sulfate and dermatan sulfate. *Curr. Op. Struct. Biol.* **13**, 612-620.
8. Iida, J., Pei, D., Kang, T., Simpson, M. A., Herlyn, M., Furcht, L. T. & McCarthy, J.B. (2001). Melanoma chondroitin sulfate proteoglycan regulates matrix

metalloproteinase-dependent human melanoma invasion into type I collagen. *J. Biol. Chem.* **276**, 18786-18794.

9. Bradbury, E. J., Moon, L. D. F., Popat, R. J., King, V. R., Bennett, G. S., Patel, P. N., Fawcett, J. W. & McMahon, S. B. (2002). Chondroitinase ABC promotes functional recovery after spinal cord injury. *Nature* **416**, 636-640.
10. Gama, C. I. & Hsieh-Wilson, L. C. (2005). Chemical approaches to deciphering the glycosaminoglycan code. *Curr. Op. Chem. Biol.* **9**, 609-619.
11. Taylor, K. R. & Gallo, R. L. (2006). Glycosaminoglycans and their proteoglycans: host-associated molecular patterns for initiation and modulation of inflammation. *FASEB J.* **20**, 9-22.
12. Feizi, T. (2000). Progress in deciphering the information content of the 'glycome' – a crescendo in the closing years of the millennium. *Glycoconj. J.* **17**, 553-565.
13. Fujikawa, S., Ohmae, M. & Kobayashi, S. (2005). Enzymatic synthesis of chondroitin 4-sulfate with well-defined structure. *Biomacromolecules* **6**, 2935-2942.
14. Peracaula, R., Tabares, G., Royle, L., Harvey, D.J., Dwek, R.A., Rudd, P.M. & de Llorens, R. (2003). Altered glycosylation pattern allows the distinction between prostate-specific antigen (PSA) from normal and tumor origins. *Glycobiology* **13**, 457-470.
15. Feizi, T., Fazio, F., Chai, W. & Wong, C.H. (2003). Carbohydrate microarrays – a new set of technologies at the frontiers of glycomics. *Curr. Op. Struct. Biol.* **13**, 637-645.

16. Shin, I., Sungjin, P. & Lee, M. (2005). Carbohydrate microarrays: an advanced technology for functional studies of glycans. *Chem. Eur. J.* **11**, 2894-2901.

17. DeRisi, J.L., Lyer, V.R. & Brown, P.O. (1997). Exploring the metabolic and genetic control of gene expression on a genomic scale. *Science* **278**, 680-686.

18. MacBeath, G. & Schreiber, S.L. (2000). Printing proteins as microarrays for high-throughput function determination. *Science* **289**, 1760-1763.

19. Shao, M.C. (1992). The use of streptavidin-biotinylglycans as a tool for characterization of oligosaccharide-binding specificity of lectin. *Anal. Biochem.* **205**, 77-82.

20. Shinohara, Y., Sota, H., Gotoh, M., Hasebe, M., Tosu, M., Nakao, J., Hasegawa, Y. & Shiga, M. (1996). Bifunctional labeling reagent for oligosaccharides to incorporate both chromophore and biotin groups. *Anal. Biochem.* **68**, 2573-2579.

21. Green, R.J., Frazier, R.A., Shakesheff, K.M., Davies, M.C., Roberts, C.J. & Tendler, S.J.B. (2000). Surface plasmon resonance analysis of dynamic biological interactions with biomaterials. *Biomaterials* **21**, 1823-1835.

22. Wang, D., Liu, S., Trummer, B.J., Deng, C. & Wang, A. (2002). Carbohydrate microarrays for the recognition of cross-reactive molecular markers of microbes and host cells. *Nat. Biotechnol.* **20**, 275-281.

23. Willats, W.G., Rasmussen, S.E., Kristensen, T., Mikkelsen, J.D. & Knox, J.P. (2002). Sugar-coated microarrays: a novel slide surface for the high-throughput analysis of glycans. *Proteomics* **2**, 1666-1671.

24. Fukui, S., Feizi, T., Galustian, C., Lawson, A.M. & Chai, W. (2002). Oligosaccharide microarrays for high-throughput detection and specificity assignments of carbohydrate-protein interactions. *Nat. Biotechnol.* **20**, 1011-1017.
25. Ko, K.S., Jaipuri, F.A. & Pohl, N.L. (2005). Fluorous-based carbohydrate microarrays. *J. Am. Chem. Soc.* **127**, 13162-13163.
26. Fazio, F., Bryan, M.C., Blixt, O., Paulson, J.C. & Wong, C.H. (2002). Synthesis of sugar arrays in microtiter plates. *J. Am. Chem. Soc.* **124**, 14397-14402.
27. Houseman, B.T. & Mrksich, M. (2002). Carbohydrate arrays for the evaluation of protein binding and enzymatic modification. *Chem. Biol.* **9**, 443-454.
28. Park, S. & Shin, I. (2002). Fabrication of carbohydrate chips for studying protein-carbohydrate interactions. *Angew. Chem. Int. Ed. Engl.* **41**, 3180-3182.
29. Ratner, D.M., Adams, E.W., Disney, M.D. & Seeberger, P.H. (2004). Tools for glycomics: mapping interactions of carbohydrates in biological systems. *ChemBioChem* **5**, 1375-1383.
30. Lee, M. & Shin, I. (2005). Facile preparation of carbohydrate microarrays by site-specific, covalent immobilization of unmodified carbohydrates on hydrazide-coated glass slides. *Org. Lett.* **7**, 4269-4272.
31. Blixt, O., Head, S., Mondala, T., Scanlan, C., Huflejt, M.E., Alvarez, R., Bryan, M.C., Fazio, F., Calarese, D., Stevens, J., Razi, N., Stevens, D.J., Skehel, J.J., van Die, I., Burton, D.R., Wilson, I.A., Cummings, R., Bovin, N., Wong, C.H. & Paulson, J.C. (2004). Printed covalent glycan array for ligand profiling of diverse glycan binding proteins. *Proc. Natl. Acad. Sci. USA* **101**, 17033-17038.

32. de Paz, J.L., Noti, C. & Seeberger, P.H. (2006). Microarrays of synthetic heparin oligosaccharides. *J. Am. Chem. Soc.* **128**, 2766-2767.

33. Sugahara, K. & Yamada, S. (2000). Structure and function of oversulfated chondroitin sulfate variants: unique sulfation patterns and neuroregulatory activities. *Trends Glycosci. Glycotech.* **12**, 321-349.

34. Deepa, S.S., Umehara, Y., Higashiyama, S., Itoh, N. & Sugahara, K. (2002). Specific molecular interactions of oversulfated chondroitin sulfate E with various heparin-binding growth factors. Implications as a physiological binding partner in the brain and other tissues. *J. Biol. Chem.* **277**, 43707-43716.

35. He, X. & Garcia, K.C. (2004). Structure of nerve growth factor complexed with the shared neurotrophin receptor p75. *Science* **304**, 870-875.

36. Shirayev, A., Thoo lin, P.K. & Moiseev, I.K. (1997). Synthesis of novel adamantylalkoxyurea derivatives from 2-(1-adamantylimino)-1,3-oxathiolane. *Synthesis* **1**, 38-40.

37. Khidekel, N., Arndt, S., Lamarre-Vincent, N., Lippert, A., Poulin-Kerstien, K.G., Ramakrishnan, B., Qasba, P.K. & Hsieh-Wilson, L.C. (2003). A chemoenzymatic approach toward the rapid and sensitive detection of *O*-GlcNAc posttranslational modifications. *J. Am. Chem. Soc.* **125**, 16162-16163.

38. Salisbury, C.M., Maly, D.J. & Ellman, J.A. (2002). Peptide microarrays for the determination of protease substrate specificity. *J. Am. Chem. Soc.* **124**, 14868-14870.

39. Kadomatsu, K., Tomomura, M. & Muramatsu, T. (1998). cDNA cloning and sequencing of a new gene intensely expressed in early differentiation stages of

embryonal carcinoma cells and in mid-gestation period of mouse embryogenesis. *Biochem. Biophys. Res. Commun.* **151**, 1312-1318.

40. Kaneda, N., Talukder, A.H., Nishiyama, H., Koizumi, S. & Muramatsu, T. (1996). Midkine, a heparin-binding growth/differentiation factor, exhibits nerve cell adhesion and guidance activity for neurite outgrowth *in vitro*. *J. Biochem.* **119**, 1150-1156.
41. Zou, K., Muramatsu, H., Ikematsu, S., Sakuma, S., Salama, R.H., Shinomura, T., Kimata, K. & Muramatsu, T. (2000). A heparin-binding growth factor, midkine, binds to a chondroitin sulfate proteoglycan, PG-M/versican. *Eur. J. Biochem.* **267**, 4046-4053.
42. Maeda, N., Nishiwaki, T., Shintani, T., Hamanaka, H. & Noda, M. (1996). 6B4 proteoglycan/phosphacan, an extracellular variant of receptor-like protein-tyrosine phosphatase zeta/RPTPbeta, binds pleiotrophin/heparin-binding growth-associated molecule (HB-GAM). *J. Biol. Chem.* **271**, 21446-21452.
43. Milev, P., Monnerie, H., Popp, S., Margolis, R.K. & Margolis, R.U. (1998). The core protein of the chondroitin sulfate proteoglycan phosphacan is a high-affinity ligand of fibroblast growth factor-2 and potentiates its mitogenic activity. *J. Biol. Chem.* **273**, 21439-21442.
44. Shuo, T., Aono, S., Matsui, F., Tokita, Y., Maeda, H., Shimada, K. & Oohira, A. (2004). Developmental changes in the biochemical and immunological characters of the carbohydrate moiety of neuroglycan C, a brain-specific chondroitin sulfate proteoglycan. *Glycoconj. J.* **20**, 267-278.

45. Herndon, M.E., Stipp, C.S. & Lander, A.D. (1999). Interactions of neural glycosaminoglycans and proteoglycans with protein ligands: assessment of selectivity, heterogeneity and the participation of core proteins in binding. *Glycobiology* **9**, 143-155.

46. Lander, A.D. (1993). Proteoglycans in the nervous system. *Curr. Opin. Neurobiol.* **3**, 716-723.

47. Ornitz, D.M. & Itoh, N. (2001). Fibroblast growth factors. *Genome Biol.* **2**, 1-12.

48. Danilenko, D.M., Montestruque, S., Philo, J.S., Li, T., Hill, D., Speakman, J., Bahru, M., Zhang, M., Konishi, M., Itoh, N., Chirica, M., Delaney, J., Hernday, N., Martin, F., Hara, S., Talvenheimo, J., Narhi, L.O. & Arakawa, T. (1999). Recombinant rat fibroblast growth factor-16: structure and biological activity. *Arch. Biochem. Biophys.* **361**, 34-46.

49. Farkas, L.M. & Krieglstein, K. (2002). Heparin-binding epidermal growth factor-like growth factor (HB-EGF) regulates survival of midbrain dopaminergic neurons. *J. Neural. Transm.* **109**, 267-277.

50. Xian, C.J. & Zhou, X.F. (1999). EGF family of growth factors: essential roles and functional redundancy in the nerve system. *Mol. Neurobiol.* **20**, 157-183.

51. Huang, E.J. & Reichardt, L.F. (2001). Neurotrophins: roles in neuronal development and function. *Annu. Rev. Neurosci.* **24**, 677-736.

52. Schlessinger, J., Plotnikov, A.N., Ibrahimi, O.A., Eliseenkova, A.V., Yeh, B.K., Yayon, A., Linhardt, R.J. & Mohammadi, M. (2000). Crystal structure of a ternary FGF-FGFR-heparin complex reveals a dual role for heparin in FGFR binding and dimerization. *Molecular Cell* **6**, 743–750.

53. Pellegrini, L., Burke, D.F., Delft, F.V., Mulloy, B. & Blundell, T.L. (2000). Crystal structure of fibroblast growth factor receptor ectodomain bound to ligand and heparin. *Nature* **407**, 1029–1034.

54. Wu. Z.L., Zhang, L., Yabe, T., Kuberan, B., Beeler, D.L., Love, A. & Rosenberg, R.D. (2003). The involvement of heparan sulfate (HS) in FGF1/HS/FGFR1 signaling complex. *J. Biol. Chem.* **278**, 17121–17129.

55. Sun, M., Kong, L., Wang, X., Lu, X., Gao, Q. & Geller, A.I. (2005). Comparison of the capability of GDNF, BDNF, or both, to protect nigrostriatal neurons in a rat model of Parkinson's disease. *Brain Res.* **1052**, 119-129.

56. Deshpande, D., Kim, Y.S., Martinez, T., Carmen, J., Dike, S., Shats, I., Rubin, L., Drummond, J., Krishnan, C., Hoke, A., Maragakis, N., Shefner, J., Rothstein, J. & Kerr, D. (2006). Recovery from paralysis in adult rats using embryonic stem cells. *Ann. Neurol.* **60**, 22-34.

57. Liu, B.P., Fournier, A., GrandPre, T. & Strittmatter, S.M. (2002). Myelin-associated glycoprotein as a functional ligand for the Nogo-66 receptor. *Science* **297**, 1190-1193.

58. Richard, M., Giannetti, N., Saucier, D., Sacquet, J., Jourdan, F. & Pellier-Monnin, V. (2005). Neuronal expression of Nogo-A mRNA and protein during neurite outgrowth in the developing rat olfactory system. *Eur. J. Neurosci.* **22**, 2145-2158.

59. Raza, A. (2000). Anti-TNF therapies in rheumatoid arthritis, Crohn's disease, sepsis, and myelodysplastic syndromes. *Micro. Res. Tech.* **50**, 229-235.

60. Feldmann, M. & Maini, R.N. (2001). Anti-TNF alpha therapy of rheumatoid arthritis: what have we learned? *Annu. Rev. Immunol.* **19**, 163-196.

61. Palladino, M.A., Bahjat, F.R., Theodorakis, E.A. & Moldawer, L.L. (2003). Anti-TNF-alpha therapies: the next generation. *Nat. Rev. Drug Disc.* **2**, 736-746.

62. Bernfield, M., Gotte, M., Park, P.W., Reizes, O., Fitzgerald, M.L., Lincecum, J. & Zako, M. (1999). Functions of cell surface heparan sulfate proteoglycans. *Ann. Rev. Biochem.* **68**, 729-777.

63. Koprivica, V., Cho, K.S., Park, J.B., Yiu, G., Atwal, J., Gore, B., Kim, J.A., Lin, E., Tessier-Lavigne, M., Chen, D.F. & He, Z. (2005). EGFR activation mediates inhibition of axon regeneration by myelin and chondroitin sulfate proteoglycans. *Science* **310**, 106-110.

64. Yu, T.W. & Bargmann, C.I. (2001). Dynamic regulation of axon guidance. *Nat. Neurosci.* **4**, 1169-1176.

65. Abel, S., Hundhausen, C., Mentlein, R., Schulte, A., Berkhout, T.A., Broadway, N., Hartmann, D., Sedlacek, R., Dietrich, S., Muetze, B., Schuster, B., Kallen, K.J., Saftig, P., Rose-John, S. & Ludwig, A. (2004). The transmembrane CXC-chemokine ligand 16 is induced by IFN-γ and TNF-α and shed by the activity of the disintegrin-like metalloproteinase ADAM10. *J. Immunol.* **172**, 6362-6372.

66. Fox, A.N. & Zinn, K. (2005). The heparan sulfate proteoglycan syndecan is an *in vivo* ligand for the *Drosophila* LAR receptor tyrosine phosphatase. *Curr. Biol.* **15**, 1701-1711.

67. Xu, Y., Liu, Y. & Yu, Q. (2004). Angiopoietin-3 is tethered on the cell surface via heparan sulfate proteoglycans. *J. Biol. Chem.* **279**, 41179-41188.

68. Taylor, K.A. & Buchanan-Smith, J.G. (1992). A colorimetric method for the quantitation of uronic acids and a specific assay for galacturonic acid. *Anal. Biochem.* **201**, 190-196.

Appendix for Chapter 5: Keys for the Microarray Grids of Chapter 5 and Binding Curve Data for Midkine and BDNF

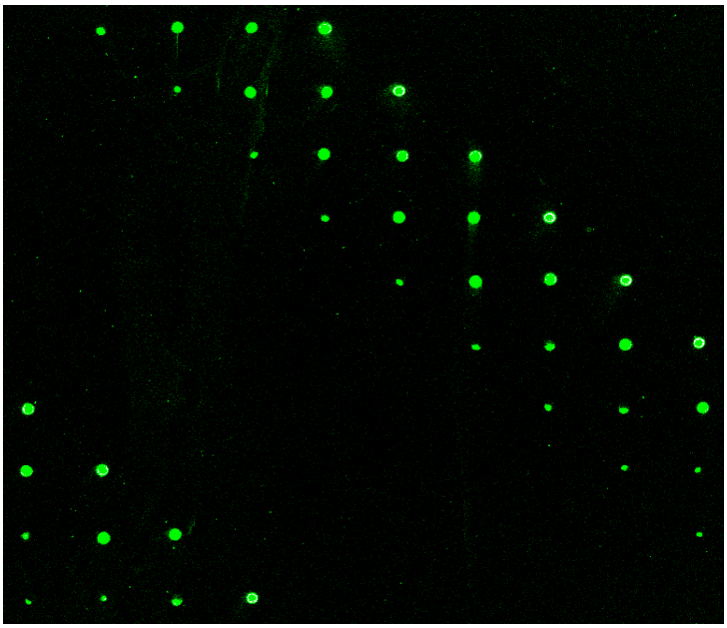

25E	5A	15A	25A	50A	70Di	200Di	0E	75E	12.5Di
12.5Di	22.5E	5A	15A	25A	50A	70Di	200Di	0E	7.5E
7.5 E	12.5Di	22.5E	5A	15A	25A	50A	70Di	200Di	0E
0E	7.5E	12.5Di	22.5E	5A	15A	25A	50A	70Di	200Di
200Di	0E	7.5E	12.5Di	22.5E	5A	15A	25A	50A	70Di
70Di	200Di	0E	7.5E	12.5Di	22.5E	5A	15A	25A	50A
50A	70Di	200Di	0E	7.5E	12.5Di	22.5E	5A	15A	25A
25A	50A	70Di	200Di	0E	7.5E	12.5Di	22.5E	5A	15A
15A	25A	50A	70Di	200Di	0E	7.5E	12.5Di	22.5E	5A
5A	15A	25A	50A	70Di	200Di	0E	7.5E	12.5Di	22.5E

Figure A5.1: Representative portion of the microarrays illustrating spot morphology and fluorescence intensity after incubation with anti-CS-A antibody 10G9-2B5. The panel below indicates the corresponding oligosaccharides and their concentrations for each spot shown. Values are in µM. A = CS-A tetrasaccharide, C = CS-C tetrasaccharide, Di = CS-E disaccharide, E = CS-E tetrasaccharide, R = CS-R tetrasaccharide. Each microarray contained 1500 spots.

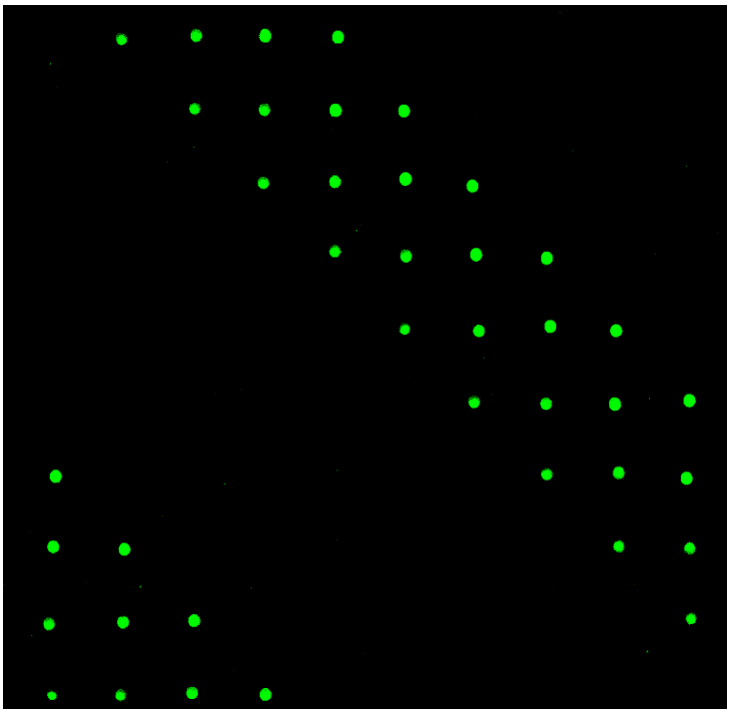

Blank	15C	25C	50C	90C	200E	0R	7.5R	17.5R	70R
70R	Blank	15C	25C	50C	90C	200E	0R	7.5R	17.5R
17.5R	70R	Blank	15C	25C	50C	90C	200E	0R	7.5R
7.5R	17.5R	70R	Blank	15C	25C	50C	90C	200E	0R
0R	7.5R	17.5R	70R	Blank	15C	25C	50C	90C	200E
200E	0R	7.5R	17.5R	70R	Blank	15C	25C	50C	90C
90C	200E	0R	7.5R	17.5R	70R	Blank	15C	25C	50C
50C	90C	200E	0R	7.5R	17.5R	70R	Blank	15C	25C
25C	50C	90C	200E	0R	7.5R	17.5R	70R	Blank	15C
15C	25C	50C	90C	200E	0R	7.5R	17.5R	70R	Blank

Figure A5.2: Representative portion of the microarrays illustrating spot morphology and fluorescence intensity after incubation with anti-CS-C antibody 2D5-1D2. The panel below indicates the corresponding oligosaccharides and their concentrations for each spot shown. Values are in μM. A = CS-A tetrasaccharide, C = CS-C tetrasaccharide, Di = CS-E disaccharide, E = CS-E tetrasaccharide, R = CS-R tetrasaccharide. Each microarray contained 1500 spots.

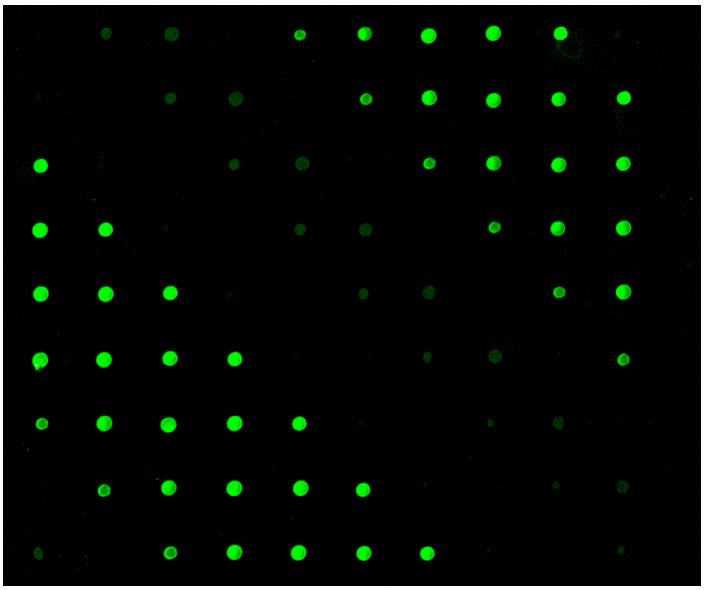

90A	400A	2.5C	12.5E	17.5E	30E	60E	100E	Blank
Blank	90A	400A	2.5C	12.5E	17.5E	30E	60E	100E
40A	Blank	90A	400A	2.5C	12.5E	17.5E	30E	60E
100E	40A	Blank	90A	400A	2.5C	12.5E	17.5E	30E
60E	100E	40A	Blank	90A	400A	2.5C	12.5E	17.5E
30E	60E	100E	40A	Blank	90A	400A	2.5C	12.5E
17.5E	30E	60E	100E	40A	Blank	90A	400A	2.5C
12.5E	17.5E	30E	60E	100E	40A	Blank	90A	400A
2.5C	12.5E	17.5E	30E	60E	100E	40A	Blank	90A
400A	2.5C	12.5E	17.5E	30E	60E	100E	40A	Blank

Figure A5.3: Representative portion of the microarrays illustrating spot morphology and fluorescence intensity after incubation with anti-CS-E antibody 2D11-2A10. The panel below indicates the corresponding oligosaccharides and their concentrations for each spot shown. Values are in µM. A = CS-A tetrasaccharide, C = CS-C tetrasaccharide, Di = CS-E disaccharide, E = CS-E tetrasaccharide, R = CS-R tetrasaccharide. Each microarray contained 1500 spots.

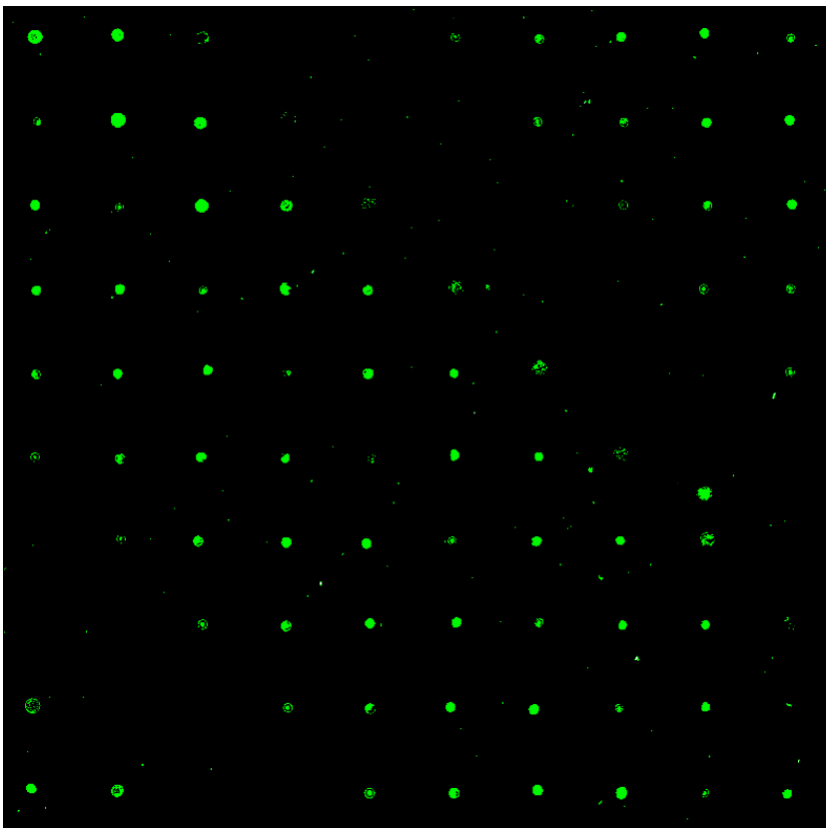

60R	70A	200A	0C	7.5C	12.5E	22.5E	40E	80E	30R
30R	60R	70A	200A	0C	7.5C	12.5E	22.5E	40E	80E
80E	30R	60R	70A	200A	0C	7.5C	12.5E	22.5E	40E
40E	80E	30R	60R	70A	200A	0C	7.5C	12.5E	22.5E
22.5E	40E	80E	30R	60R	70A	200A	0C	7.5C	12.5E
12.5E	22.5E	40E	80E	30R	60R	70A	200A	0C	7.5C
7.5C	12.5E	22.5E	40E	80E	30R	60R	70A	200A	0C
0C	7.5C	12.5E	22.5E	40E	80E	30R	60R	70A	200A
200A	0C	7.5C	12.5E	22.5E	40E	80E	30R	60R	70A
70A	200A	0C	7.5C	12.5E	22.5E	40E	80E	30R	60R

Figure A5.4: Representative portion of the microarrays illustrating spot morphology and fluorescence intensity after incubation with midkine. The panel below indicates the corresponding oligosaccharides and their concentrations for each spot shown. Values are in µM. A = CS-A tetrasaccharide, C = CS-C tetrasaccharide, Di = CS-E disaccharide, E = CS-E tetrasaccharide, R = CS-R tetrasaccharide. Each microarray contained 1500 spots.

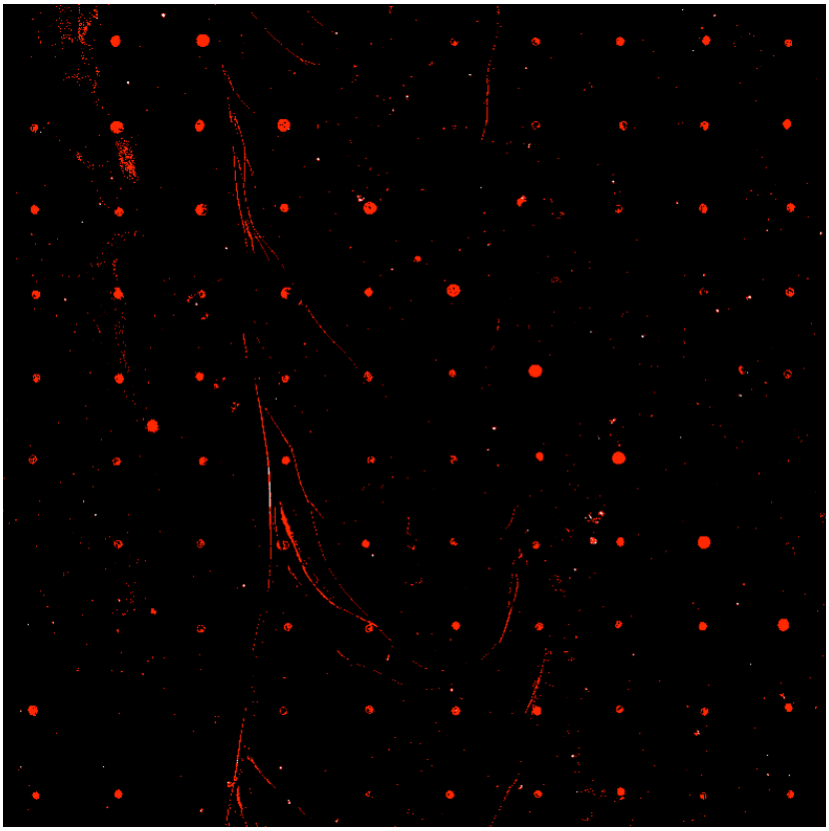

60R	70A	200A	0C	7.5C	12.5E	22.5E	40E	80E	30R
30R	60R	70A	200A	0C	7.5C	12.5E	22.5E	40E	80E
80E	30R	60R	70A	200A	0C	7.5C	12.5E	22.5E	40E
40E	80E	30R	60R	70A	200A	0C	7.5C	12.5E	22.5E
22.5E	40E	80E	30R	60R	70A	200A	0C	7.5C	12.5E
12.5E	22.5E	40E	80E	30R	60R	70A	200A	0C	7.5C
7.5C	12.5E	22.5E	40E	80E	30R	60R	70A	200A	0C
0C	7.5C	12.5E	22.5E	40E	80E	30R	60R	70A	200A
200A	0C	7.5C	12.5E	22.5E	40E	80E	30R	60R	70A
70A	200A	0C	7.5C	12.5E	22.5E	40E	80E	30R	60R

Figure A5.5: Representative portion of the microarrays illustrating spot morphology and fluorescence intensity after incubation with pleiotrophin. The panel below indicates the corresponding oligosaccharides and their concentrations for each spot shown. Values are in μM. A = CS-A tetrasaccharide, C = CS-C tetrasaccharide, Di = CS-E disaccharide, E = CS-E tetrasaccharide, R = CS-R tetrasaccharide. Each microarray contained 1500 spots.

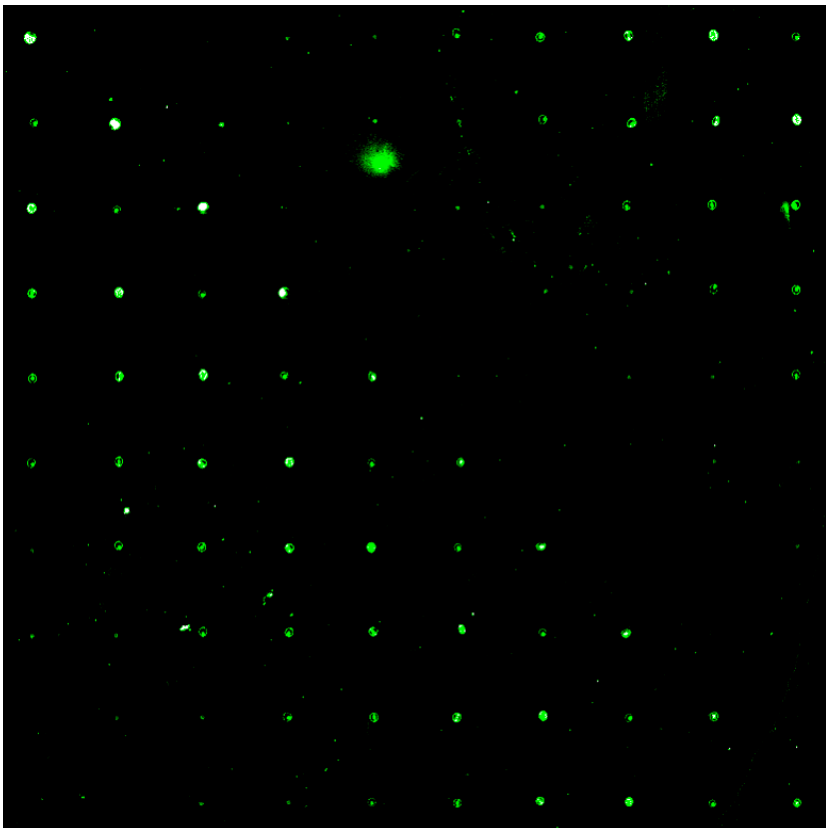

60R	70A	200A	0C	7.5C	12.5E	22.5E	40E	80E	30R
30R	60R	70A	200A	0C	7.5C	12.5E	22.5E	40E	80E
80E	30R	60R	70A	200A	0C	7.5C	12.5E	22.5E	40E
40E	80E	30R	60R	70A	200A	0C	7.5C	12.5E	22.5E
22.5E	40E	80E	30R	60R	70A	200A	0C	7.5C	12.5E
12.5E	22.5E	40E	80E	30R	60R	70A	200A	0C	7.5C
7.5C	12.5E	22.5E	40E	80E	30R	60R	70A	200A	0C
0C	7.5C	12.5E	22.5E	40E	80E	30R	60R	70A	200A
200A	0C	7.5C	12.5E	22.5E	40E	80E	30R	60R	70A
70A	200A	0C	7.5C	12.5E	22.5E	40E	80E	30R	60R

Figure A5.6: Representative portion of the microarrays illustrating spot morphology and fluorescence intensity after incubation with FGF-16. The panel below indicates the corresponding oligosaccharides and their concentrations for each spot shown. Values are in μM. A = CS-A tetrasaccharide, C = CS-C tetrasaccharide, Di = CS-E disaccharide, E = CS-E tetrasaccharide, R = CS-R tetrasaccharide. Each microarray contained 1500 spots.

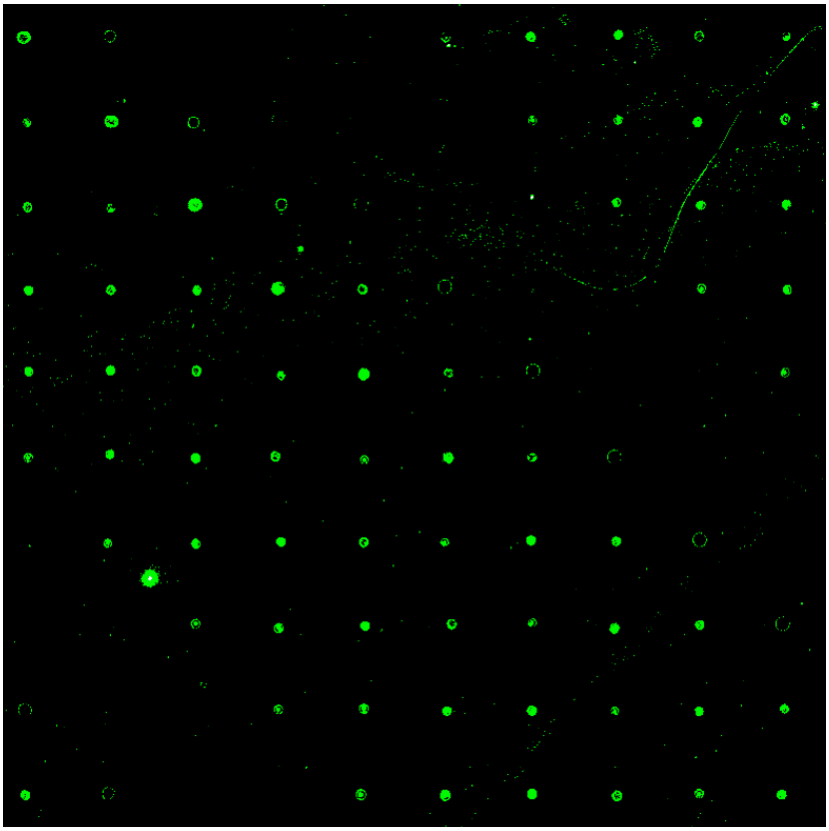

60R	70A	200A	0C	7.5C	12.5E	22.5E	40E	80E	30R
30R	60R	70A	200A	0C	7.5C	12.5E	22.5E	40E	80E
80E	30R	60R	70A	200A	0C	7.5C	12.5E	22.5E	40E
40E	80E	30R	60R	70A	200A	0C	7.5C	12.5E	22.5E
22.5E	40E	80E	30R	60R	70A	200A	0C	7.5C	12.5E
12.5E	22.5E	40E	80E	30R	60R	70A	200A	0C	7.5C
7.5C	12.5E	22.5E	40E	80E	30R	60R	70A	200A	0C
0C	7.5C	12.5E	22.5E	40E	80E	30R	60R	70A	200A
200A	0C	7.5C	12.5E	22.5E	40E	80E	30R	60R	70A
70A	200A	0C	7.5C	12.5E	22.5E	40E	80E	30R	60R

Figure A5.7: Representative portion of the microarrays illustrating spot morphology and fluorescence intensity after incubation with BDNF. The panel below indicates the corresponding oligosaccharides and their concentrations for each spot shown. Values are in μM. A = CS-A tetrasaccharide, C = CS-C tetrasaccharide, Di = CS-E disaccharide, E = CS-E tetrasaccharide, R = CS-R tetrasaccharide. Each microarray contained 1500 spots.

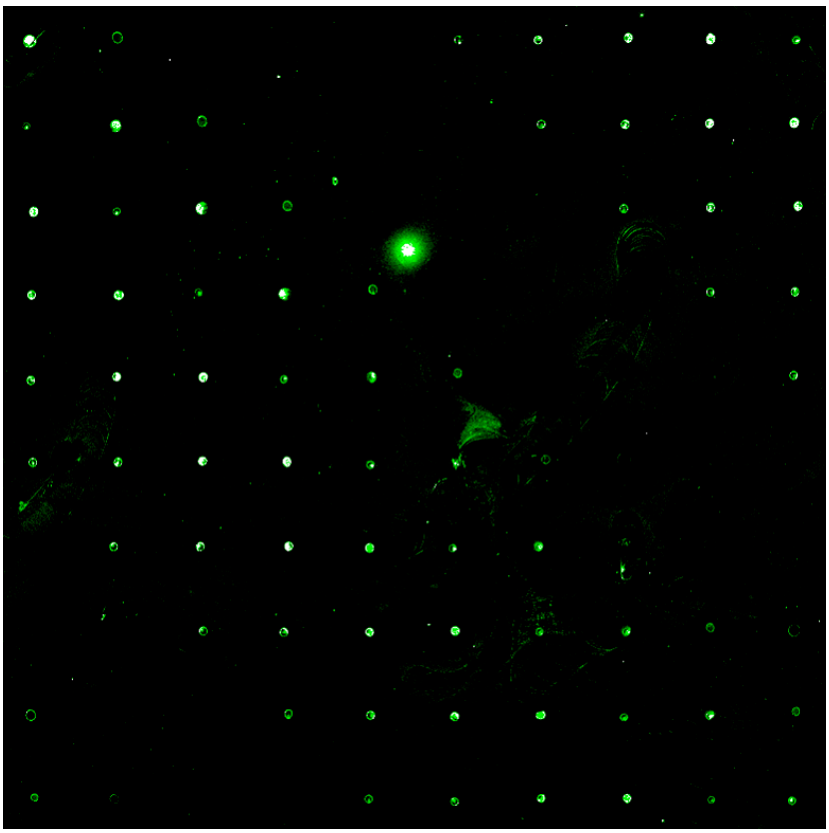

60R	70A	200A	0C	7.5C	12.5E	22.5E	40E	80E	30R
30R	60R	70A	200A	0C	7.5C	12.5E	22.5E	40E	80E
80E	30R	60R	70A	200A	0C	7.5C	12.5E	22.5E	40E
40E	80E	30R	60R	70A	200A	0C	7.5C	12.5E	22.5E
22.5E	40E	80E	30R	60R	70A	200A	0C	7.5C	12.5E
12.5E	22.5E	40E	80E	30R	60R	70A	200A	0C	7.5C
7.5C	12.5E	22.5E	40E	80E	30R	60R	70A	200A	0C
0C	7.5C	12.5E	22.5E	40E	80E	30R	60R	70A	200A
200A	0C	7.5C	12.5E	22.5E	40E	80E	30R	60R	70A
70A	200A	0C	7.5C	12.5E	22.5E	40E	80E	30R	60R

Figure A5.8: Representative portion of the microarrays illustrating spot morphology and fluorescence intensity after incubation with NGF. The panel below indicates the corresponding oligosaccharides and their concentrations for each spot shown. Values are in μM. A = CS-A tetrasaccharide, C = CS-C tetrasaccharide, Di = CS-E disaccharide, E = CS-E tetrasaccharide, R = CS-R tetrasaccharide. Each microarray contained 1500 spots.

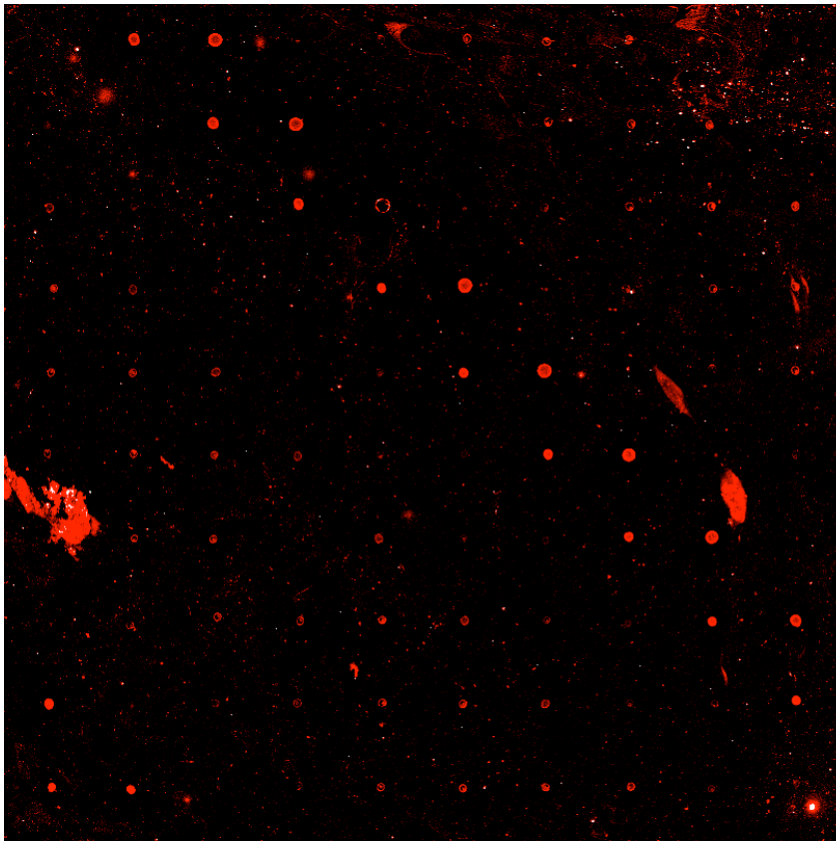

60R	70A	200A	0C	7.5C	12.5E	22.5E	40E	80E	30R
30R	60R	70A	200A	0C	7.5C	12.5E	22.5E	40E	80E
80E	30R	60R	70A	200A	0C	7.5C	12.5E	22.5E	40E
40E	80E	30R	60R	70A	200A	0C	7.5C	12.5E	22.5E
22.5E	40E	80E	30R	60R	70A	200A	0C	7.5C	12.5E
12.5E	22.5E	40E	80E	30R	60R	70A	200A	0C	7.5C
7.5C	12.5E	22.5E	40E	80E	30R	60R	70A	200A	0C
0C	7.5C	12.5E	22.5E	40E	80E	30R	60R	70A	200A
200A	0C	7.5C	12.5E	22.5E	40E	80E	30R	60R	70A
70A	200A	0C	7.5C	12.5E	22.5E	40E	80E	30R	60R

Figure A5.9: Representative portion of the microarrays illustrating spot morphology and fluorescence intensity after incubation with TrkB. The panel below indicates the corresponding oligosaccharides and their concentrations for each spot shown. Values are in µM. A = CS-A tetrasaccharide, C = CS-C tetrasaccharide, Di = CS-E disaccharide, E = CS-E tetrasaccharide, R = CS-R tetrasaccharide. Each microarray contained 1500 spots.

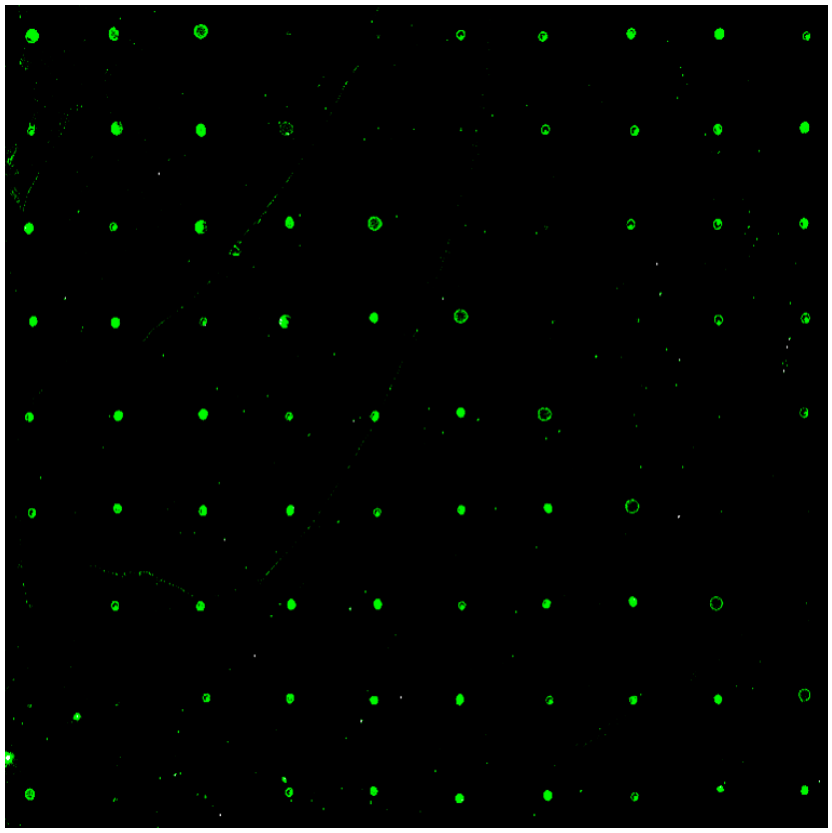

60R	70A	200A	0C	7.5C	12.5E	22.5E	40E	80E	30R
30R	60R	70A	200A	0C	7.5C	12.5E	22.5E	40E	80E
80E	30R	60R	70A	200A	0C	7.5C	12.5E	22.5E	40E
40E	80E	30R	60R	70A	200A	0C	7.5C	12.5E	22.5E
22.5E	40E	80E	30R	60R	70A	200A	0C	7.5C	12.5E
12.5E	22.5E	40E	80E	30R	60R	70A	200A	0C	7.5C
7.5C	12.5E	22.5E	40E	80E	30R	60R	70A	200A	0C
0C	7.5C	12.5E	22.5E	40E	80E	30R	60R	70A	200A
200A	0C	7.5C	12.5E	22.5E	40E	80E	30R	60R	70A
70A	200A	0C	7.5C	12.5E	22.5E	40E	80E	30R	60R

Figure A5.10: Representative portion of the microarrays illustrating spot morphology and fluorescence intensity after incubation with GDNF. The panel below indicates the corresponding oligosaccharides and their concentrations for each spot shown. Values are in μM. A = CS-A tetrasaccharide, C = CS-C tetrasaccharide, Di = CS-E disaccharide, E = CS-E tetrasaccharide, R = CS-R tetrasaccharide. Each microarray contained 1500 spots.

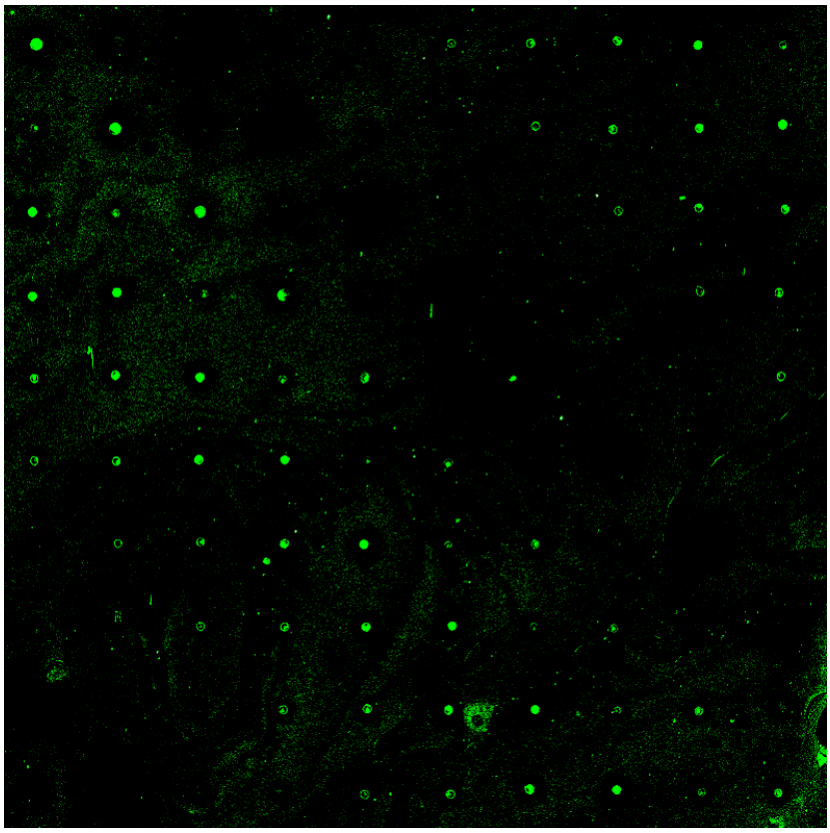

60R	70A	200A	0C	7.5C	12.5E	22.5E	40E	80E	30R
30R	60R	70A	200A	0C	7.5C	12.5E	22.5E	40E	80E
80E	30R	60R	70A	200A	0C	7.5C	12.5E	22.5E	40E
40E	80E	30R	60R	70A	200A	0C	7.5C	12.5E	22.5E
22.5E	40E	80E	30R	60R	70A	200A	0C	7.5C	12.5E
12.5E	22.5E	40E	80E	30R	60R	70A	200A	0C	7.5C
7.5C	12.5E	22.5E	40E	80E	30R	60R	70A	200A	0C
0C	7.5C	12.5E	22.5E	40E	80E	30R	60R	70A	200A
200A	0C	7.5C	12.5E	22.5E	40E	80E	30R	60R	70A
70A	200A	0C	7.5C	12.5E	22.5E	40E	80E	30R	60R

Figure A5.11: Representative portion of the microarrays illustrating spot morphology and fluorescence intensity after incubation with Nogo-A. The panel below indicates the corresponding oligosaccharides and their concentrations for each spot shown. Values are in μM. A = CS-A tetrasaccharide, C = CS-C tetrasaccharide, Di = CS-E disaccharide, E = CS-E tetrasaccharide, R = CS-R tetrasaccharide. Each microarray contained 1500 spots.

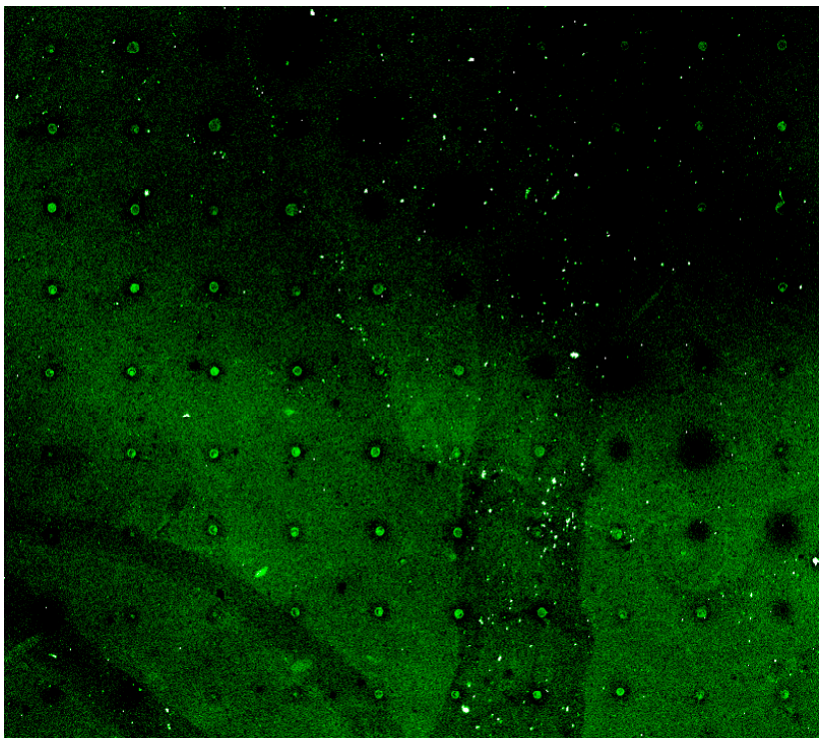

60R	70A	200A	0C	7.5C	12.5E	22.5E	40E	80E	30R
30R	60R	70A	200A	0C	7.5C	12.5E	22.5E	40E	80E
80E	30R	60R	70A	200A	0C	7.5C	12.5E	22.5E	40E
40E	80E	30R	60R	70A	200A	0C	7.5C	12.5E	22.5E
22.5E	40E	80E	30R	60R	70A	200A	0C	7.5C	12.5E
12.5E	22.5E	40E	80E	30R	60R	70A	200A	0C	7.5C
7.5C	12.5E	22.5E	40E	80E	30R	60R	70A	200A	0C
0C	7.5C	12.5E	22.5E	40E	80E	30R	60R	70A	200A
200A	0C	7.5C	12.5E	22.5E	40E	80E	30R	60R	70A
70A	200A	0C	7.5C	12.5E	22.5E	40E	80E	30R	60R

Figure A5.12: Representative portion of the microarrays illustrating spot morphology and fluorescence intensity after incubation with Nogo-R. The panel below indicates the corresponding oligosaccharides and their concentrations for each spot shown. Values are in μM. A = CS-A tetrasaccharide, C = CS-C tetrasaccharide, Di = CS-E disaccharide, E = CS-E tetrasaccharide, R = CS-R tetrasaccharide. Each microarray contained 1500 spots.

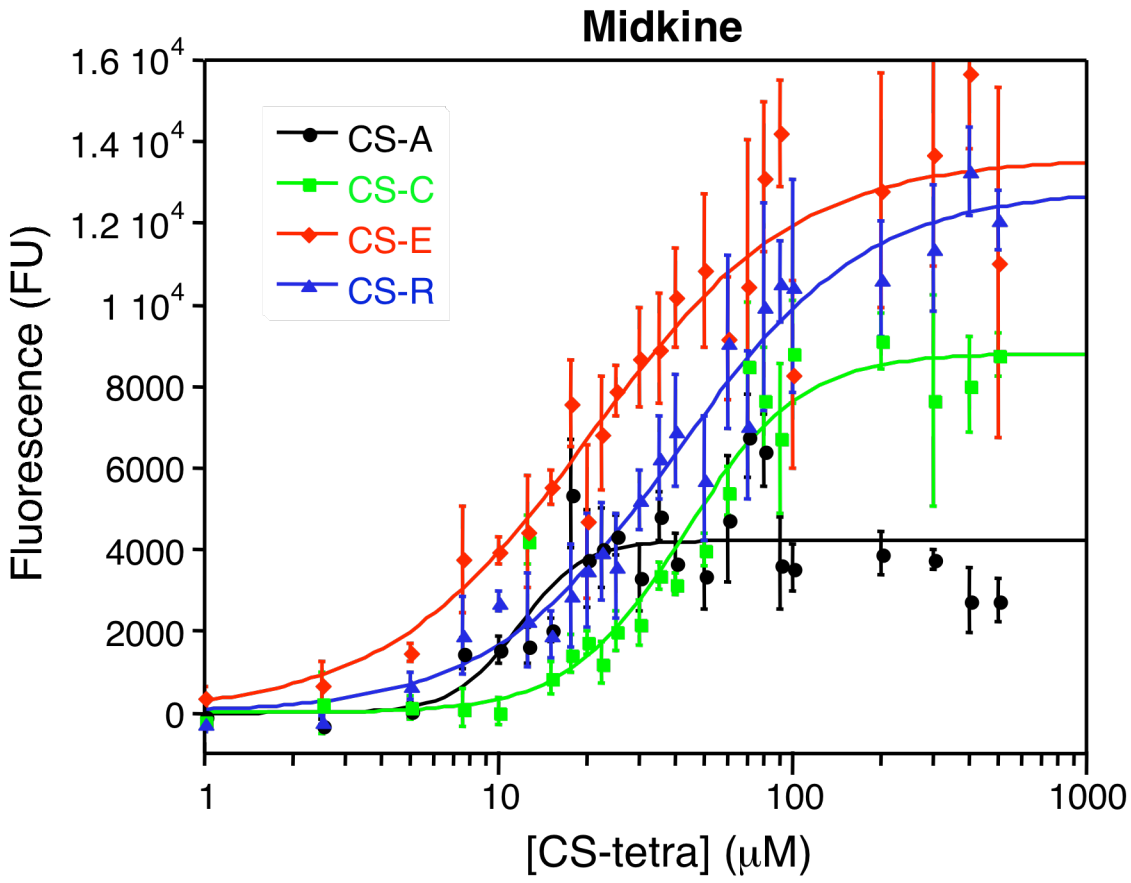

Figure A5.13: Binding curves obtained from microarray data of the CS tetrasaccharides bound to midkine. Curves are fit to the Hill equation, m1*x^m2/(m3^m2+x^m2).

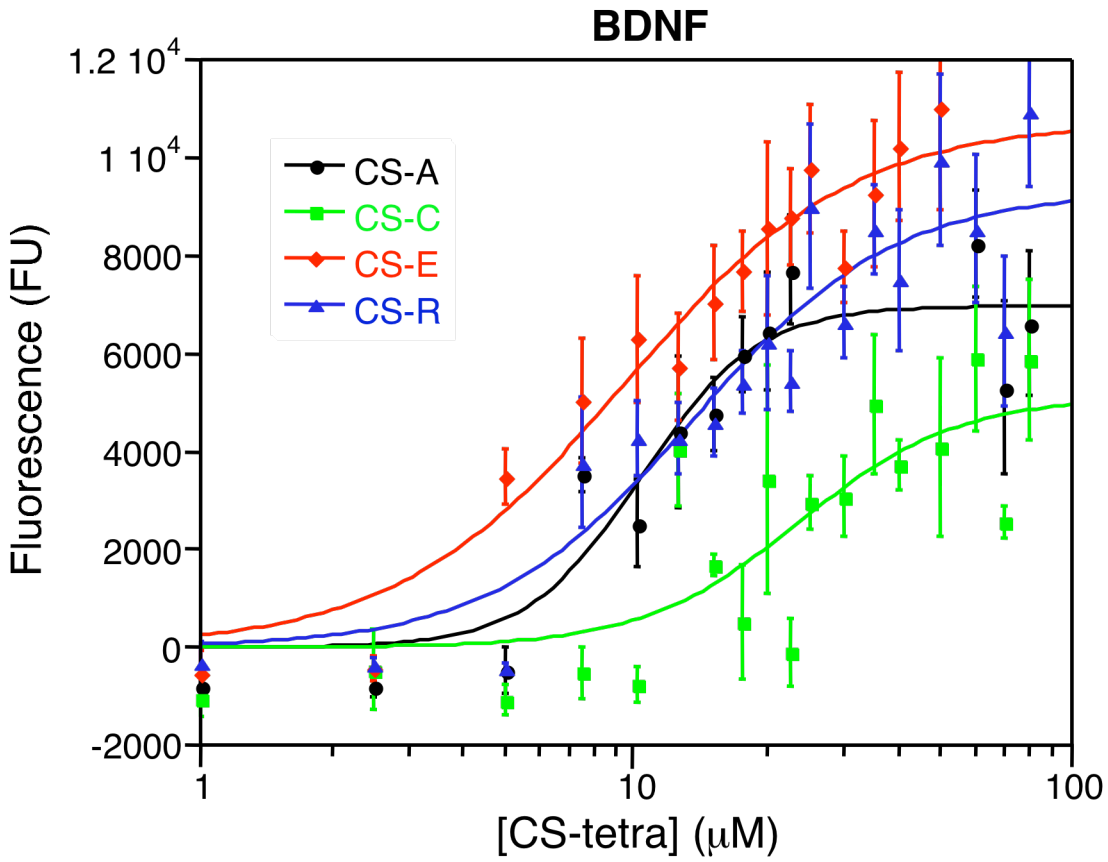

Figure A5.14: Binding curves obtained from microarray data of the CS tetrasaccharides bound to BDNF. Curves are fit to the Hill equation, m1*x^m2/(m3^m2+x^m2).